# Thermal Induced Stresses in Thin-Shell Structures

**Shaahid Hansa**

A research report submitted to the Faculty of Engineering and the Built Environment, of the University of the Witwatersrand, in partial fulfilment of the requirements for the degree of Master of Science in Engineering.

Johannesburg 2012

## Declaration

I declare that this thesis is my own work. It is being submitted to the University of the Witwatersrand, Johannesburg, in partial fulfilment of the requirements for the degree of Master of Science in Engineering. It has not been submitted before for any degree or examination in any other University.

Shaahid Hansa

Signature _____

## Abstract

Thin shell structures constructed from stabilised earth were assumed to be fully compressive structures as the loading conditions applied by the designers indicated this. However, it was found that these structures were experiencing extremely high tensile stresses and strains. These tensile stresses and strains are assumed to originate from thermal induced loading. This thesis investigates the temperature distribution and thermal induced stresses in a typical thin shell structure.

In order to determine the temperature distribution across a typical thin shell structure, a model was built and the temperature distribution was then determined. It was found that the temperature in the model was higher than expected. This temperature distribution was processed in a finite element model to produce typical magnitudes of the thermal induced stresses. It was found that thermal induced stresses are not negligible in these types of structures and a design engineer would need to account for theses stresses. This inspired the formulation of a design guide for these types of structures so as to adequately design these structures in the future.

## Acknowledgements

The author of this thesis is indebted to his supervisor; Professor Mitchell Gohnert, who sacrificed his time, and who has been a constant source of wholehearted encouragement throughout the research project.

The author is obligated, and forever appreciative to his father who supported him financially, academically and spiritually throughout the author's academic career.

# Table of Contents

# 1. Introduction

As defined by Chen and Lui, “Thin-shell structures are light weight constructions using shell elements. These elements are typically curved and are assembled to large structures. Typical applications are fuselages of airplanes, boat hulls and roof structures in some buildings.

A thin shell is defined as a shell with a thickness which is small compared to its other dimensions and in which deformations are not large compared to thickness. A primary difference between a shell structure and a plate structure is that, in the unstressed state, the shell structure has curvature as opposed to plate structures which are flat. Membrane action in a shell is primarily caused by in-plane forces (plane stress), though there may be secondary forces resulting from flexural deformations. Where a flat plate acts similar to a beam with bending and shear stresses, shells are analogous to a cable which resists loads through tensile stresses. Though the ideal thin shell must be capable of developing both tension and compression.” [1]

According to Statistics South Africa, about 40% of households in rural areas are traditional households and about 20% of households in urban areas are informal households or shacks, thereby there is a great need for cost effective household construction for the poor. Traditional construction is inexpensive, but low in quality and high in maintenance. Un-reinforced thin-shell structures constructed from stabilized earth tiles and local labour is a sustainable option that could be used in rural areas to construct structures for not only houses, but for schools, clinics and recreation facilities as well. This method of construction would result in empowerment of the poor in as well as cost effective and efficient structures. As the majority of the materials can be sourced in-situ, the overall cost of these structures is expected to be more economical than traditional structures.

There is potential to create employment through the construction of stabilised earth, thin shell structures, provided it is based on comprehensive planning relating to all activities. The framework for the integration of management, design, detailing and specification, construction

and manufacturing processes forms the basis for future construction of thin shell structures with labour intensive activities.

The design of un-reinforced thin shell structures constructed of stabilized earth tiles (or bricks) is a subject in structural engineering, which has no direct guidelines. There are many undiscovered sectors within this study which require a clear and accurate scientific approach. A particular sector, which requires special attention, is the thermal induced stresses within a stabilized earth thin-shell structure. An investigation is required here as in most cases in stabilized earth, thin-shell structures; cracking of the thin shell is due to thermal induced strains caused by varying temperature conditions. This thesis introduces the platform for this particular field of research.

# 2. Research objectives

## Problem statement

It has been observed by thin shell specialists, who are trying to implement low cost housing with shell structures, that the design forces are not accurately determined within conventional loading combinations, such as dead, live and wind combinations. Observations have indicated that tensions have been developing on the outer surface of thin shell structures which were thought to have been fully compressive structures. An example of this is the Sparrow Aids Village in Johannesburg, South Africa. The cracking observed in these thin shell structures is postulated to thermal stresses. Failures of shell structures have been directly attributed to large and rapid temperature changes [Gred, Paul (1986), "Students Narrowly Escape Dome Collapse", Engineers Australia, August 22, 82 1986], and therefore this type of loading must be considered. Besides failure, thermal cracking is aesthetically unpleasant and it causes waterproofing of the structure to be compromised.

These thermally induced stresses originate from a natural phenomenon; that is the day which heats the structure and the night which cools it. This exposure to differential temperature causes structures to expand and contract. Contraction induces compressive forces, which structures usually resist. However, expanding may induce tensile forces, and the structures'

strength may be exceeded. Thus, the focal point of this research is to determine fairly accurate temperature loading, the range of thermally induced stresses and a temperature loading design guide within a thin shell structure, constructed from stabilised earth.

### Research programme

The research programme was strategically planned whereby each subject and research objects within the programme complimented each other. The ultimate goal was to determine thermal induced stresses, thus temperature distributions on a model were to be established. After completing this, the thermally induced stresses were to be determined by a finite element model using the experimental data. Evolving from the focal point of the research was methods of attenuating the thermally induced stresses and temperature loading design curves for thin shell structures constructed from stabilised earth. This thesis unfolds the stream of events of the research programme in order to determine the thermal induced stresses.

## 3. Literature review

### Thin shell theory

As defined by Mark Fintel et al, “A structure is considered to be a shell if the thickness of the structure is much smaller than any other dimension. This structure is constructed as a curved, faceted or folded structure so that geometry activates axial forces to be the dominant load carrying system.

Shells may have curvature of the surface in one or more directions. Shells are of positive curvature if for any point on the surface the origins of both principal radii of curvature of that point are on the same side of the surface, i.e. both curvatures are in the same direction e.g. elliptical parabola shells and handkerchief shells. Negative curvature of a shell is when the curvatures of a single point have different directions (e.g. hyperbolic paraboloids). Positive curvature shells react to pressures normal to the surface with direct forces of the same sign in any two perpendicular directions, compared to negative curvature shells which have direct forces of opposite sign in any two perpendicular directions. The sign of the curvature of a shell is therefore indicative of the structural behaviour of the shell.

Shells may be classified according to the manner of generating the mathematical model of the shell. Rotational shells are formed by revolving a plane curve about an axis. Translational shells are formed by translating one curve along another, e.g. the handkerchief shell. However, classification provides little information on the structural behaviour of the shell.

Shell usage covers many sectors. This thesis is motivated by shell structures being used in low-cost developments with large spans, as shell structures used for roof systems are inspired by large spans and aesthetics. The cost of this type of structure will be much cheaper with stabilised earth tiles than conventional concrete, as the need for formwork is significantly reduced by the ingenious method of construction with earth tiles (or bricks). With conventional concrete shell structures, the high cost of formwork can severely restrict the large spans which would be considered economic. However, as the spans increase in size, buckling may become a controlling factor.

The ideal behaviour of a shell is to carry its load by in-plane or membrane forces or axial forces, and have these forces almost constant throughout the shell. This behaviour is activated by the shape of the shell and the support conditions. Variations in shell stiffness or loading will result in bending moments developing to either carry the load or to restore compatibility. The extent of this region in which bending occurs depends entirely on the geometry of the structure.

Shells with positive curvature transmit loads to the supports primarily by axial arching forces, provided some support exists along each edge. However, disturbances along the edges tend to damp out quickly. Negative curvature shells utilize in-plane shear as a prime mechanism to carry the imposed loads. Singly curved shells behave as curved beams. These shells tend to propagate edge disturbances in the form of moments much farther into the shell, as compared to positive curvature shells." [5]

## Thin shell structure for research

The thin shell structure chosen for the research was a handkerchief shell structure. The structure is inspired by a free-hanging handkerchief-type cloth supported by its four corners,

which is in tension under self-weight. Compression forces are noticed in this free-hanging structure as the cloth buckles near the supports, as shown in the following figure:

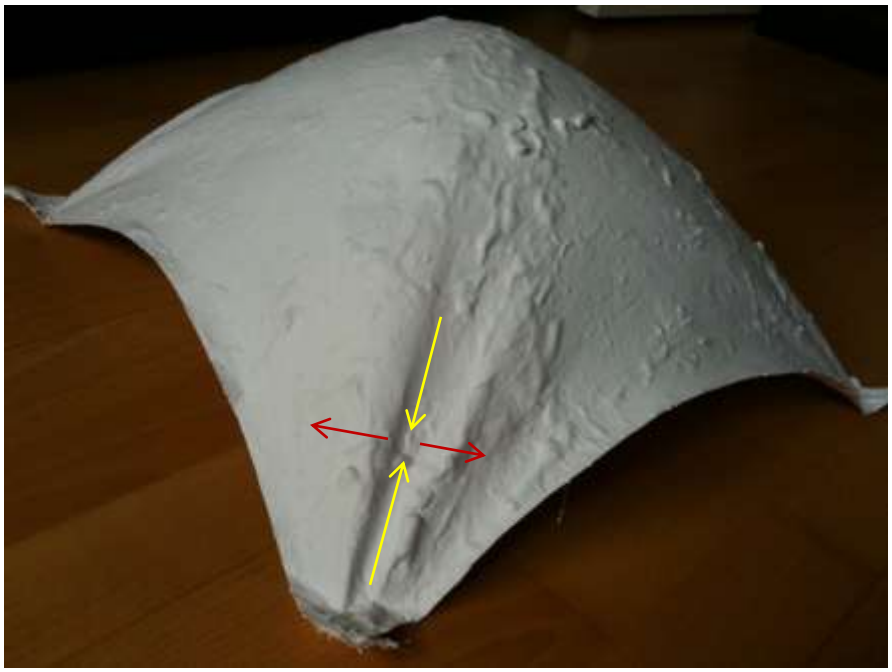

Figure 1: Illustrative display of the internal forces in a free-hanging structure. The yellow arrows indicate tension and the red arrows indicate compression in the structure.

From the figure it appears that there exists an internal compressive force due to the Poisson effect. Nonetheless, when the structure is hypothetically inverted, the structure is in compression under self-weight. When this hypothesis is extended, a handkerchief structure will be in compression under the conventional design load case of dead and live imposed loads. The handkerchief shell structure was then chosen on the basis of optimal resistance to conventionally imposed loads.

## Handkerchief shell theory

The handkerchief shell structure is classified as a translational shell. This category of shell classification probably has the largest variety of different shell surfaces and this form of shell is almost exclusively used for roofing systems. Principal shells of this classification are the elliptical parabola (similar to the handkerchief shell), hyperbolic parabola and the conoid. The popularity

of these shells is attributed to the vast range and variety of appearances that can be achieved with the same basic shell configurations.

The basic construction of the shells in this classification is to translate a curve along a fixed curve. This translational activity sweeps out the desired shell surface. Depending upon the selection of curves, the surface may have negative, zero or positive curvature.

A handkerchief left to hang only under its self-weight does not develop edges where negative curvatures form. The cloth resembles the elliptical parabola thin shell surface quite accurately. When additional load is placed onto it, these flattened edges form. This is a natural phenomenon which the cloth adapts in order to carry the additional loading.

## Materials and construction

### Materials

The material ideology for erecting the low-cost shells follows that of Hassan Fathy. Fathy's primary concern in the field of low-cost housing was that the conventional material of reinforced concrete was unaffordable in poverty stricken areas of Egypt. Fathy proposed that the materials used for constructing low cost houses in the area should be primarily sourced in-situ. Keeping this ideology in mind, the material for the structures evolved as unreinforced, stabilised earth.

Since the majority of the material will be sourced in-situ, job opportunities in the area will increase and fundamental construction skills and techniques will be acquired. By using materials that could be sourced almost exclusively from the site itself, more structures may be built from the project budget, and the bulk of the project cost could be retained within the community by means of community employment. By reverting to techniques of construction that are thousands of years old, the need for machines will be minimal.

### Construction methods

The method of construction of Rafael Guastavino and his son has been adopted for the construction of shells, using stabilised earth tiles, in this research domain. This system of construction appears to have its origins in 14$^{th}$ Century Spain, and the methodology of this

system is seamlessly applied to low cost shells. During construction, the vertical and horizontal joints of the tiles are staggered, thus the structure supports itself while being constructed, and this reduces cracking along the joints.

The construction of the shells will be executed with tiles and mortar, whereby the first layer of tiles will use a very strong, rapid hydrating high grade alpha particle gypsum mortar, which is a product called Crystacal. This is done in order to support the additional layers of tiles during construction, whereby these additional layers will use conventional mortar. This self-supporting construction method almost eliminates the need for formwork and it activates labour intensive construction. An example of where this innovative construction method was used is the Mapungubwe Interpretation Center. Shown below is a picture illustrating a minimal amount of formwork:

Figure 2: The Mapungubwe Interpretation Center during construction (compliments from Dezeen Limited)

# 4. Temperature distribution

In attempting to identify the temperature distribution across a handkerchief thin shell structure, several models were built. The models aimed at accurately capturing the actual structures properties. In order to obtain an accurate model, a scale of the materials in an actual structure was envisaged and simplified erection techniques were applied to construct the model. It was presumed that the shape, material, position, location and orientation of a structure all influence the temperature distribution across the structure.

## Description of model structure

The model was built as a handkerchief thin shell structure. This structure was chosen as it is a structurally efficient thin shell structure. The behaviour of this structure is that it carries most of the applied load by in-plane or membrane forces, as explained above. The shape of the model structure was determined by hanging a piece of cloth, soaked in plaster of Paris, at the four corners of the cloth. The deformed shape had then indicated the desired handkerchief shell model shape. The plaster of Paris structure was then stiffened with wood, on the inner surface, in order to create a mould/rig for developing 5 other handkerchief shells, created from stabilised earth.

Figure 3: A hanging plaster of Paris mould without wood stiffeners

Figure 4: Typical stabilised earth model

As explained previously, a handkerchief left to hang only under its self-weight does not develop edges where negative curvatures form. This hanging cloth resembles the elliptical parabola thin shell surface quite accurately. When additional load is placed onto it i.e. the plaster of Paris, these flattened edges form. When creating the mould for the structure, the material used for the cloth had a high tensile capacity, thus these edges did not fully form. With the wooden stiffeners inserted into the mould, this led to the stabilised earth models having very slight upward curves. Nonetheless, the model did have these flattened edges, albeit barely visible, which were purposely avoided because according to the theory these negative curvature edges induce in-plane shear stresses in the structure, thus increasing the total stress within the structure.

## Model materials

The material used for the construction of life-size thin shell structures consists ideally of 60% pit sand, 40% river sand and 10% cement. The model structure required a particle scale of this mix in order to accurately determine the temperature distribution across the structure. In search for the ideal model material, plaster sand was seen as a close approximation. The particle size

distribution of the material was then determined and compared to the real structures' material. The results are displayed below:

| Sieve size (mm) | Plaster Sand | Pit & River Sand | Size difference |
|---|---|---|---|
| | Percentage Passing | Percentage Passing | Percentage |
| 6.7 | 100 | 98.7 | 1.3 |
| 4.75 | 100 | 86.3 | 13.2 |
| 2.36 | 99.4 | 71.8 | 27.0 |
| 1.18 | 98.3 | 59.7 | 36.3 |
| 0.6 | 93.7 | 51.2 | 38.6 |
| 0.425 | 83.4 | 39.2 | 41.8 |
| 0.3 | 67.4 | 16.6 | 46.4 |
| 0.15 | 30.9 | 7.9 | 59.3 |
| 0.075 | 19.4 | 0.0 | |

| | |
|---|---|
| Average | 33.0 |
| Standard error | 6.0 |

Table 1: Particle size difference

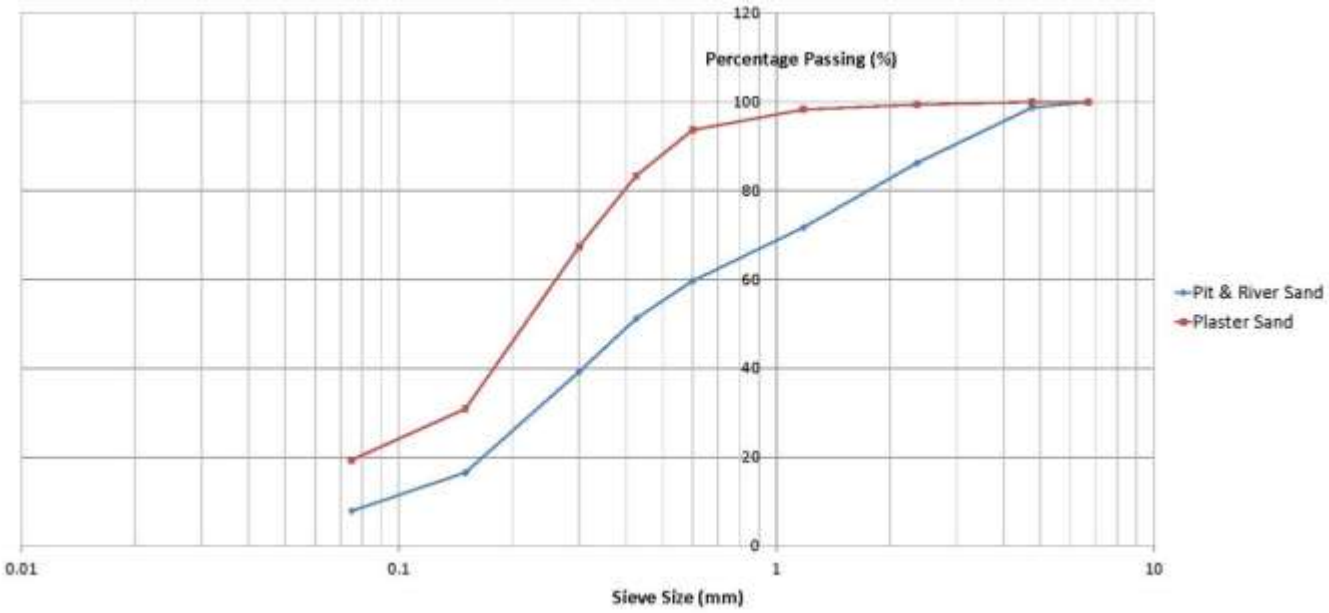


Figure 5: Particle size graph

The table presents the size difference of the two soil types. These results indicate that the particle size of the plaster sand is on average about thirty three times smaller than the plaster and river sand mix, with a standard error of six percent. The approximation is complimented with the graphical result, indicating the different soils having a fairly average difference in their particle sizes. This implies that the model structure which has a span of 700mm, a real structure would have a span of 23m, which is an ordinary size for a school hall or something of similar activity. The scaling of the materials is an attempt to match the geometrical dimensions of the scaled model. The plaster sand was then accepted and used to create the model.

## Model dimensions

After many attempts of trying to create a handkerchief shell mould, the final dimensions of the stabilised earth shell structures created from the mould were as follows (All the dimensions in these diagrams are approximate in millimetres. These diagrams do not clearly display the upward curved edges of the model. These edges are shown in the FEM model and in the pictures):

## Plan view

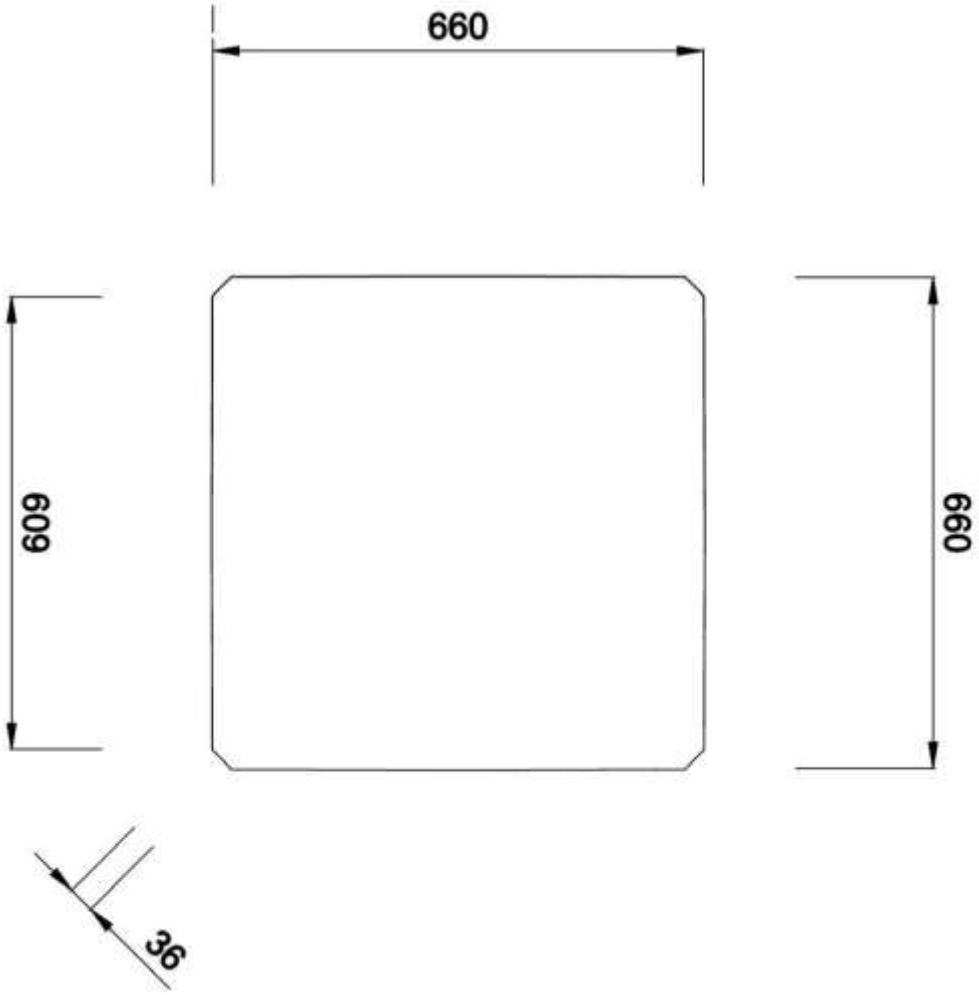


Figure 6: Plan view of model

## Side view

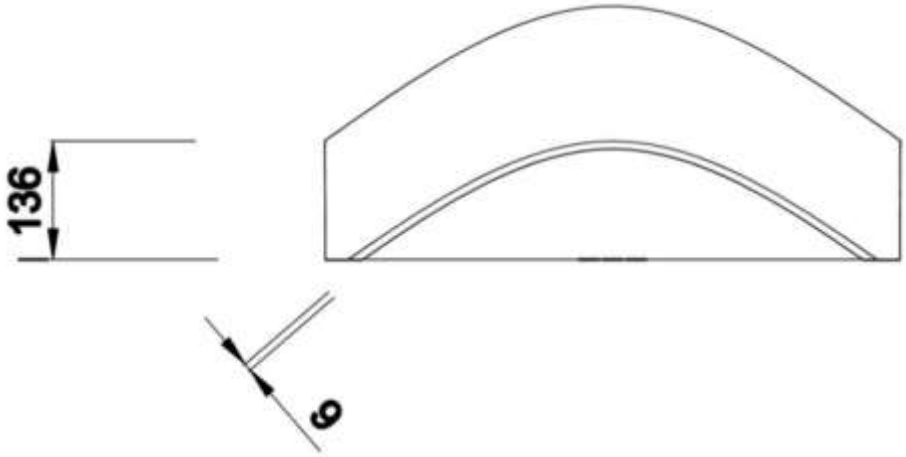


Figure 7: Side view of model

## 3D view

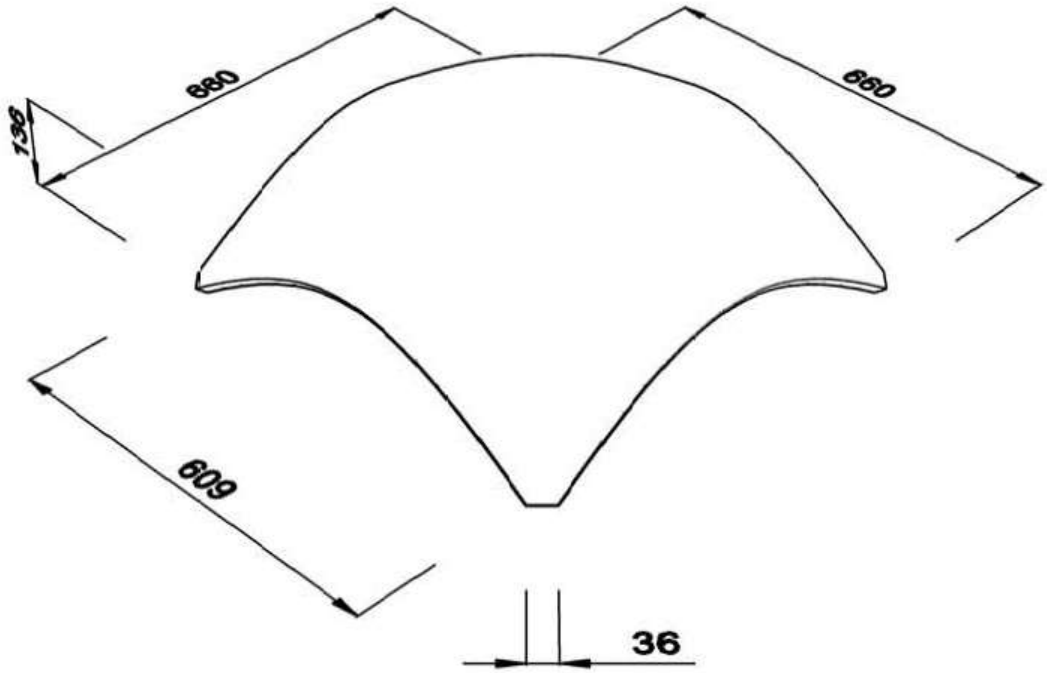


Figure 8: 3D view of model

## Surface temperature distribution

The temperature of the inner and outer surfaces of the structure was determined by placing the structure in a position where it would encounter the most severe temperature variations that a real structure would be exposed to. This position was established as where the structure would be exposed to direct sunlight during the day.

The temperature across the surface of the shell structure was estimated by means of a gun-type infrared thermometer (manufacturer-Top Tronic, model-T111). This reading was taken along with the ambient air temperature reading, the suns inclination and declination angles, the date and the time. Initially readings were taken at regular intervals during the day, in order to establish the time when the shells surface would yield the highest temperature.

Experience dictated that the time for measuring the temperature across the surface was at sunrise, when the surface was the coolest, at the suns zenith and an hour and a half after zenith when the shells surface temperature was the highest. The inner and outer surface of the shell structure was measured in order to determine the differential temperature across the thickness of the shell.

## Surface types

In an attempt to attenuate the thermally induced stresses within the thin shell structures, different surface textures and colours were applied to the shells. The types of surfaces used were:

1. A plain, untouched surface (control model)

Figure 9: Plain surface model

2. A white painted surface. The paint used was Plascon, white gloss enamel paint.

Figure 10: White surface model

3. Applied granite crusher stone surface (approximately 75% covered)

Figure 11: Crusher stone surface model

4. Applied pumice stone surface (approximately 90% of critical areas covered)

Figure 12: Pumice stone surface model

## Location

The location of the models influences the temperature distribution in more than one way. For example, the sun will project its rays onto the model from different angles in different locations. These angles are known as the azimuth angle and the elevation angle. The azimuth angle is the angle between the model and the sun in plan, while the elevation angle is the angle between the model and the sun in elevation or section. Also the local weather conditions influence the temperature on the surface of the structure. The model structures were tested for the temperature distribution in the following location:

15 Blossom Road, Bakerton, Springs, Gauteng;

GPS coordinates: 26°13’13” S, 28°28’28” E;

Balloon A on map;


Figure 13: Map showing the location of the thin shell model structures under observation

## Sun charts

Sun path charts can be plotted either in Cartesian (rectangular) or polar coordinates. The charts display the azimuth and the elevation angle of the sun relative to the point of interest i.e. the models. The azimuth angle indicates the direction of the sun in the horizontal plain from a given location. North is defined to have an azimuth of 0° and south has an azimuth of 180°. The various trajectories of the sun are bounded by those of the longest and shortest days. Although both coordinate systems display the azimuth and elevation angle, the Cartesian coordinate plot illustrates the elevation better than the polar coordinate plot and the polar coordinate plot illustrates the azimuth better.

Herewith below is a polar coordinate representation of the sun's position relative to the models, which illustrates the azimuth clearly. All angles displayed below are given relative to the model. Polar coordinates are based on a circle where the solar elevation is read on the various concentric circles, from 0° to 90° degrees, the azimuth is the angle going around the

circle from 0° to 360° degrees, the horizon is represented by the outermost circle, at the perimeter.

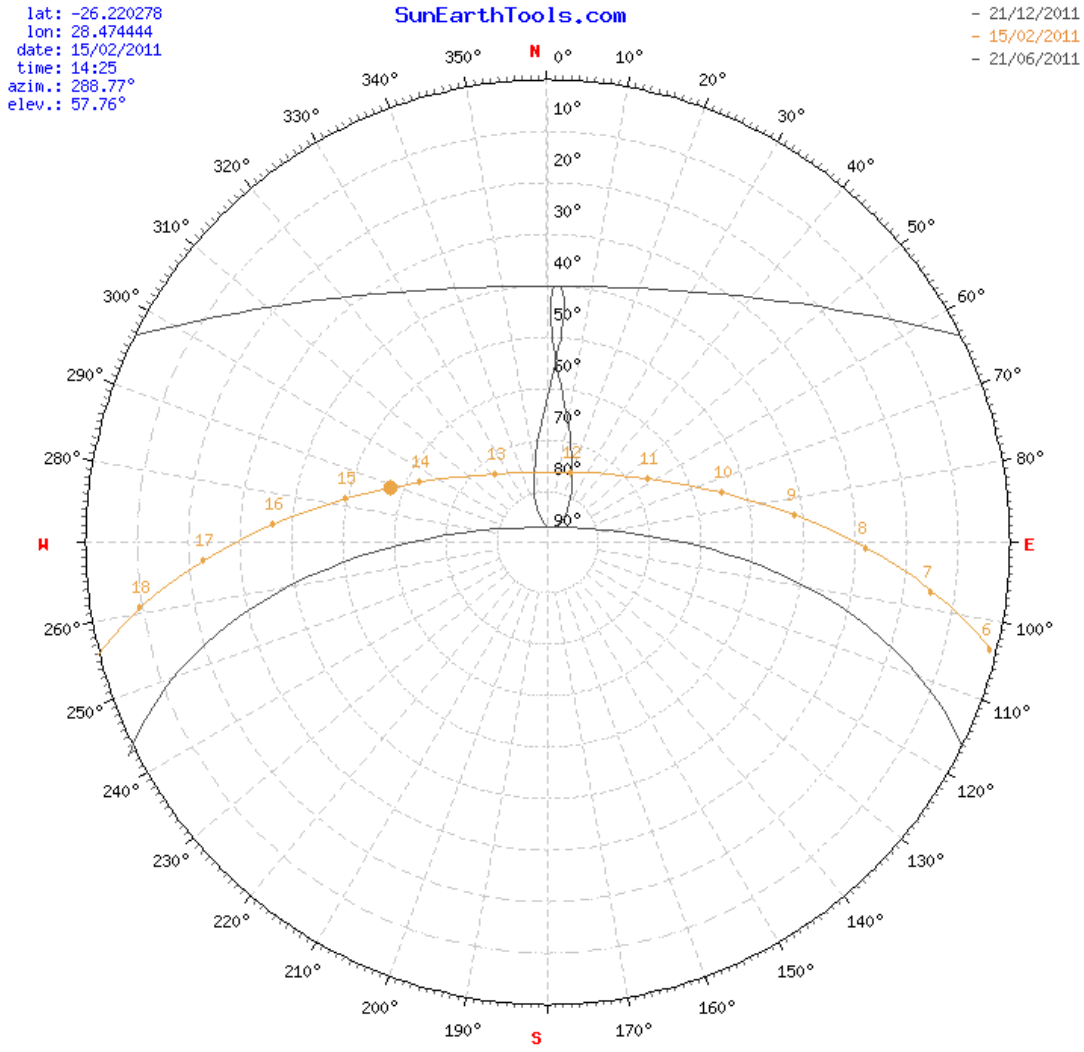


Figure 14: Illustration of the azimuth. The centre of the diagram indicates the models' positions (compliments from sunearthtools.com)

The Cartesian coordinates plot is where the solar elevation is plotted on Y axis and the azimuth is plotted on the X axis.

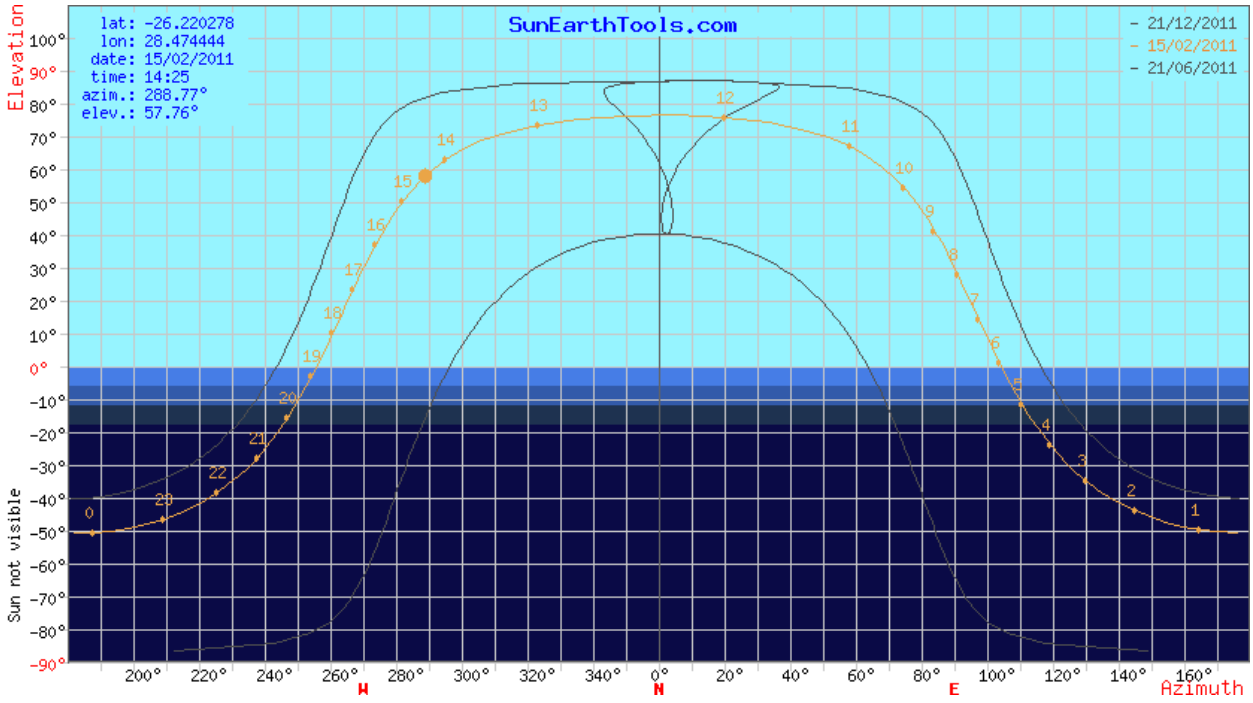


Figure 15: Illustration of the elevation angle. The centre of the diagram indicates the models position (compliments from sunearthtools.com)

## Orientations

The orientation of the structure considerably influences the temperature distribution across the entire surface. As the models were located in the southern hemisphere, the north-facing slopes/faces of the structure would be exposed to the most high temperature variations. Thus, the models were placed in multiple orientations in order to determine the acute temperature distributions.

1.

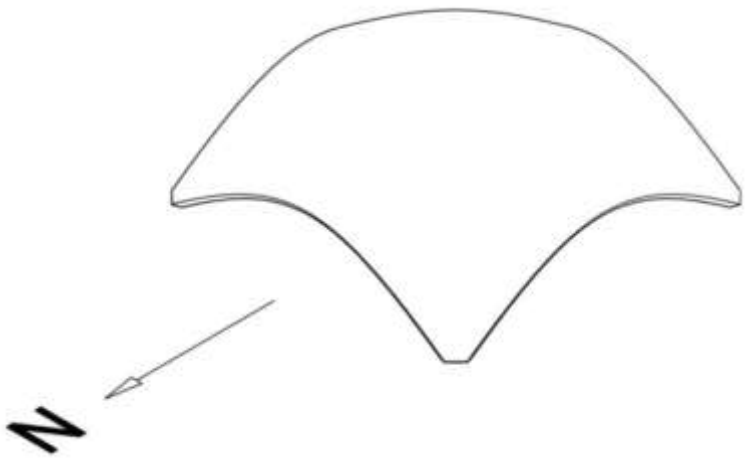


Figure 16: Illustration of orientation one of the models whereby a single face of the structure is north facing

2.


Figure 17: Illustration of orientation two of the models whereby multiple faces of the structure are north facing

## Observation

The results displayed a trend that the coolest temperature readings were taken just before sunrise and the hottest temperature readings at about an hour and a half after the suns zenith. Higher readings were also noted for the orientation of the structures where multiple faces of the structure were north facing, as shown in Figure 17. The number of readings taken on the outer surface of the models was thirty six and on the inner surface was nine, the total being forty five readings on each model. The number of readings was limited by the time taken to measure and annotate the surface temperature distribution, as more than forty five readings on each model resulted in large differences in the time at temperature measurements for all the models.

The following pages present the most intense results which were processed into contour maps by MATLAB. These contour maps have their axis labelled as relative to the span of the structure i.e. dimensionless; this was done so that the temperature distribution contour map may be mapped onto any handkerchief shell structure of any span.

## Results

The orientation of the temperature contour maps displayed hereafter mimic the orientation of the structure as shown below in plan view.

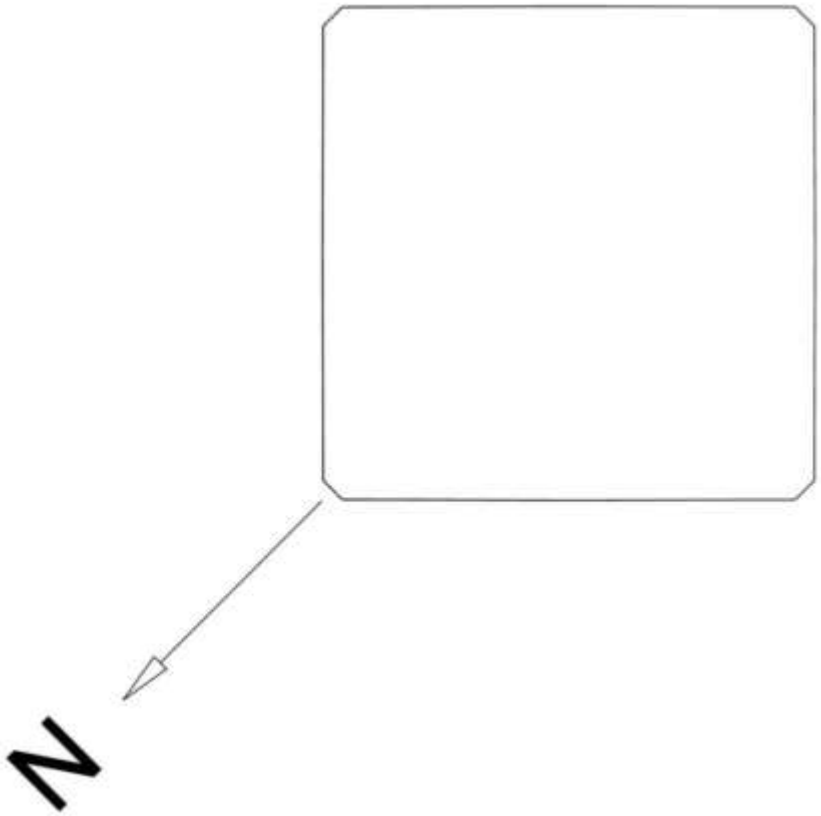


Figure 18: Model orientation

**Date**: 15/02/2011

**Time**: 06:00 (sunrise)

**Ambient temperature**: 15°C

**Weather description**: Clear, cool

**Suns position**: Azimuth - 103.71°; elevation - 1.19°

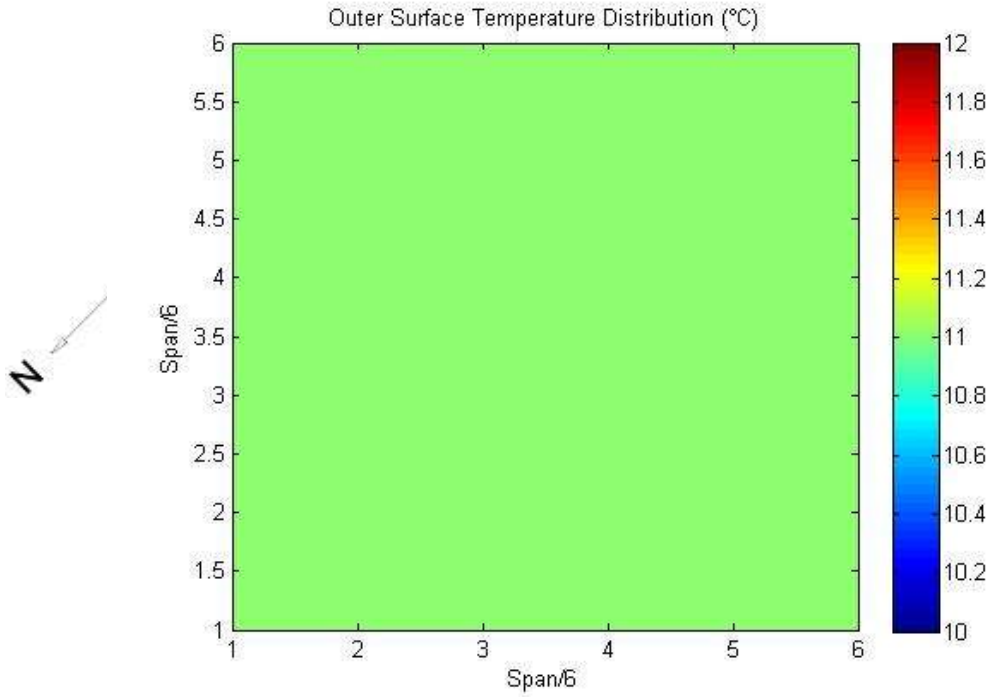


Figure 19: Outer surface temperature-Plain, crusher stone and white paint surfaces

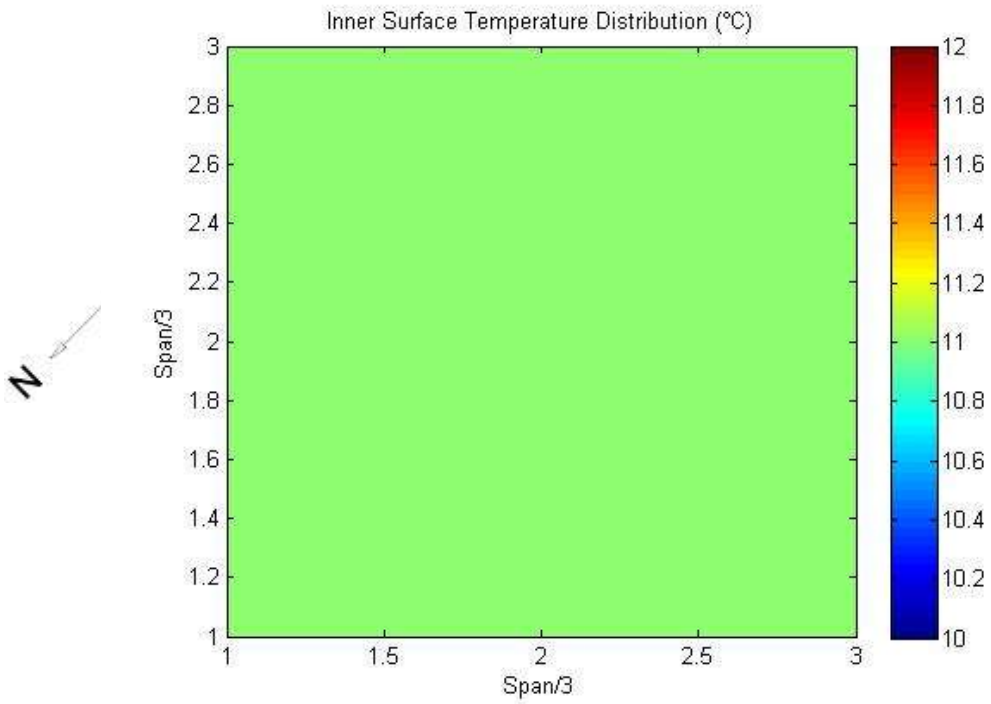


Figure 20: Inner surface temperature-Plain, crusher stone and white paint surfaces

**Date**: 15/02/2011

**Time**: 12:20 (suns zenith)

**Ambient temperature**: 25°C

**Weather description**: Clear, warm

**Suns position**: Azimuth – 0.28°; elevation – 76.5°

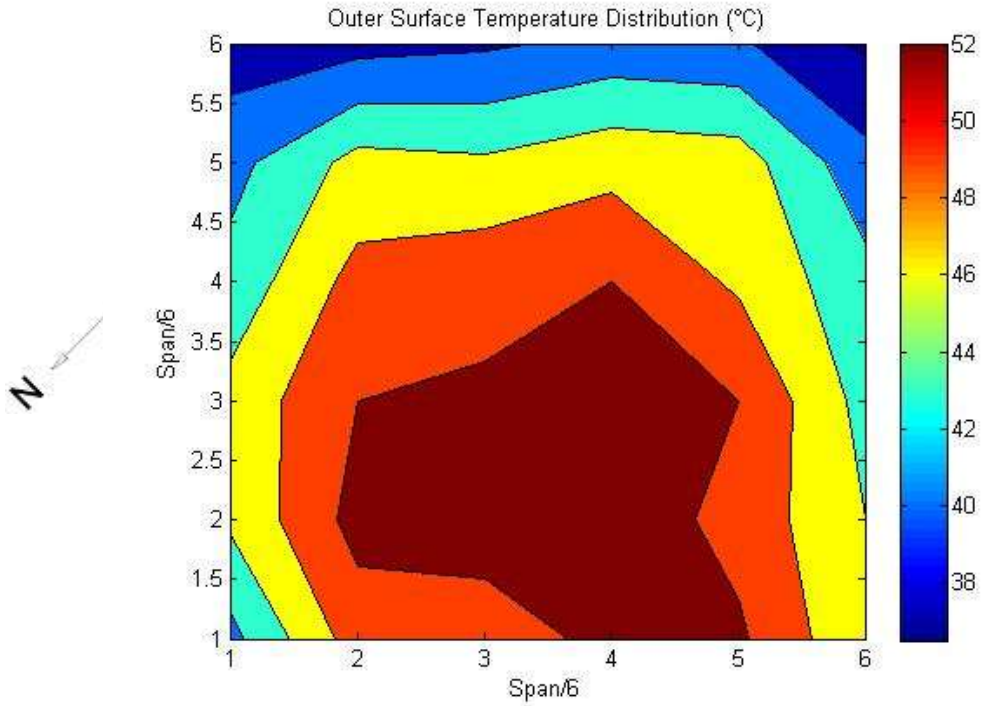


Figure 21: Outer surface temperature-Plain surface

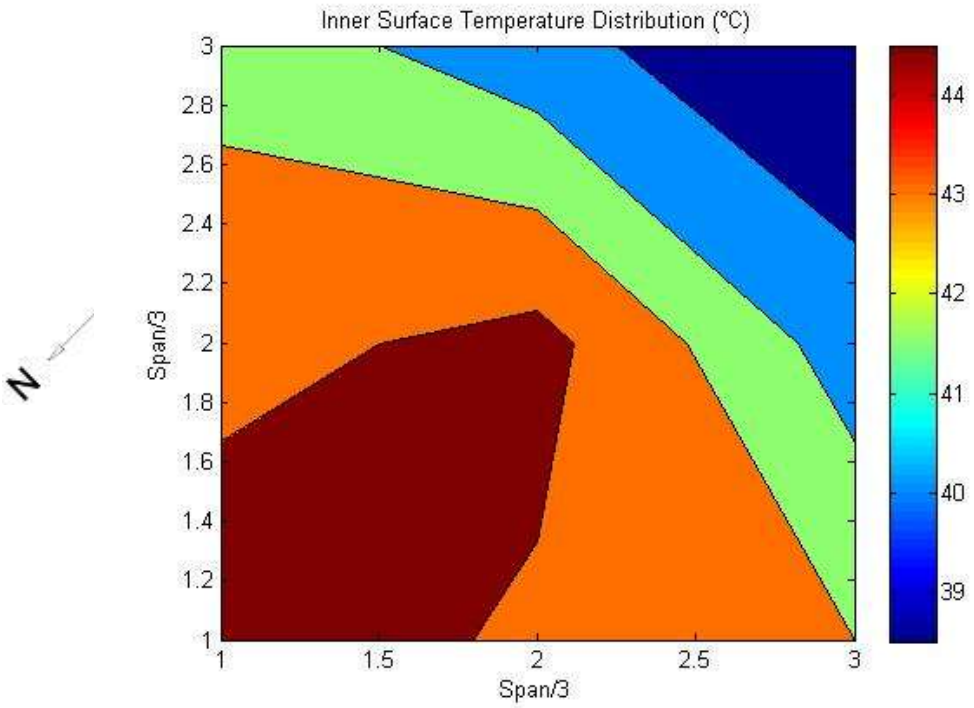


Figure 22: Inner surface temperature-Plain surface

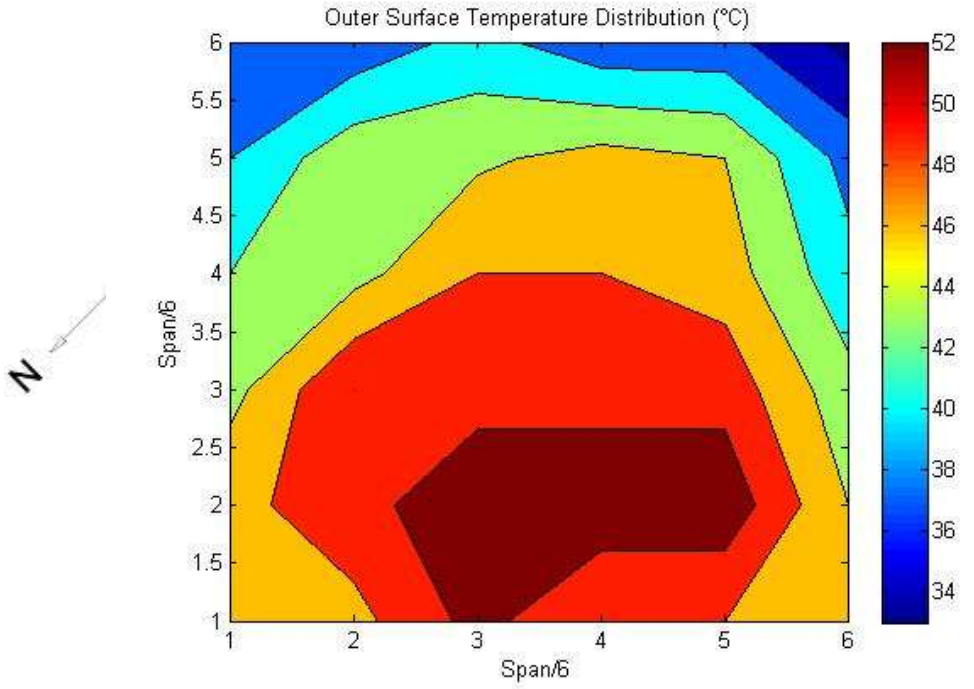


Figure 23: Outer surface temperature-Crusher stone surface

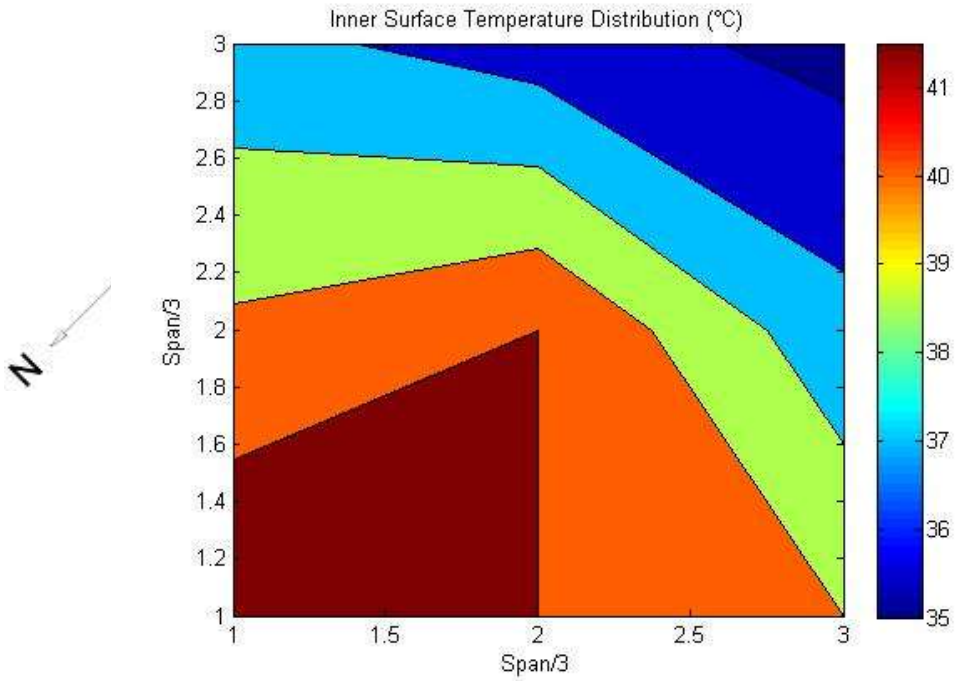


Figure 24: Inner surface temperature-Crusher stone surface

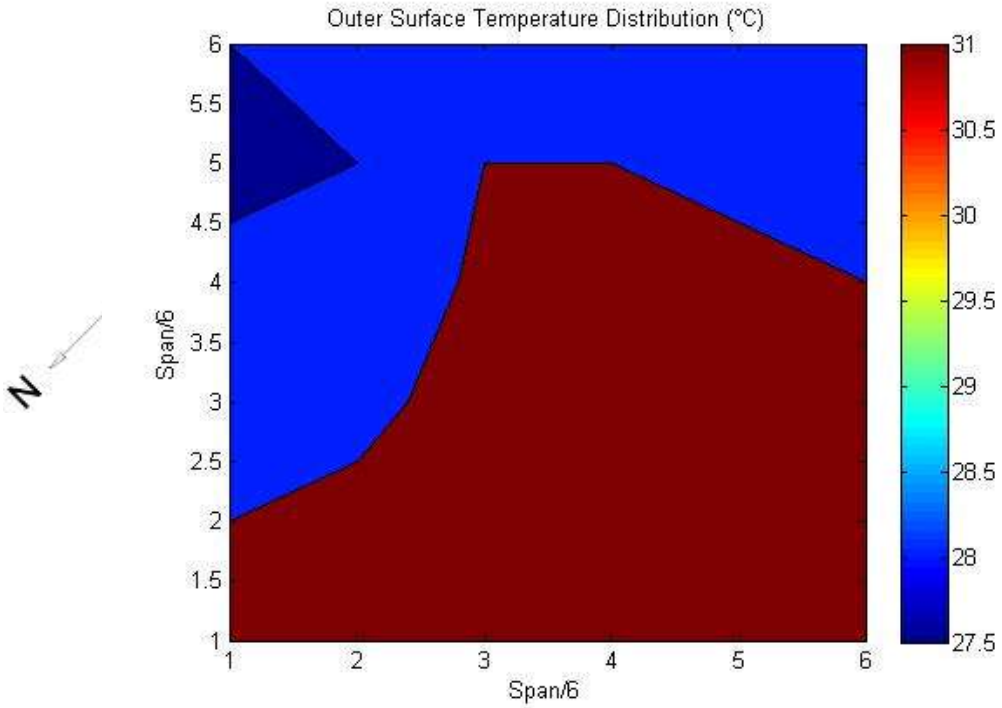


Figure 25: Outer surface temperature-White paint surface

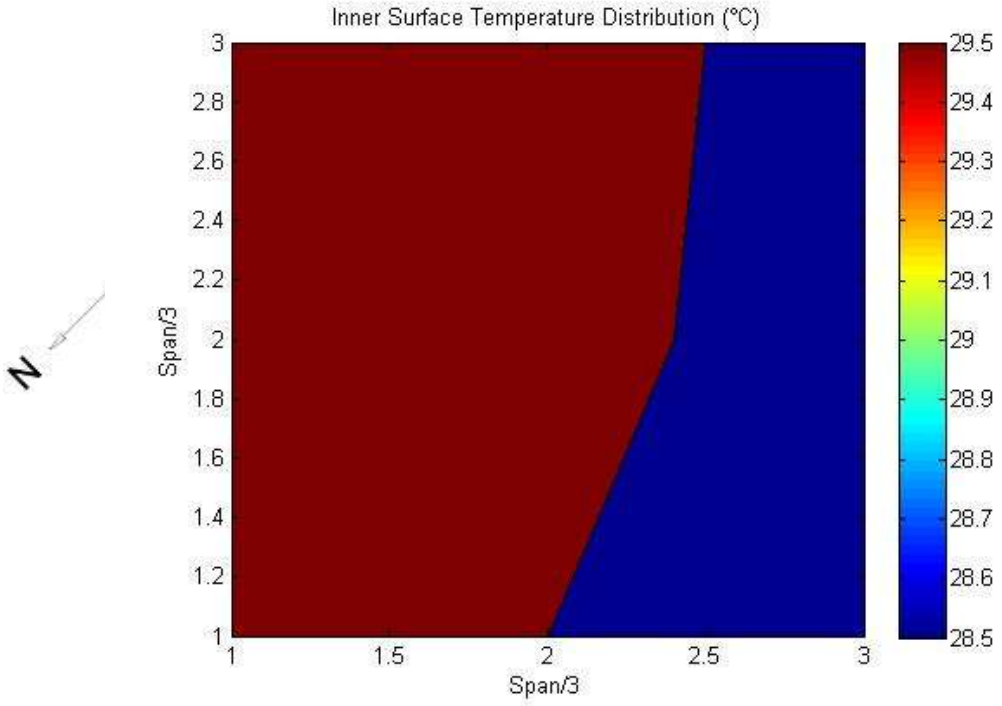


Figure 26: Inner surface temperature-White paint surface

**Date**: 15/02/2011

**Time**: 14:25

**Ambient temperature**: 28°C

**Weather description**: Clear, warm

**Suns position**: Azimuth – 288.77°; elevation – 57.76°

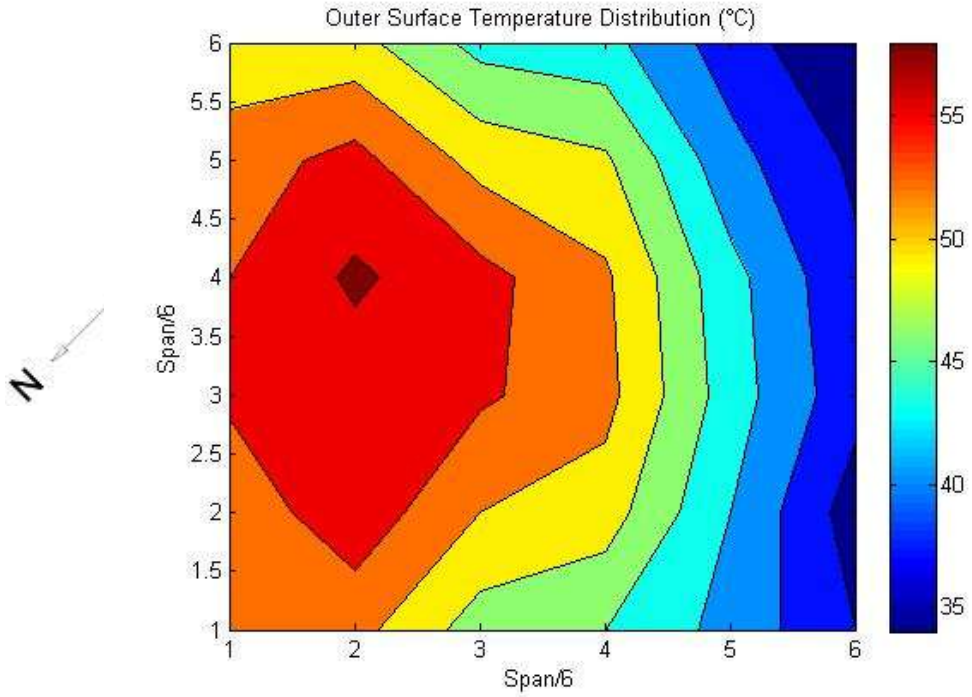


Figure 27: Outer surface temperature-Plain surface

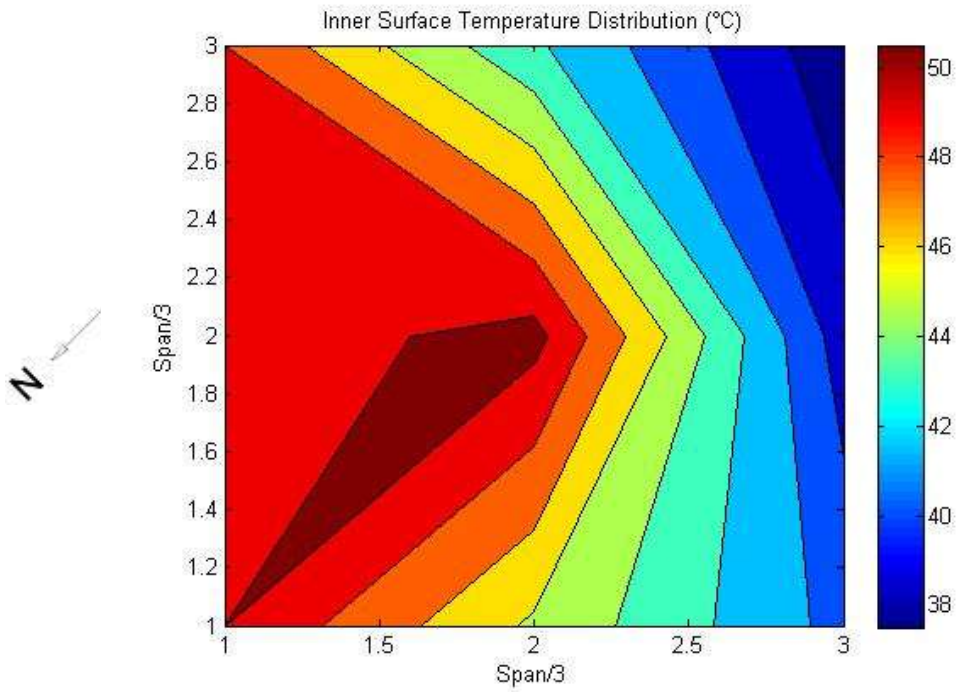


Figure 28: Inner surface temperature-Plain surface

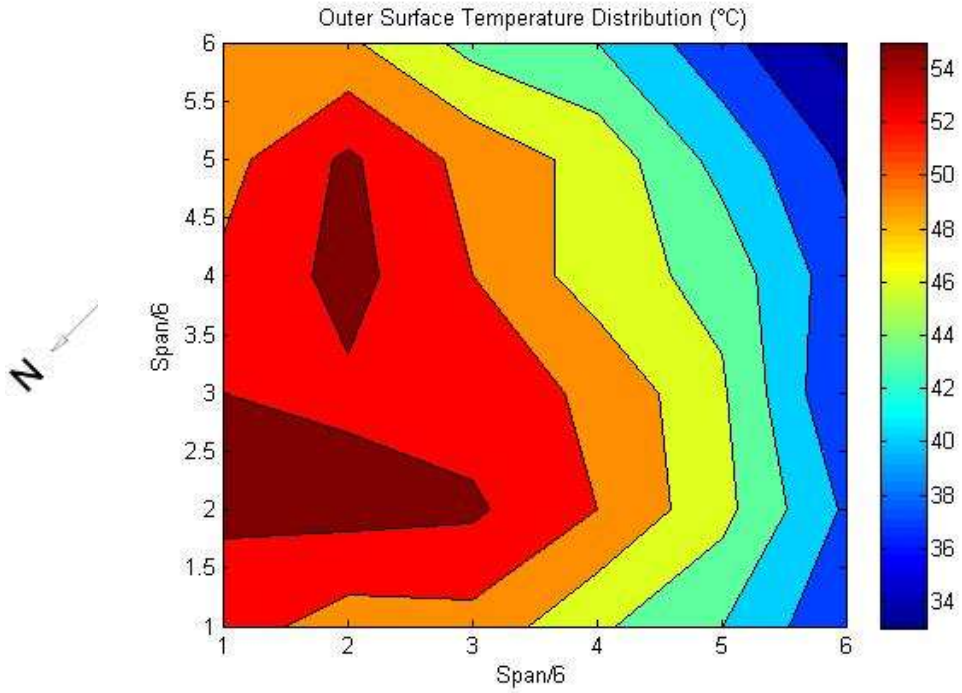


Figure 29: Outer surface temperature-Crusher stone surface

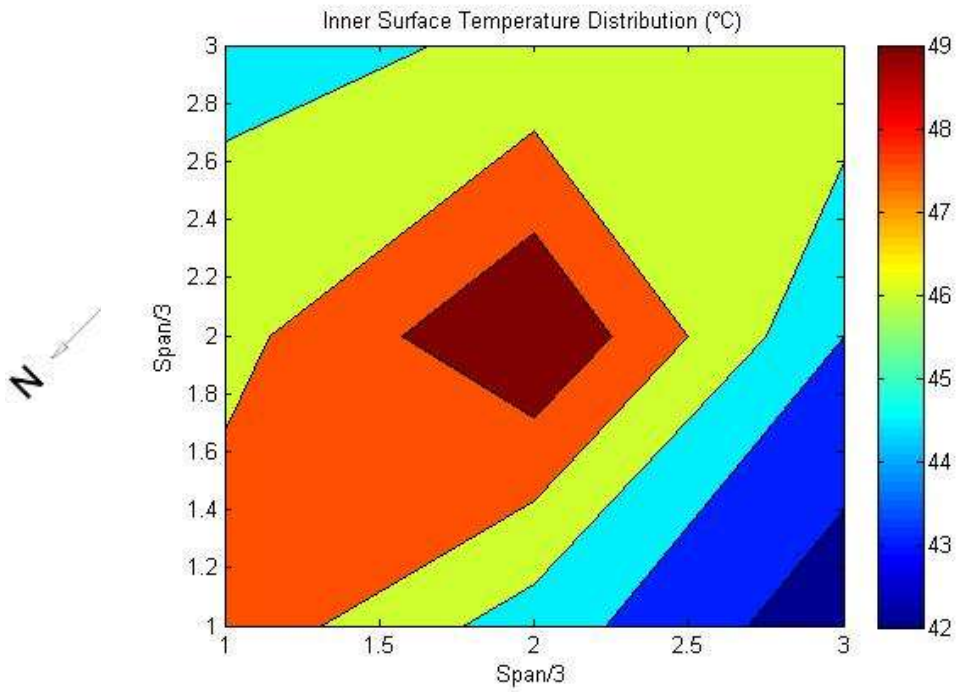


Figure 30: Inner surface temperature-Crusher stone surface

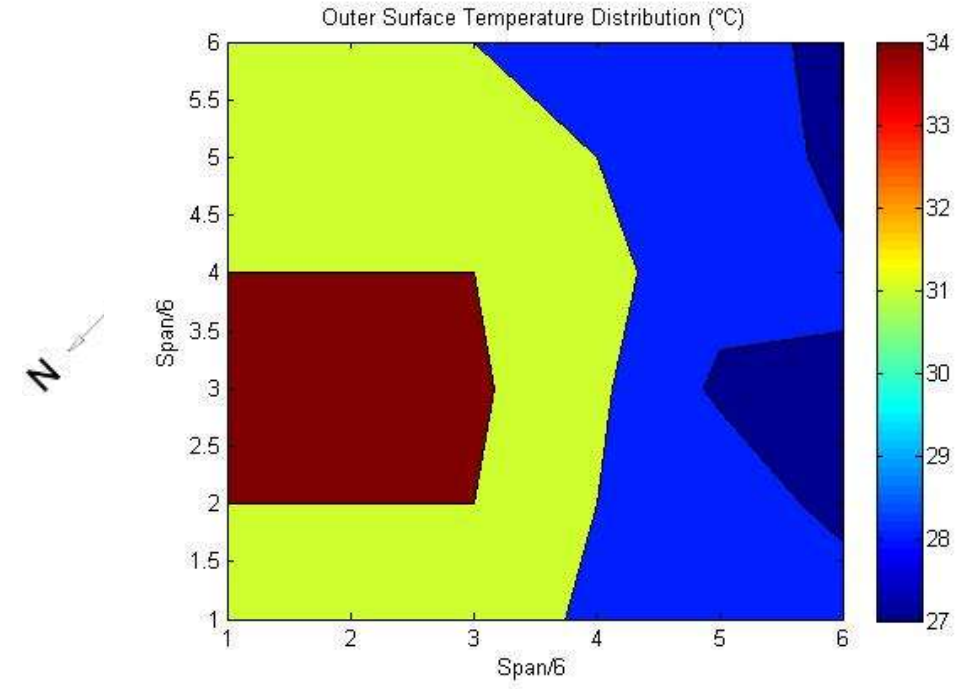


Figure 31: Outer surface temperature-White paint surface

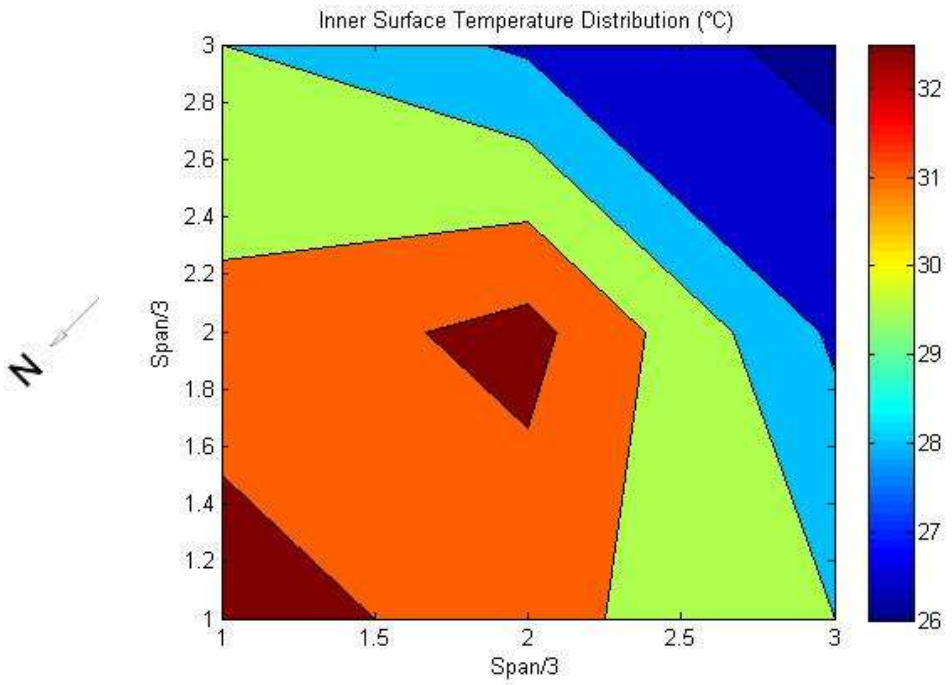


Figure 32: Inner surface temperature-White paint surface

**Date**: 19/07/2011

**Time**: 07:00 (sunrise)

**Ambient temperature**: 1°C

**Weather description**: Clear, cold

**Suns position**: Azimuth - 72.29°; elevation - -11.71°

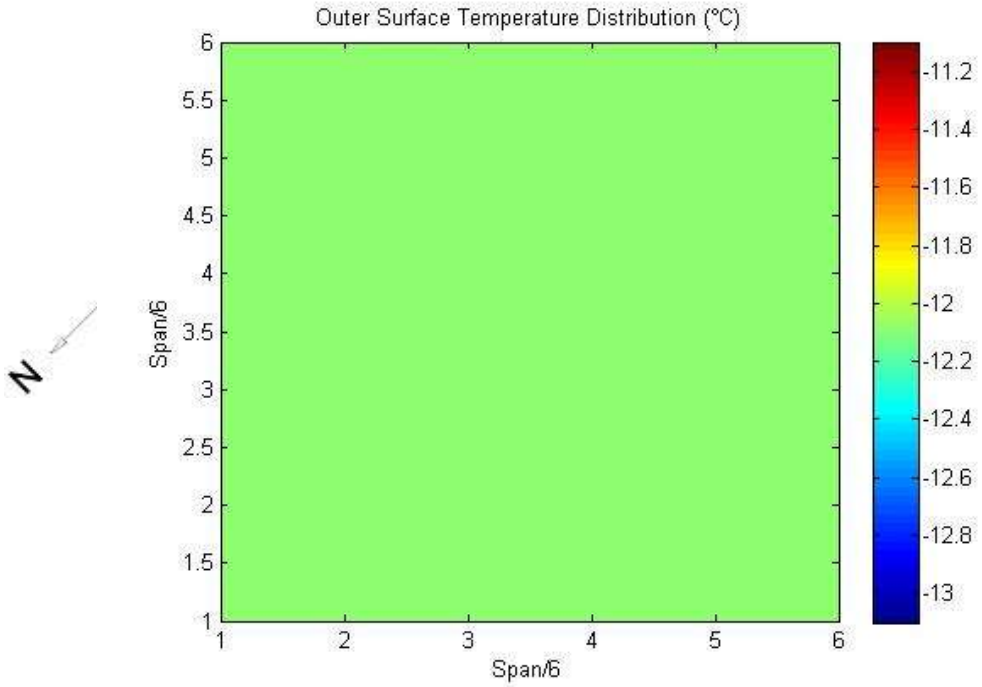


Figure 33: Outer surface temperature-Plain, crusher stone and white paint surface (note negative temperature)

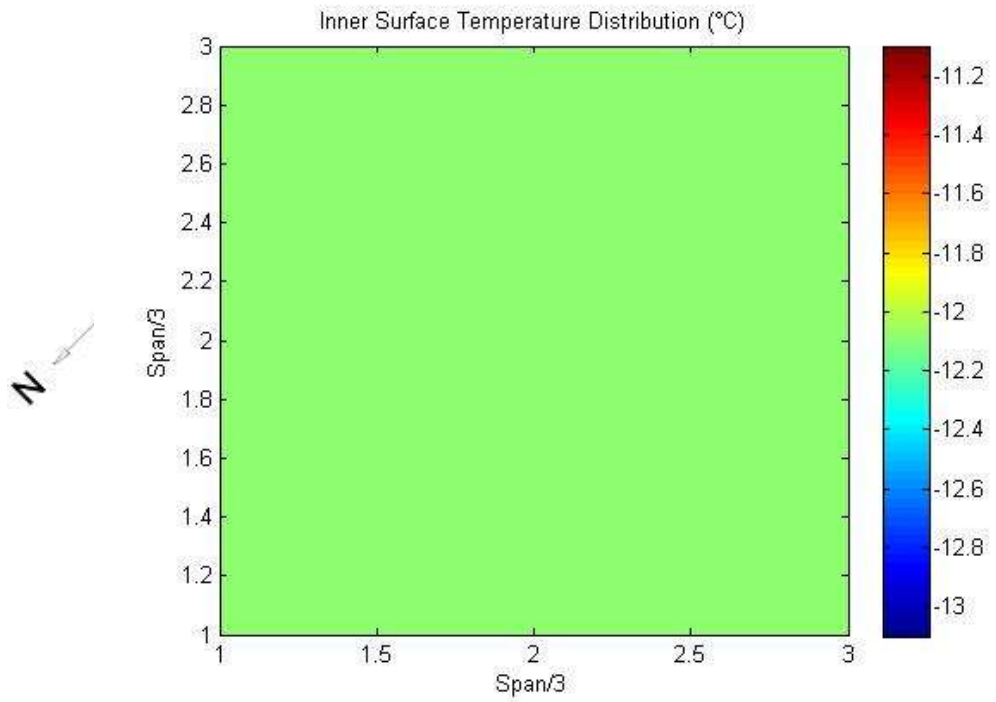


Figure 34: Inner surface temperature-Plain, crusher stone and white paint surface (note negative temperature)

**Date**: 19/07/2011

**Time**: 12:15 (suns zenith)

**Ambient temperature**: 23°C

**Weather description**: Clear, warm

**Suns position**: Azimuth – 0.13°; elevation – 42.91°

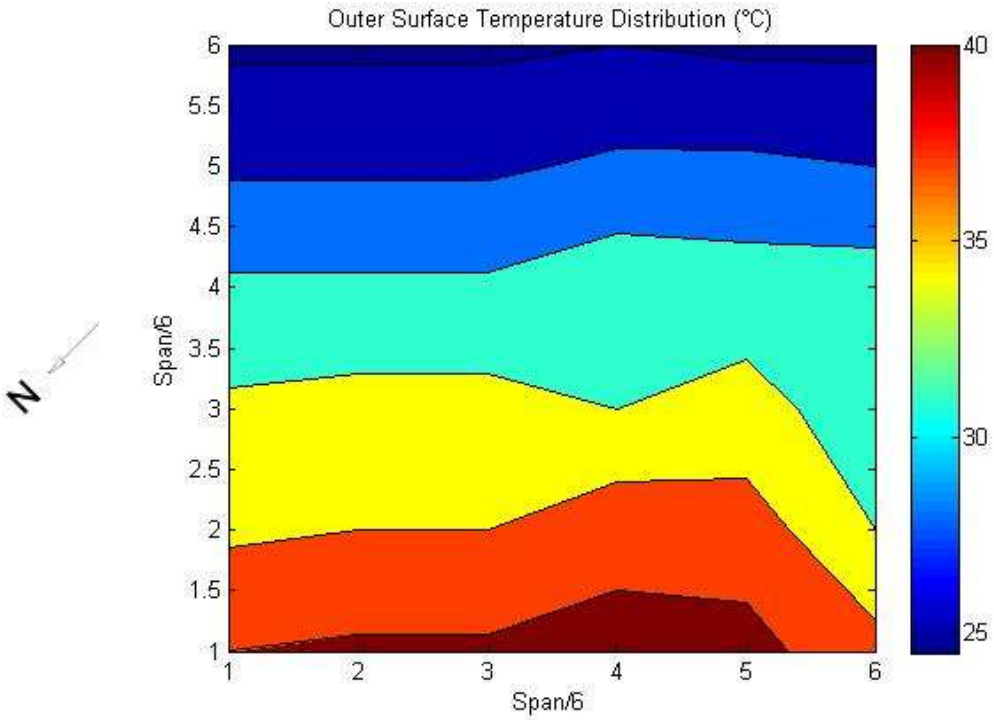


Figure 35: Outer surface temperature-Plain surface

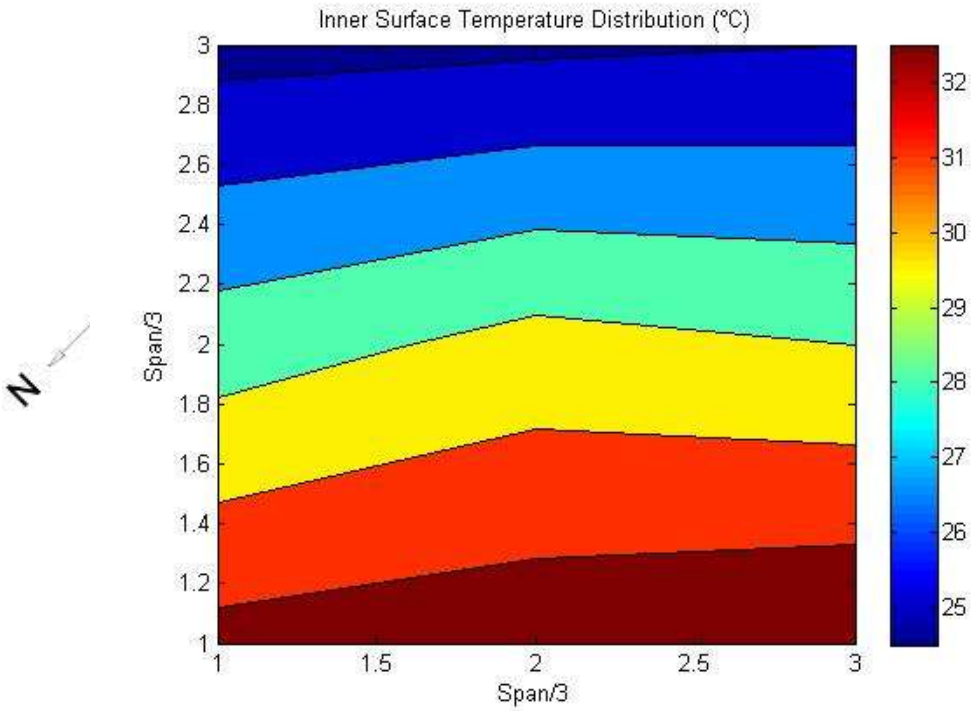


Figure 36: Inner surface temperature-Plain surface

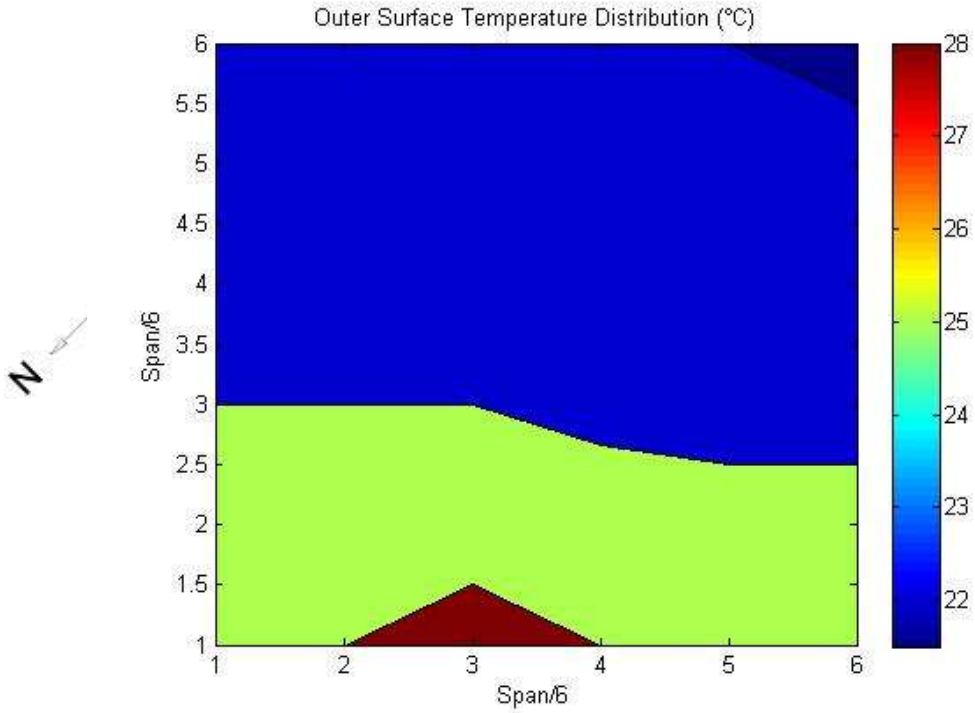


Figure 37: Outer surface temperature-Pumice stone surface

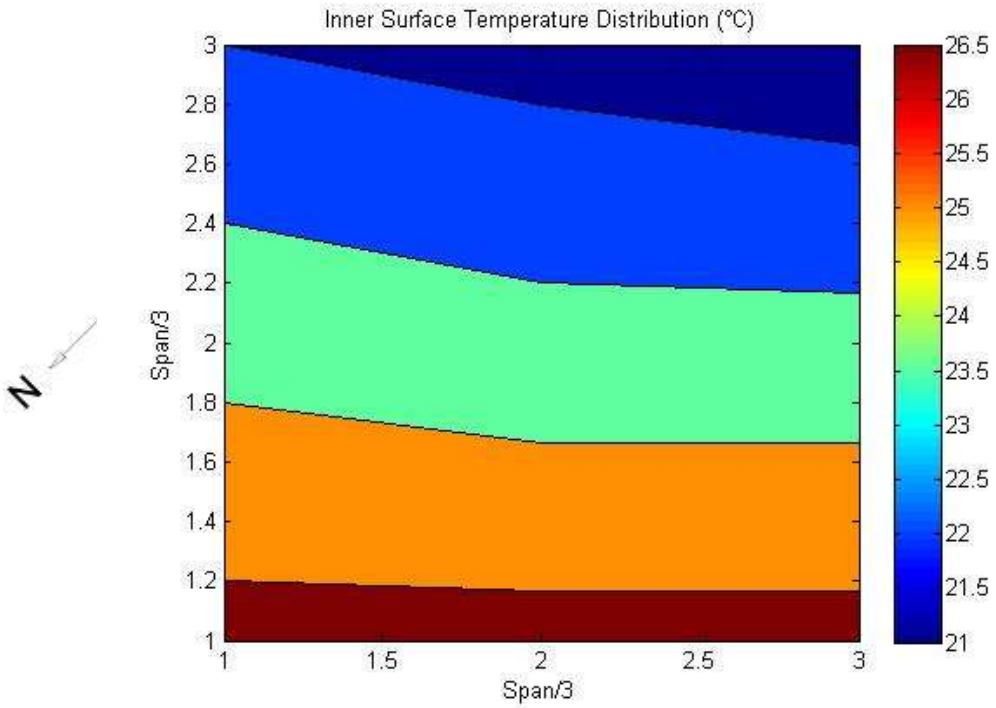


Figure 38: Inner surface temperature-Pumice stone surface

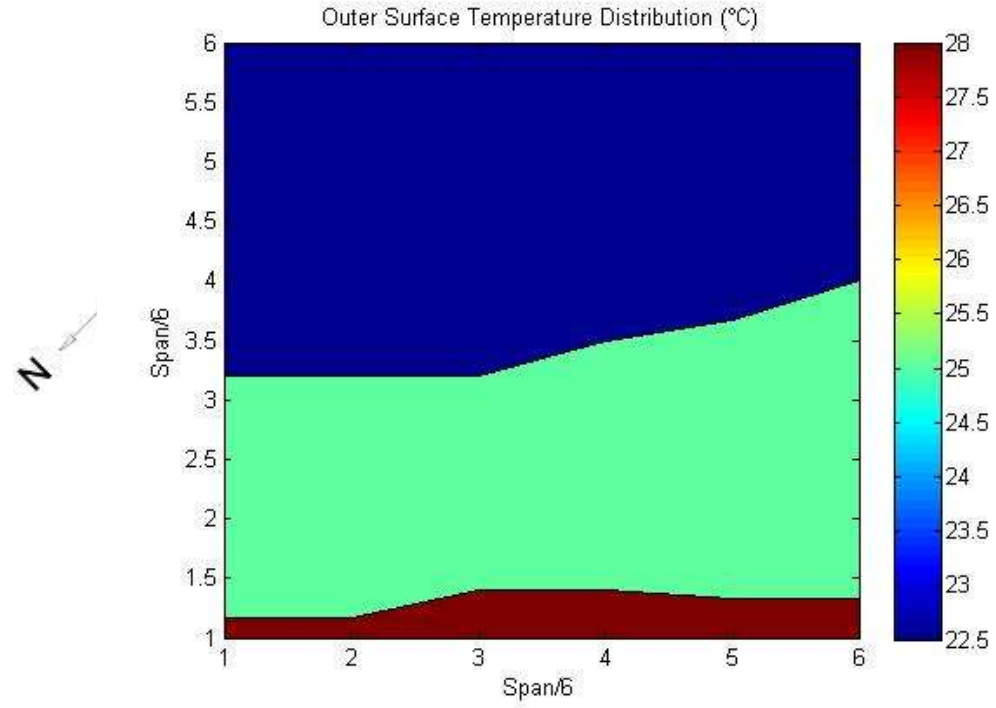


Figure 39: Outer surface temperature-White paint surface

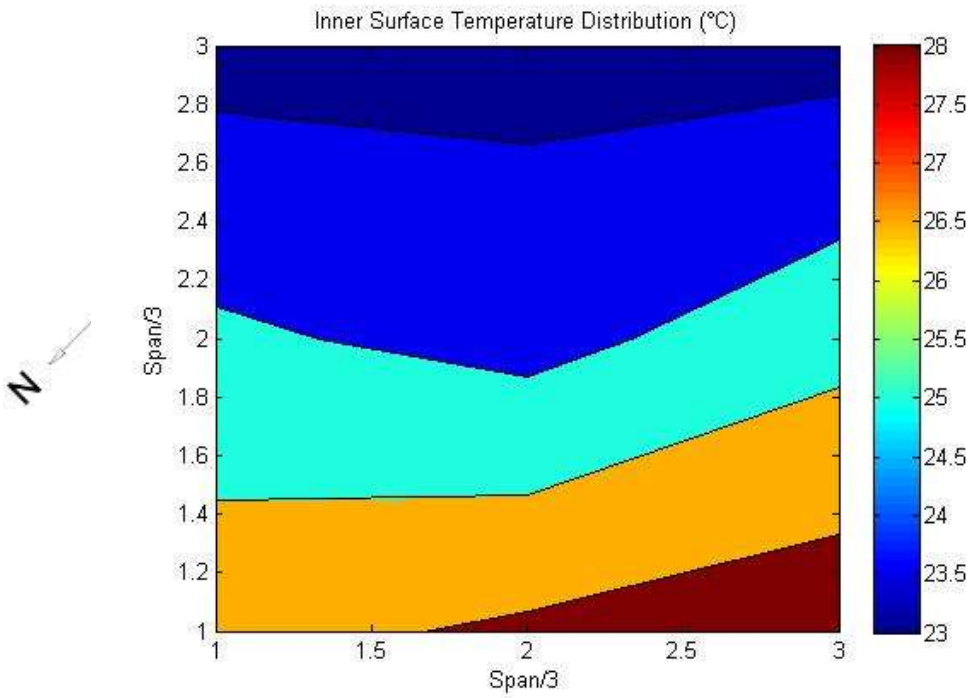


Figure 40: Inner surface temperature-White paint surface

**Date**: 19/07/2011

**Time**: 13:45

**Ambient temperature**: 25°C

**Weather description**: Clear, warm

**Suns position**: Azimuth – 332.28°; elevation – 37.85°

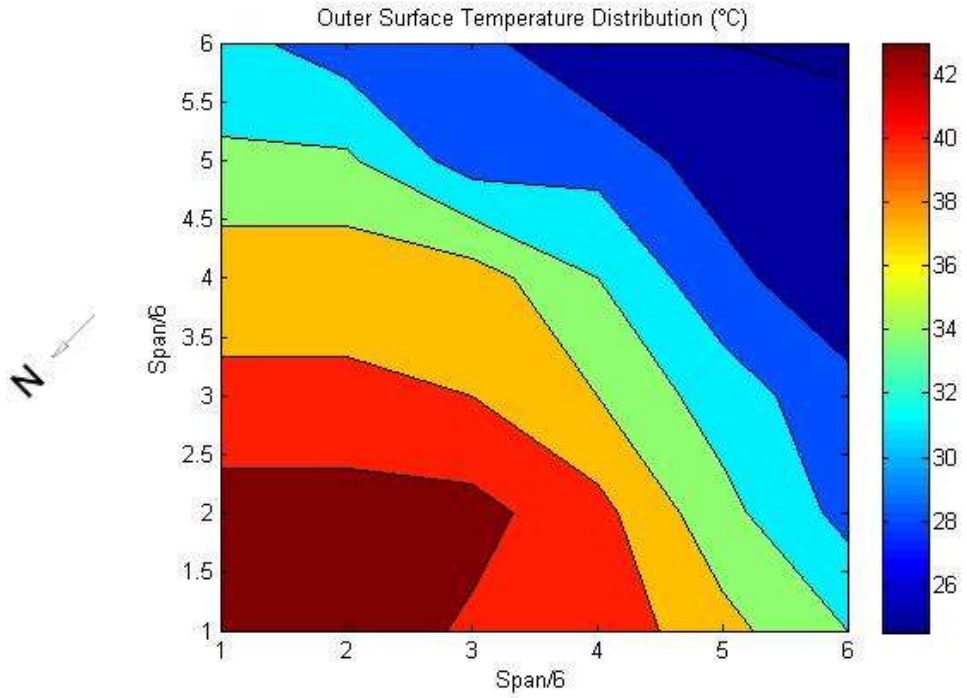


Figure 41: Outer surface temperature-Plain surface

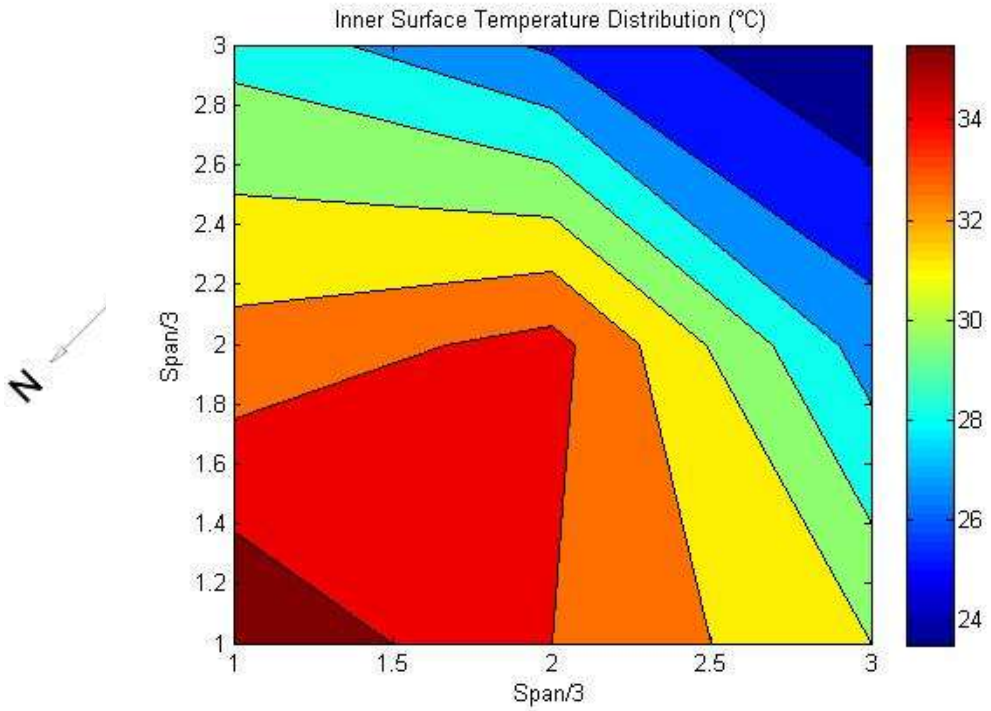


Figure 42: Inner surface temperature-Plain surface

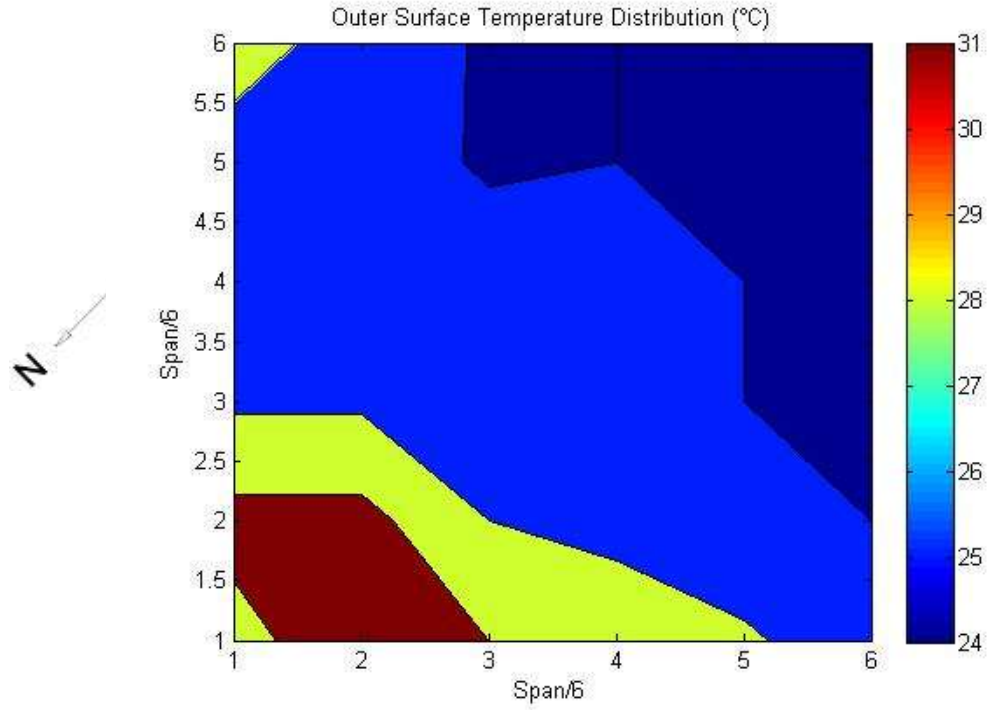


Figure 43: Outer surface temperature-Pumice stone surface

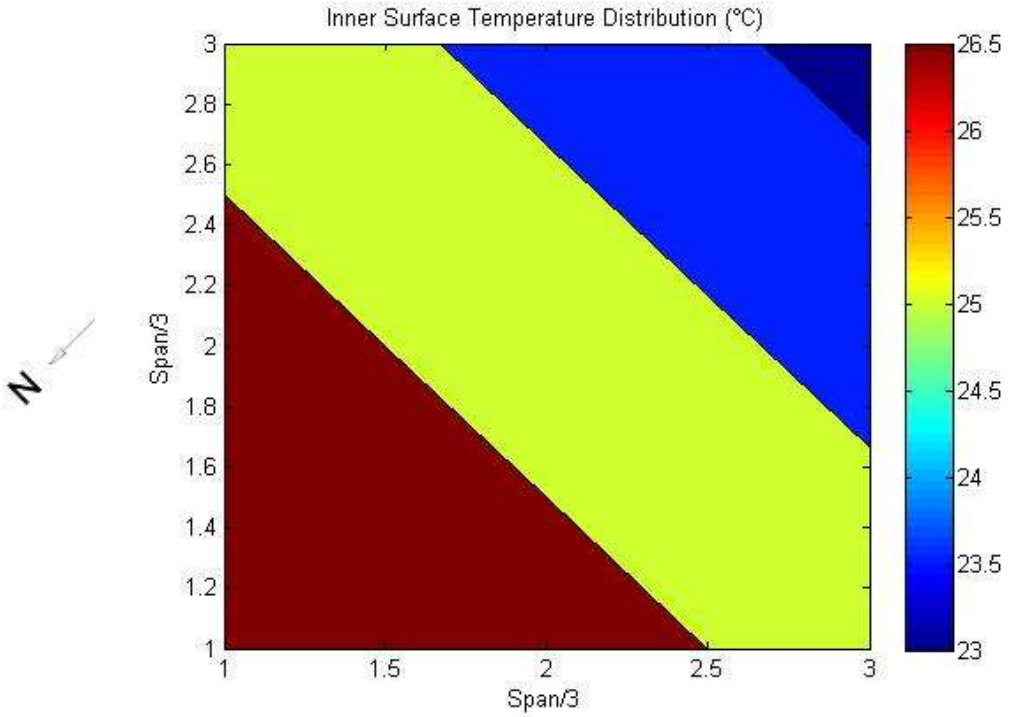


Figure 44: Inner surface temperature-Pumice stone surface

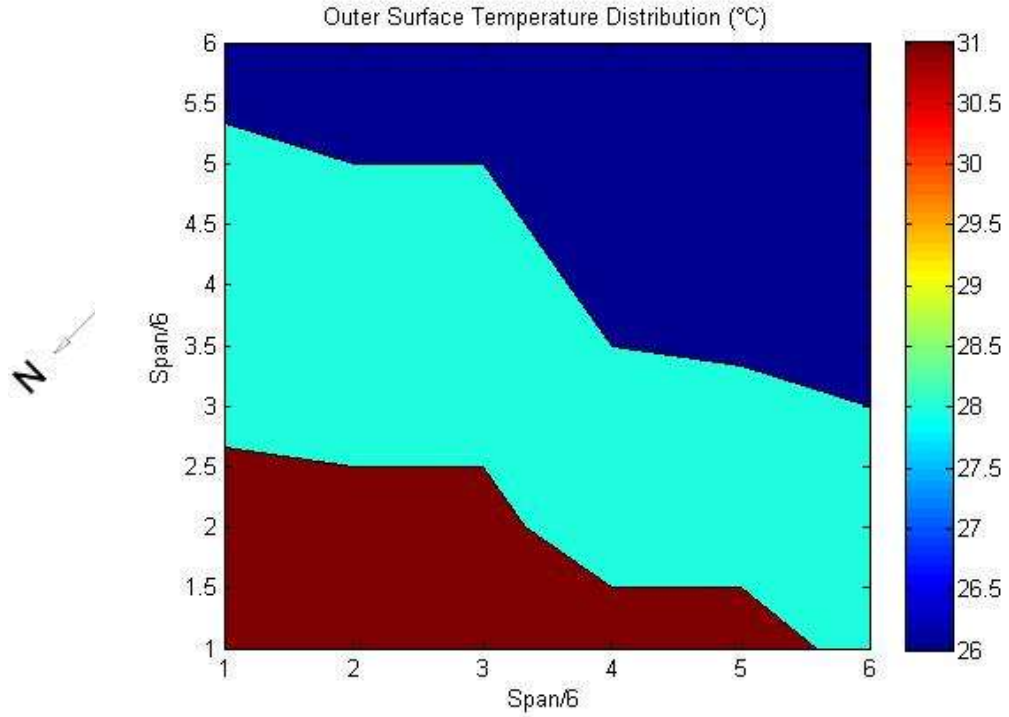


Figure 45: Outer surface temperature-White paint surface

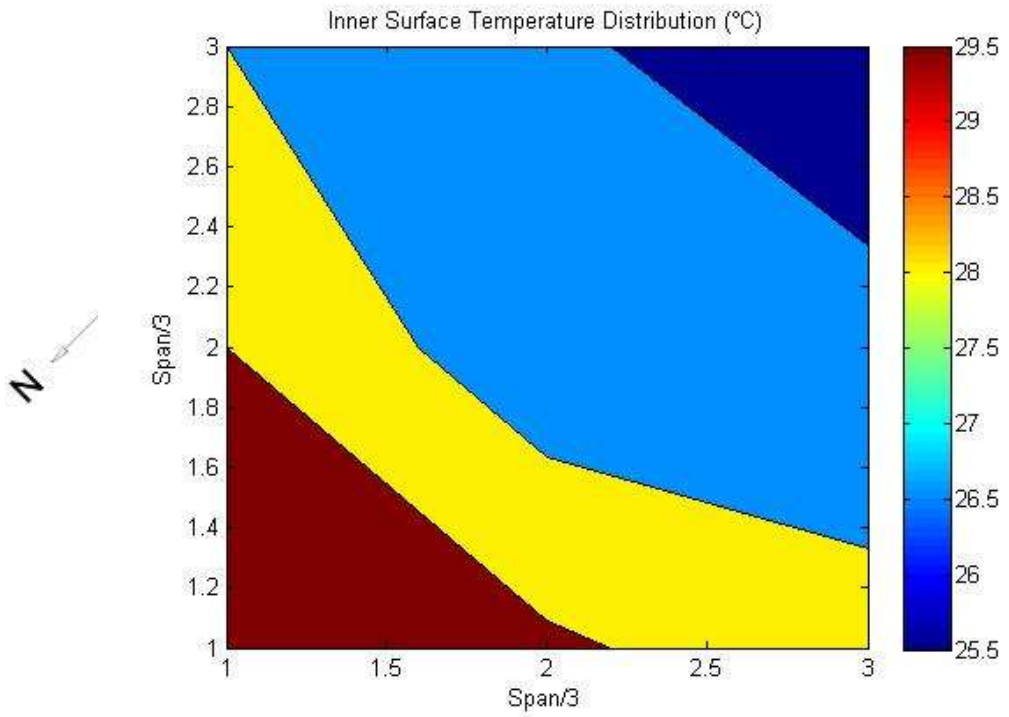


Figure 46: Inner surface temperature-White paint surface

## 5. Interpretation of results

The transformation of the results into temperature distribution contour maps may be interpreted in various ways. As discussed in the introduction, we require the thermal induced stresses in the shell structure. The thermal induced stresses are directly proportional to the change in temperature of the structure. Thereby, contour plots of the intense change in temperature results were determined. Developing a relationship between the ambient air temperature and the change in temperature in the structure would be a useful tool for future design work, thus an attempt was made in this regard. An important feature sought in the results was the efficiency of the attenuation methods.

### Attenuation methods

As mentioned before, the primary method for attenuating the thermal induced stresses was through different surface conditions, where the structure was exposed to direct sunlight. When

analysing the temperature distribution maps of the different surfaces, the following results were extrapolated:

| Outer surface | Average Temperature (°C) | Percentage attenuation (%) |
|---|---|---|
| Plain (Control model) | 53 | |
| Crusher stone | 50 | 5.6 |
| White paint | 33 | 37.7 |
| Pumice stone | 30 | 43.4 |

Table 2: Analysis of the temperature attenuation of the different surface textures and colours

The crusher stone surface appears to make a minor attenuation; therefore I will not consider it. The pumice stone surface has performed the best in terms of reducing the temperature; however, the price of the pumice stone is extremely high for low cost projects. The price of the stone alone for this small project was over R2000. It is thus an uneconomical option, definitely not suited for low cost housing or low cost projects. The white paint surface performed the best overall; the paint was a fraction of the pumice stone, without compromising much on performance.

It is important to note that the colour of the surface plays a vital role in the temperature distribution. A structure with a dark, earth-like colour had the same temperature as the plain surface temperature. Thus, it was not the paint's ability to reduce the temperature in the structure, it was merely due to the fact that white colour was able to reflect most of the sunlight, keeping the structure at an almost constant temperature as displayed in the results.

The pumice stone surface was able to attenuate the temperature the most as the colour of the stone was white and the stone is very porous. This gave this surface the leading edge in temperature attenuation. A very important aspect of the temperature distribution was the fact that when the sky was cloudy, the ambient temperature almost matched the surface temperatures.

It has been shown that the temperature distribution across the structure may be attenuated by forty percent, however the thermal induced stresses are not known, and if they were adequately attenuated. This will be explored in the next chapter of application of results, where the plain surface thermal induced stresses will be compared to the white paint surface, as the white paint surface performed the best.

## Change in temperature maps

The change in temperature maps was determined from the difference of the maximum and minimum temperatures of the model structure. The following contour maps illustrate the change in temperature of the plain surface structure and the white paint surface structure. These contour maps were developed to indicate the temperature distribution maps to be used in the following chapter (application of results):

**Date**: 15/02/2011

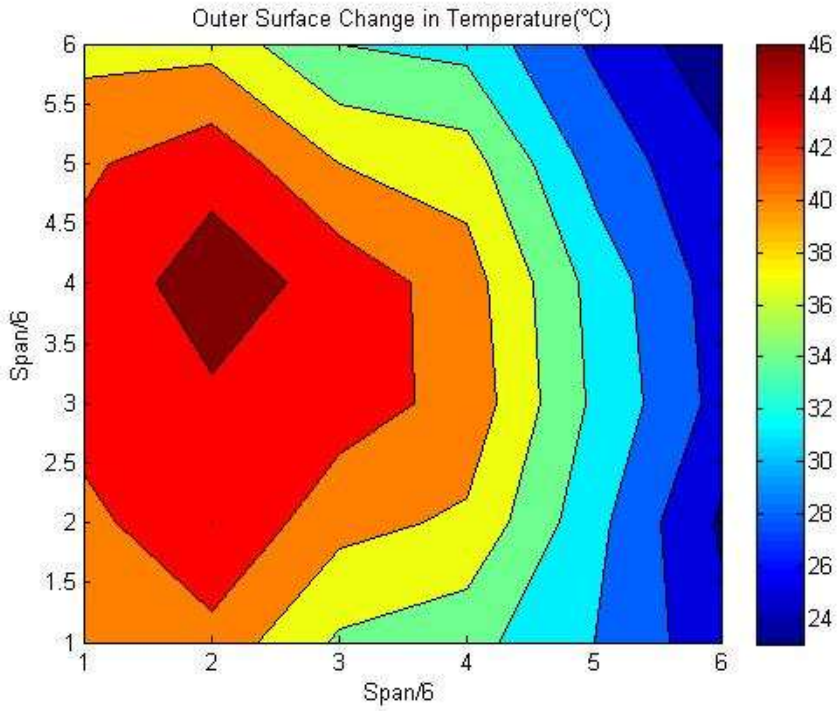


Figure 47: Outer surface temperature change-Plain surface

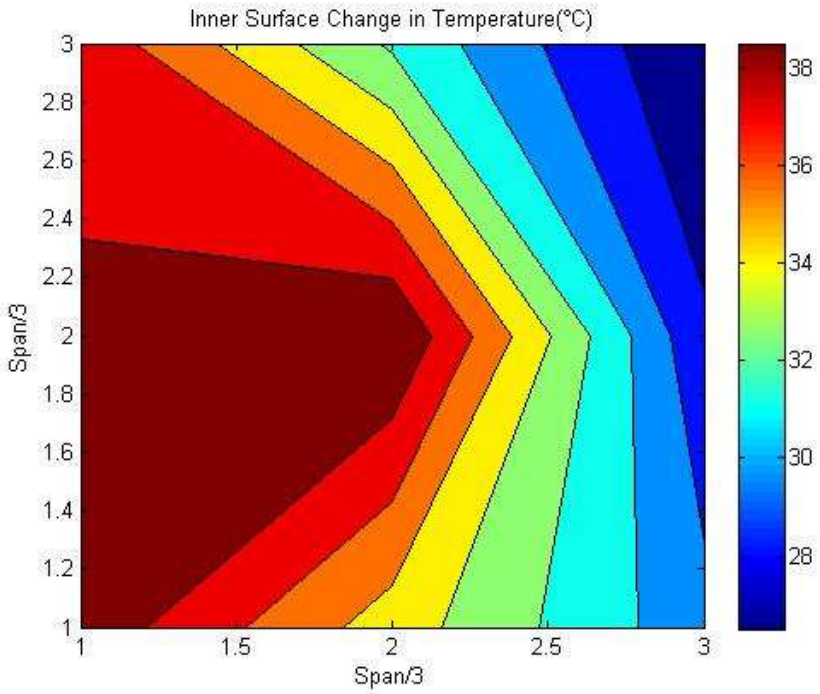


Figure 48: Inner surface temperature change-Plain surface

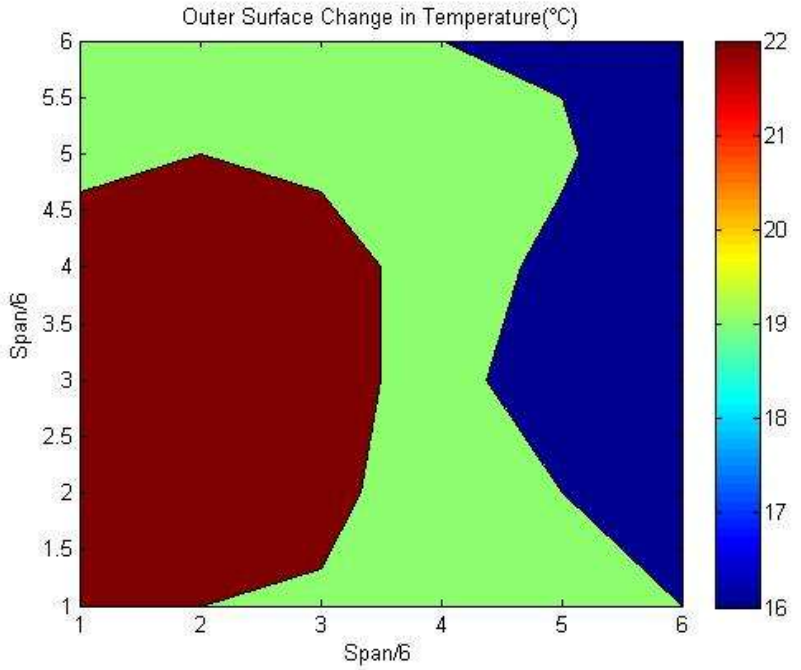


Figure 49: Outer surface temperature change-White paint surface

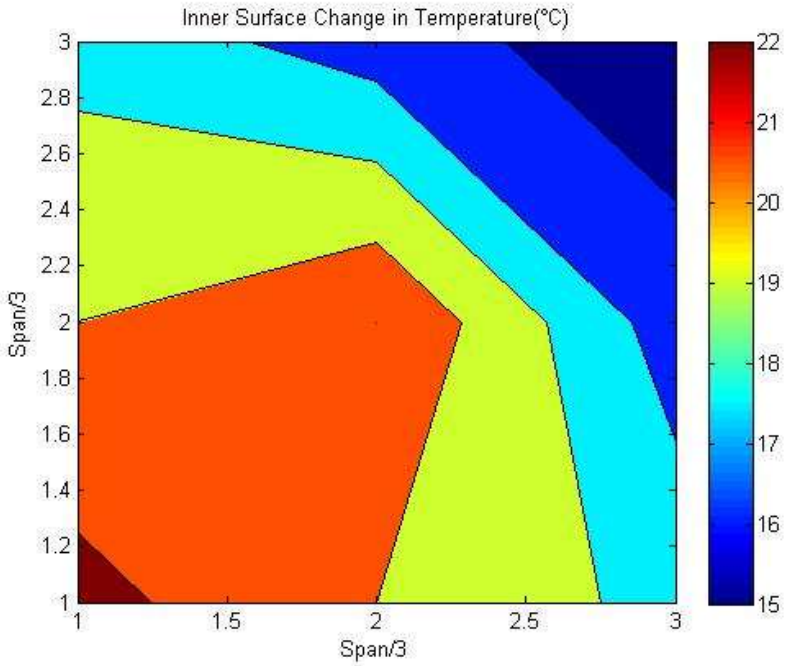


Figure 50: Inner surface temperature change-White paint surface

**Date**: 19/07/2011

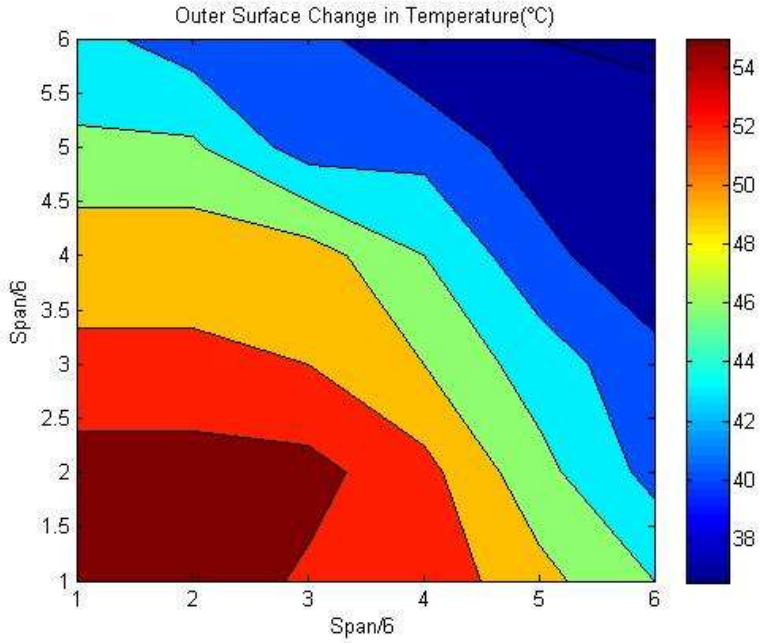


Figure 51: Outer surface temperature change-Plain surface

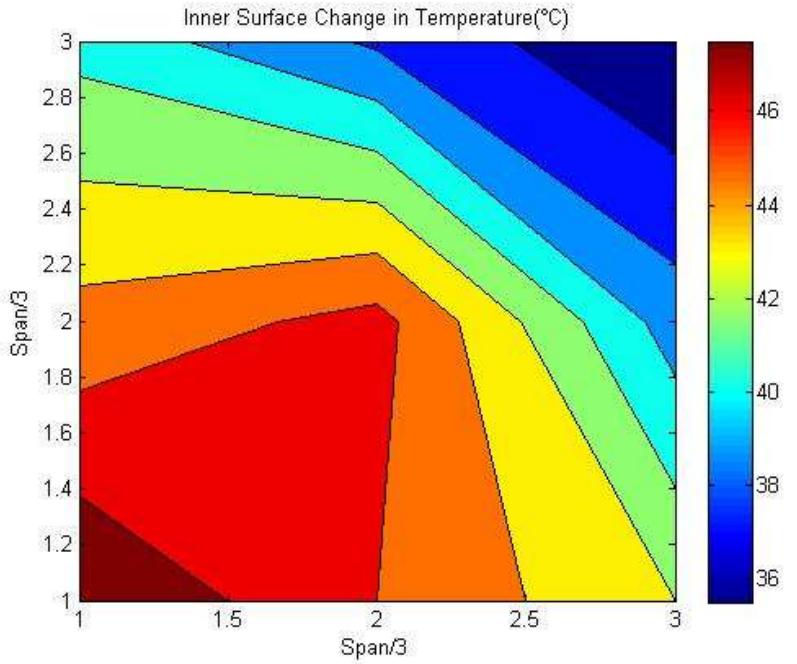


Figure 52: Inner surface temperature change-Plain surface

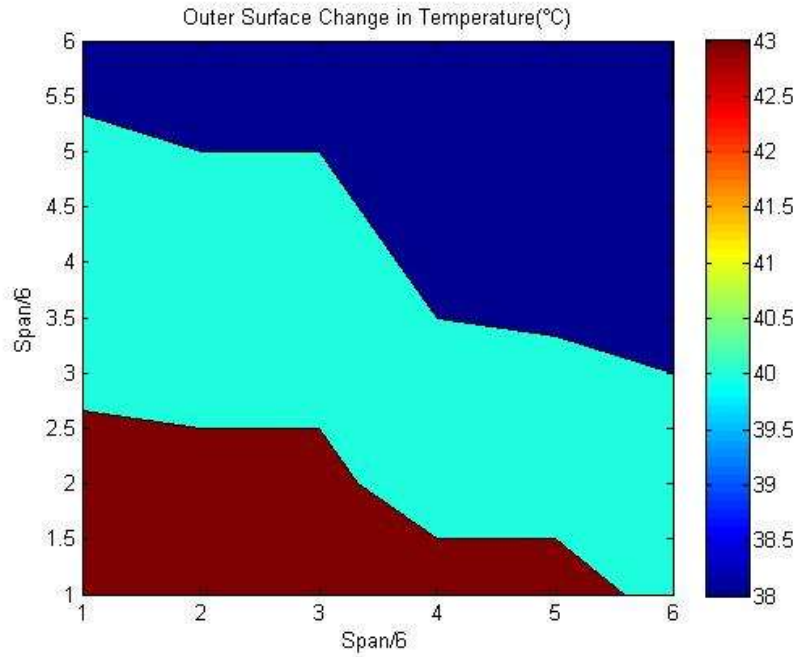


Figure 53: Outer surface temperature change-White paint surface

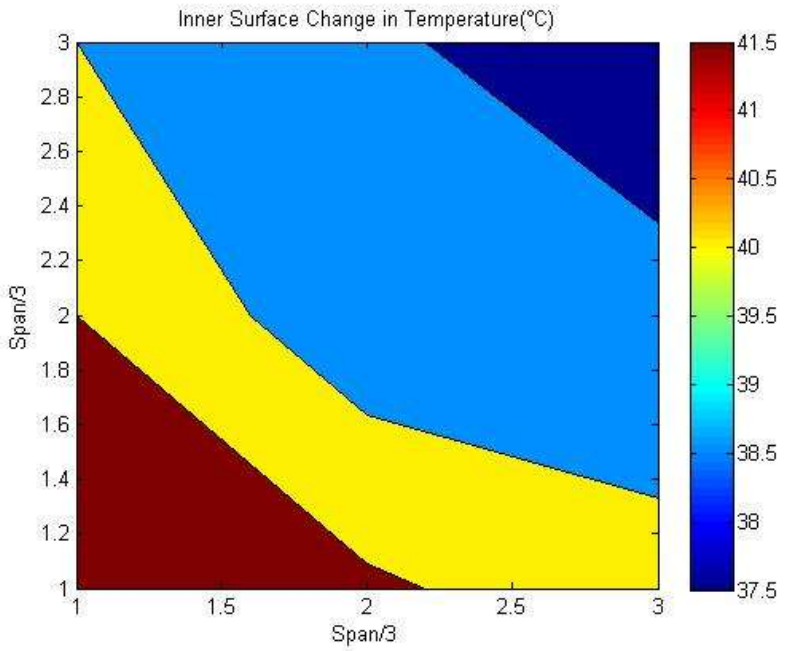


Figure 54: Inner surface temperature change-White paint surface

## Discussion of results

The change in temperature maps were produced to indicate which temperature distribution maps are to be used in the finite element model. It was presumed that the acute temperature distribution changes would occur in the summer months in South Africa. However, as the results have shown, the acute change in temperature distribution changes occur in winter.

The finite element model would need to analyse for both the summer and the winter month's change in temperature distribution, as I may then conclude which temperature loading is the most severe.

## Proposed design temperature loading

The temperature loading design tool which is presented below is an attempt at creating a conservative design tool. The tool is aimed at predicting the temperature as a function of the ambient temperature. It may be applied in any design application of thin shell structures constructed from stabilised earth, without any thermal insulation.

This design tool was intended to apply the temperature loading onto the structure in a swift, easy and efficient method. In order to achieve this, the method of application is divided into two parts. In the first part, the surface temperature is predicted from a graph or a given equation. Two readings are taken in order to determine the change in temperature of the structure from the maximum and minimum ambient temperatures in winter. This single scalar quantity is then processed in the second part of the design application. The second part consists of two simplified maps of the outer and inner surface change in temperature distributions, as a proportion of the change in temperature determined in the first part. These maps are then applied to the structure to obtain the final design temperature loading.

Presented below is the design temperature loading for plain surfaces and the white painted surfaces, as they are practical surfaces for low-cost projects. The design change in temperature curves were obtained by choosing a curve which had a ninety five percent confidence interval above the actual readings, according to the British Standard; BS 2846: Guide to statistical interpretation of data (see reference seven and eight). The change in temperature maps were derived from the average change in temperature maps in the winter months, as the change in temperature was higher in winter. Both the curves and the maps were simplified for swift application in a design environment.

## Plain surface

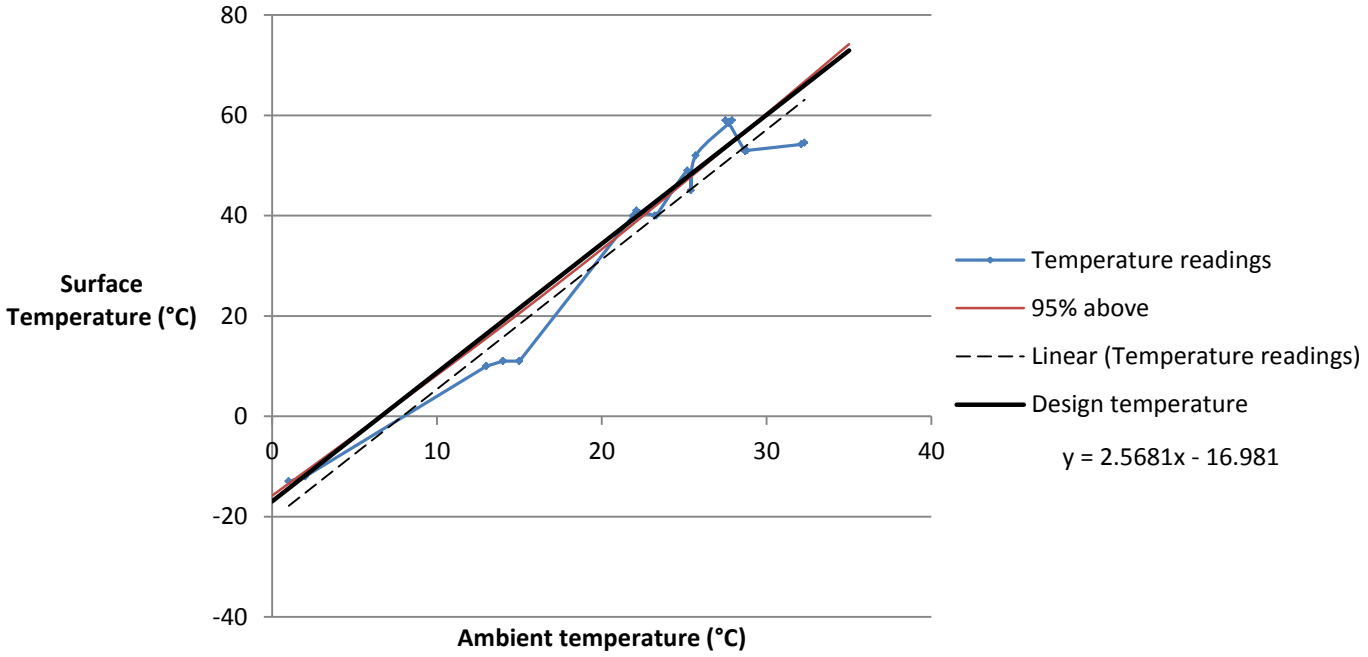


Figure 55: Design temperature loading curve for a plain surface structure

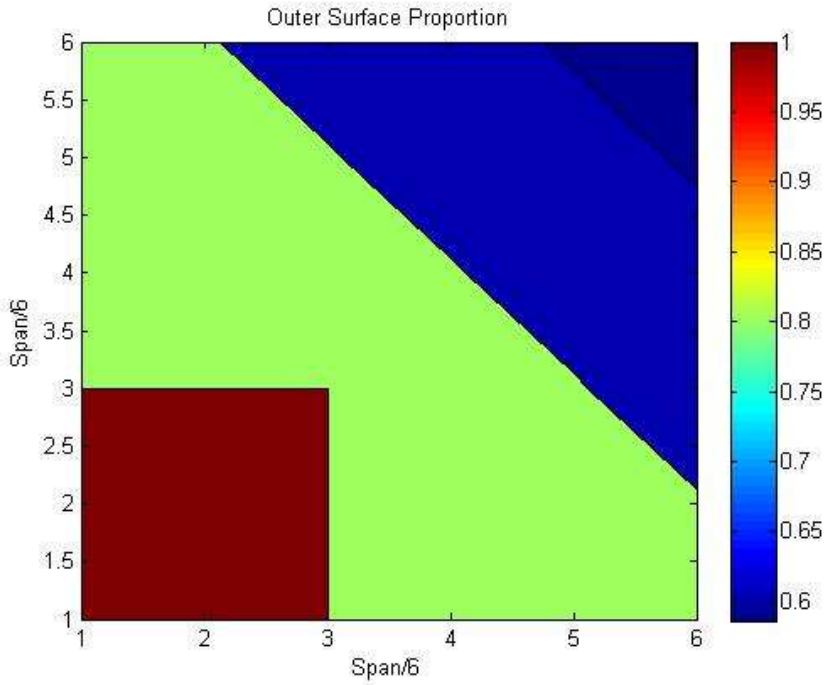


Figure 56: Design change in temperature proportions for a plain outer surface

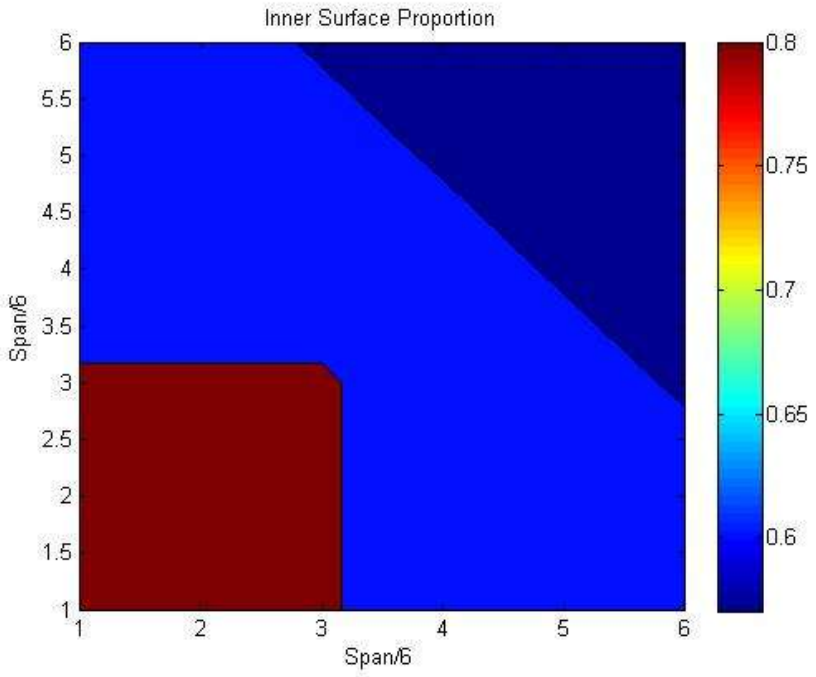


Figure 57: Design change in temperature proportions for a plain inner surface

If one analyses the design temperature graph, particular attention is drawn at the upper limits where there is considerable scatter in the results. What is disturbing is the fact that where there is a higher ambient temperature there is not necessarily a higher surface temperature. This is due to the structures physical orientation to the sun, where the sun's rays are at different angles on the structure at different times of the day. This graph cannot be produced for the temperature on the surface at a certain time only, as this would not yield accurate design change in temperature of the surface throughout the day. Thus, the entire readings were considered in this design tool.

The graph, however, does have some stable and appealing characteristics. For example at lower temperatures, fairly stable results are noticed. This is due to the ambient temperature alone affecting the surface temperature of the structure at night or on cold, windy days. The most appealing characteristic of this graph is the linear design tool attached to the results. This graph will make a complicated design task of assuming a temperature distribution on the surface of the curved structure fairly simple. The only concern is how effective is this design graph, which will be explored in detail in the following chapter.

## White surface

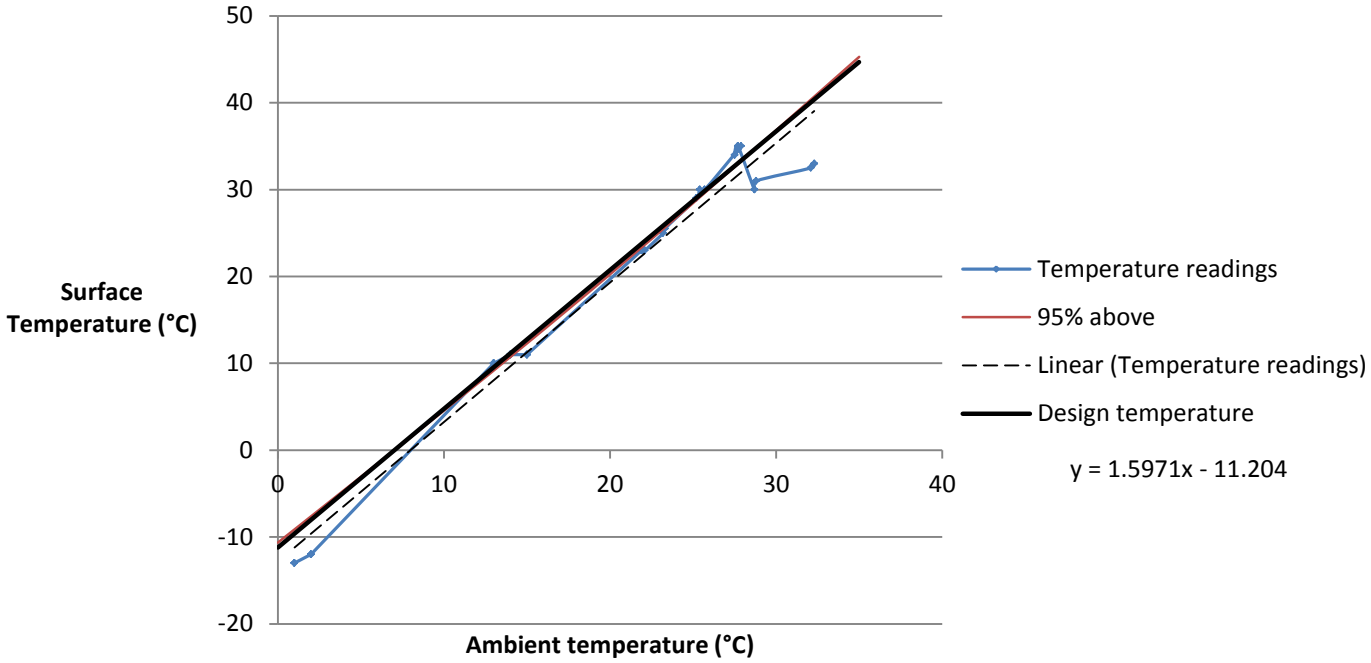


Figure 58: Design temperature loading curve for a white surface structure

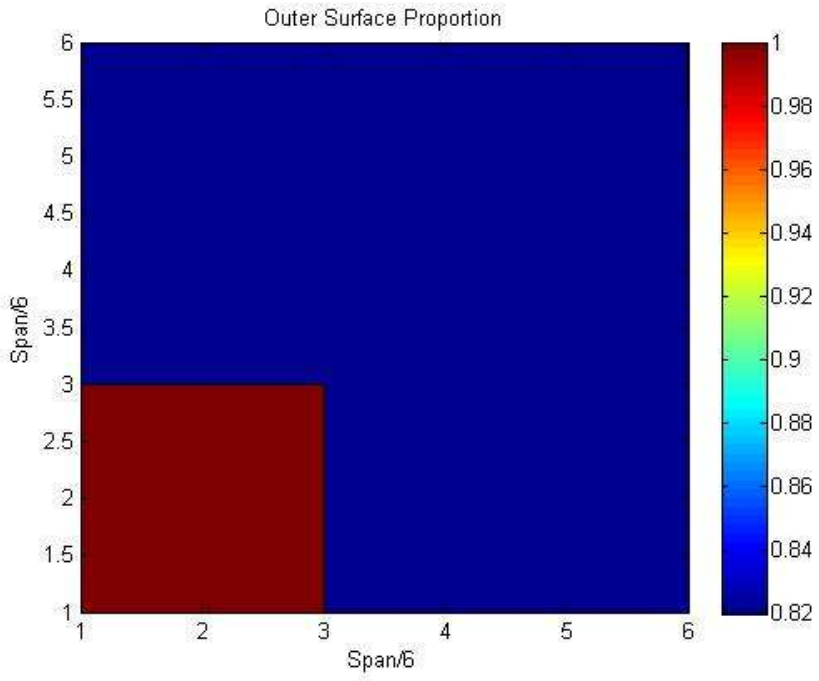


Figure 59: Design change in temperature proportions for a white outer surface

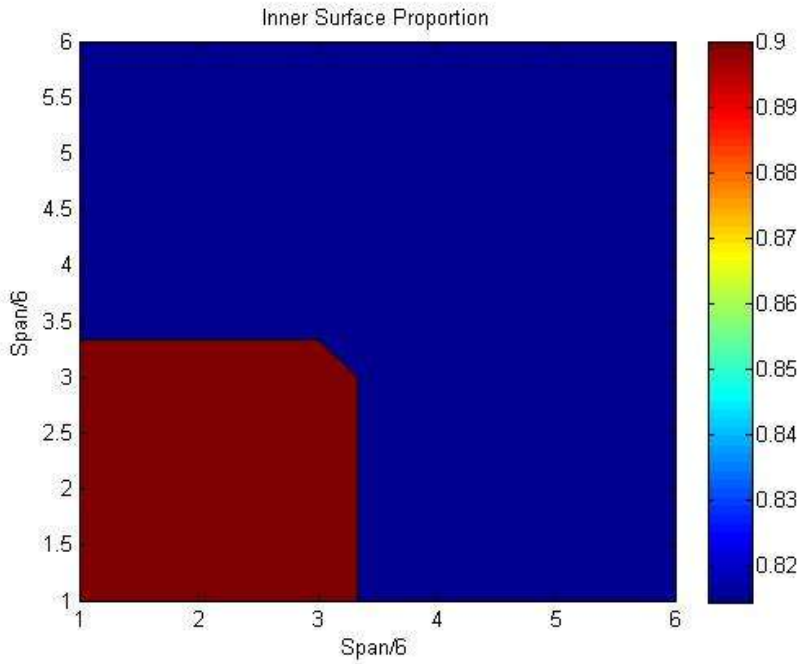


Figure 60: Design change in temperature proportions for a white inner surface

The design temperature graph and the temperature maps for a white surface thin shell structure follow a similar configuration to the plain surface shell structure. Moreover, the white surface design tools display more stable characteristics, such as less scatter in the design temperature graph and a fairly even change in temperature distribution map for both the inner and outer surfaces of the structure.

## 6. Application of research

The temperature distribution has been established for the handkerchief shell structure. The temperature contour maps will be used in an assumed real life application. A finite element model will be now created, simulating the model in temperature loading. However, it will have realistic dimensions in order to establish realistic thermal induced stresses in the structure.

The determination of the dimensions of the finite element model presented a few concerns. The most important concern was that if the thermal induced stress was related linearly or non-linearly to the span of the structure. According to the handkerchief shell theory, the loads are distributed to the supports by axial forces, and since axial forces are linearly related to stresses

in a structure, it was assumed that the thermal induced stresses were linearly related to the span of the structure. This assumption allows the dimensions of the finite element model to be large.

The finite element model was then chosen to be thirty three times larger than the model, as this was acceptable in terms of the material scale in the model and the stress to span assumption. A structure of this span would be used for a hall, indoor sports arena or something of that nature.

## Finite element model

The models which were used to measure the temperature distribution were scaled exactly by thirty three times, which produced the following structure;

## Plan view

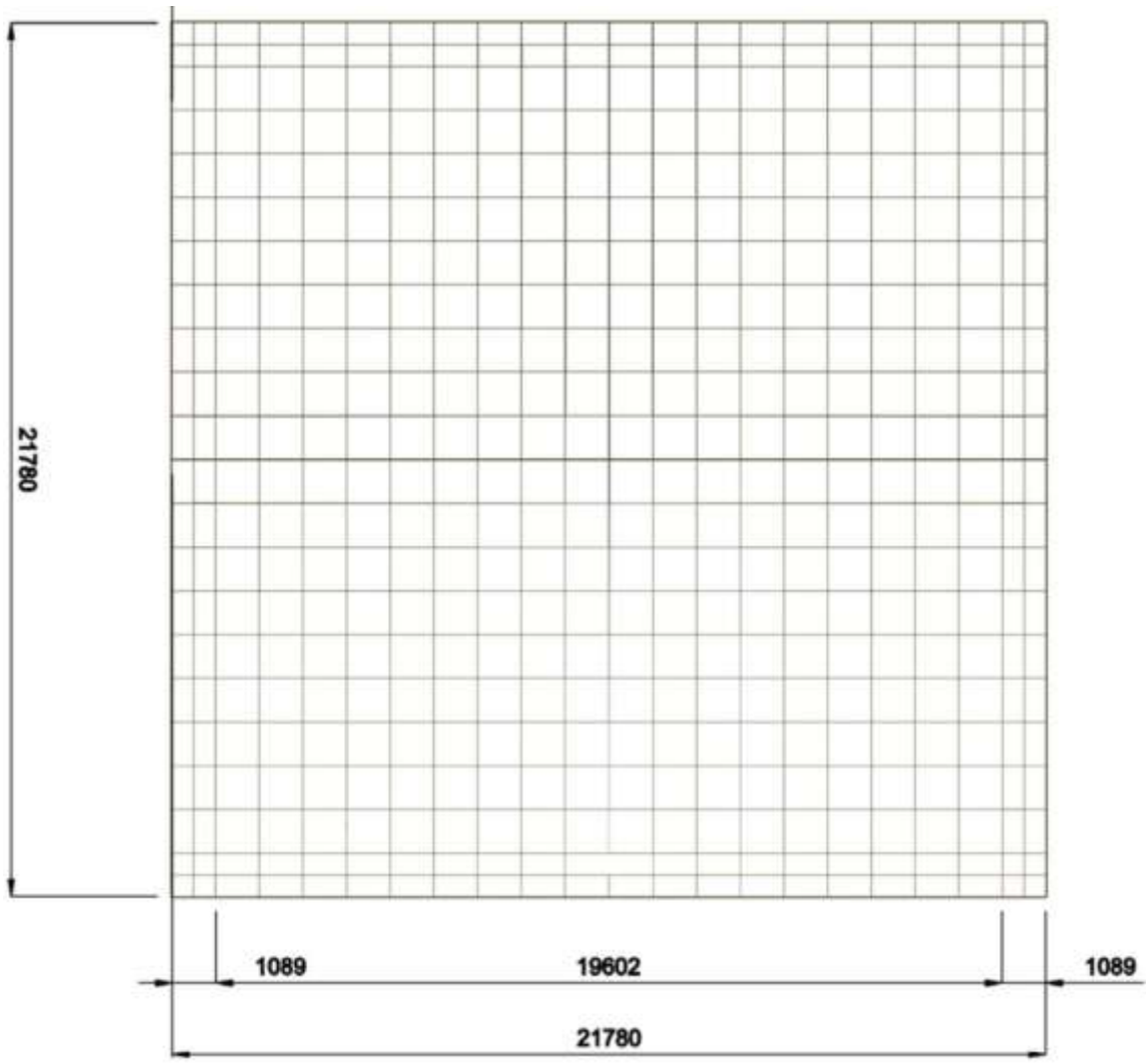


Figure 61: Plan view of finite element model

## Side view

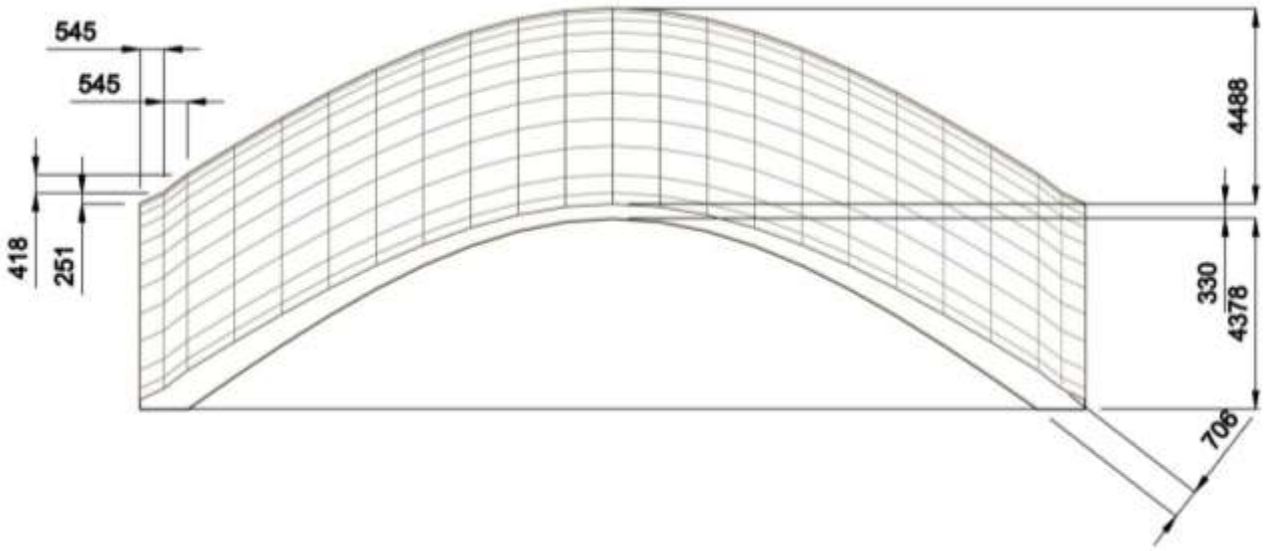


Figure 62: Side view of finite element model

## 3D view

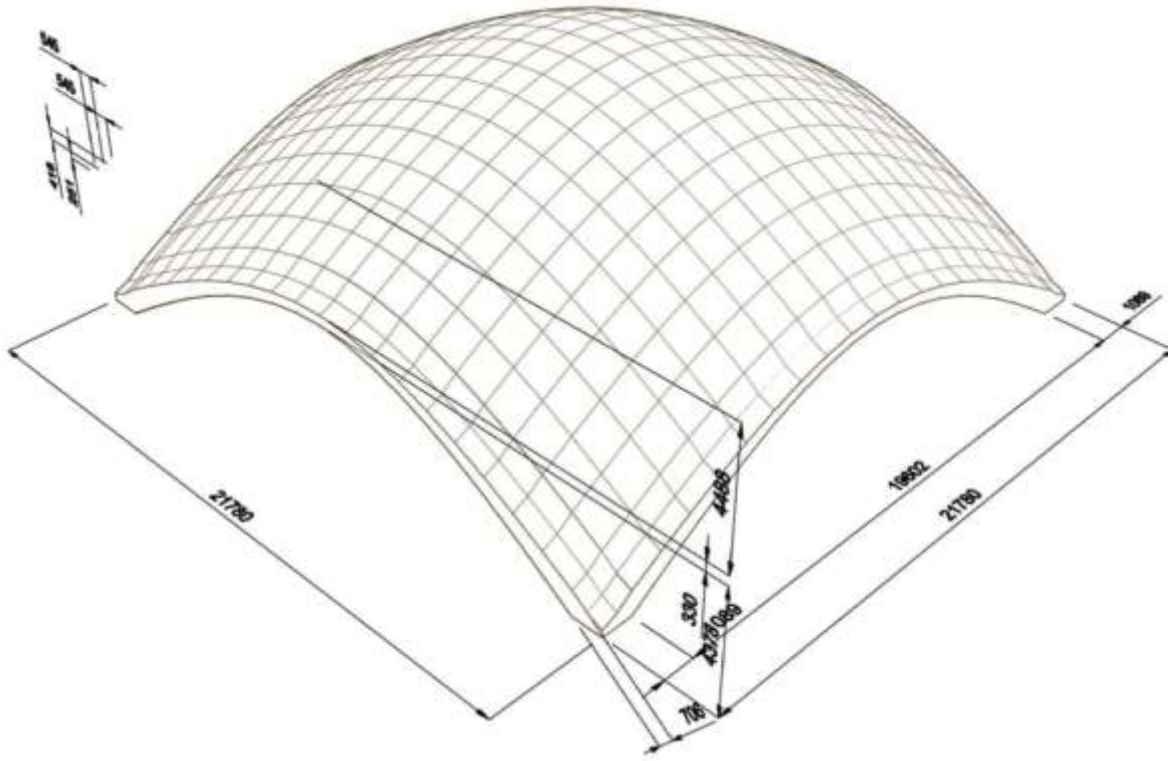


Figure 63: Three dimensional view of finite element model

## Overview of ANSYS

The package which was used for the analysis was ANSYS version 13.0. This version compels the user to draw the structure, either in ANSYS or in a drawing package which the user is familiar with and then the geometry is imported into ANSYS. This handkerchief structure was drawn in AutoCAD, exported as an ACIS file and then finally imported into ANSYS. Some aspects of the structure within ANSYS are;

- ANSYS automatically meshes the structure and the user may only introduce a few constraints, such as the majority of element shapes, approximate size of elements etc.
- One cannot locate the nodes or the elements of the structure within ANSYS for the input of external forces. Rather discreetly defined parts of the geometry, as indicated in the drawings as faces of the structure, are accessible for this.
- Results are displayed graphically only; however, specific points of deformations or stresses are determined through a probing tool which ANSYS provides.
- The structure was analysed as a full 3 dimensional structure, thus the element shapes were either tetrahedral or hexahedral, with all the elements having mid-side nodes. The structure was chosen to be modelled in full three dimensional space so as to model the change in temperature distribution of the outer and inner surface accurately and to obtain a varying thickness of the shell.
- The sign convention for direct stresses and strains used throughout the ANSYS program is that tension is positive and compression is negative. For shears, positive is when the two applicable positive axes rotate toward each other.

## ANSYS model

The structure was drawn with many faces on the top surface because there was a varying change in temperature distribution across the top and bottom surfaces in the real model. This would then be introduced in the ANSYS model correctly, and this configuration of the structure gave rise to tetrahedral elements.

I encountered a problem in ANSYS where the supports could not be pinned in a full three dimensional structure as compared to a shell element structure. To allow full rotation at the

support, only a single vertex at the ends of the arches may be selected as a support. This configuration gave rise to stress singularities at the supports, which were undesirable. The structure was then modelled at the supporting column or foundation with a frictionless roller, in all three principle axis. Each frictionless roller was placed on a single face of the faceted geometry, as shown below:

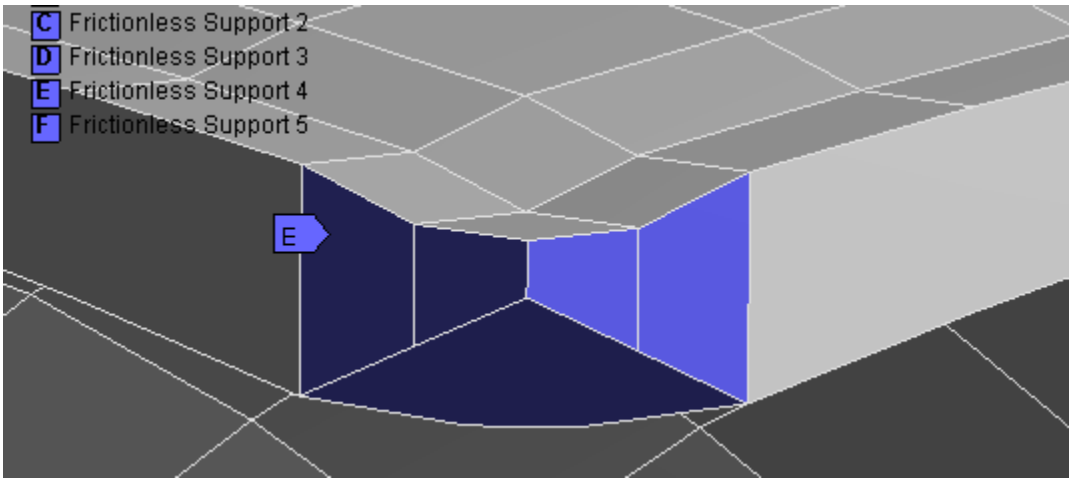


Figure 64: Frictionless support configuration for the handkerchief shell structure

Although the frictionless rollers provide support in a direction perpendicular to the face of the support only, the configuration shown above would not allow the structure to rotate at the support. However, this configuration was presumed to represent the actual structure most accurately as a column or pad footing would support the structure. And it would induce higher thermal induced stress due to the structure being constrained more than an assumed simply supported edge in a shell element structure.

The following table presents the assumed material properties for stabilized earth [2];

| Density | Coefficient of thermal expansion | Young's modulus | Poisson's ratio | Tensile ultimate strength | Compressive ultimate strength | Thermal conductivity |
|---|---|---|---|---|---|---|
| ($kg/m^3$) | ($C^{-1}$) | (MPa) | | (MPa) | (MPa) | ($Wm^{-1}C^{-1}$) |
| 1870 | 7.60E-06 | 7750 | 0.17 | 0.63 | 11.5 | 0.72 |

Table 3: Material properties for stabilized earth

Convergence testing was required to determine the accuracy of the results of the initial mesh which the ANSYS mesh generator produced. The following figures illustrate the accuracy of the ANSYS mesh generator.

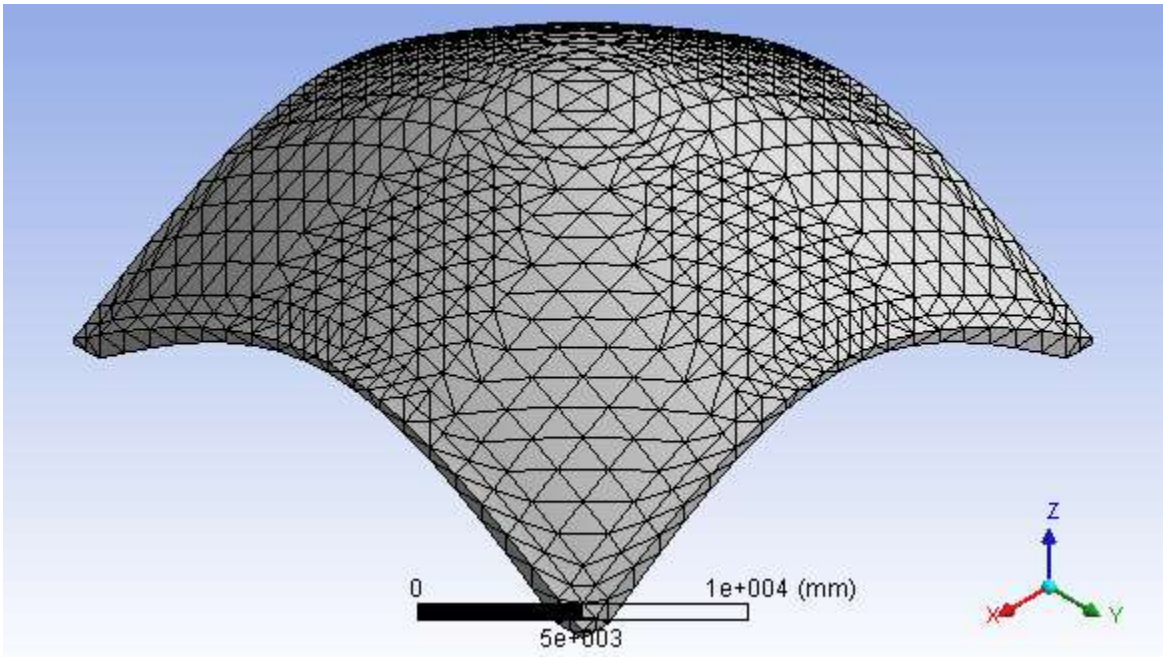


Figure 65: Initial mesh of the finite element model

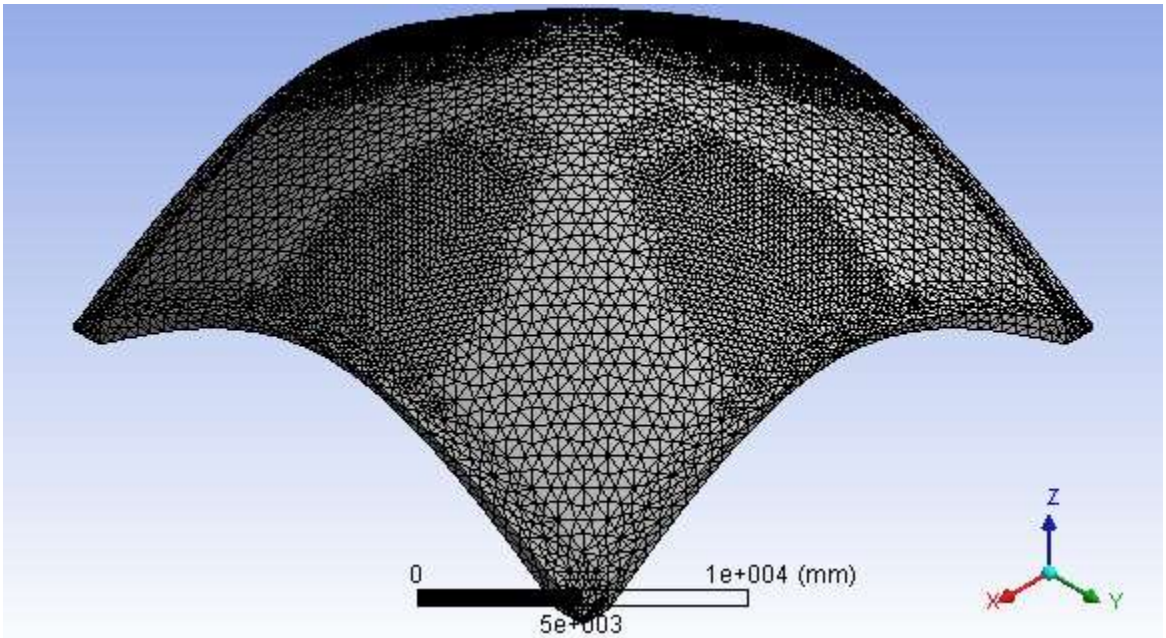


Figure 66: Refined mesh of the finite element model

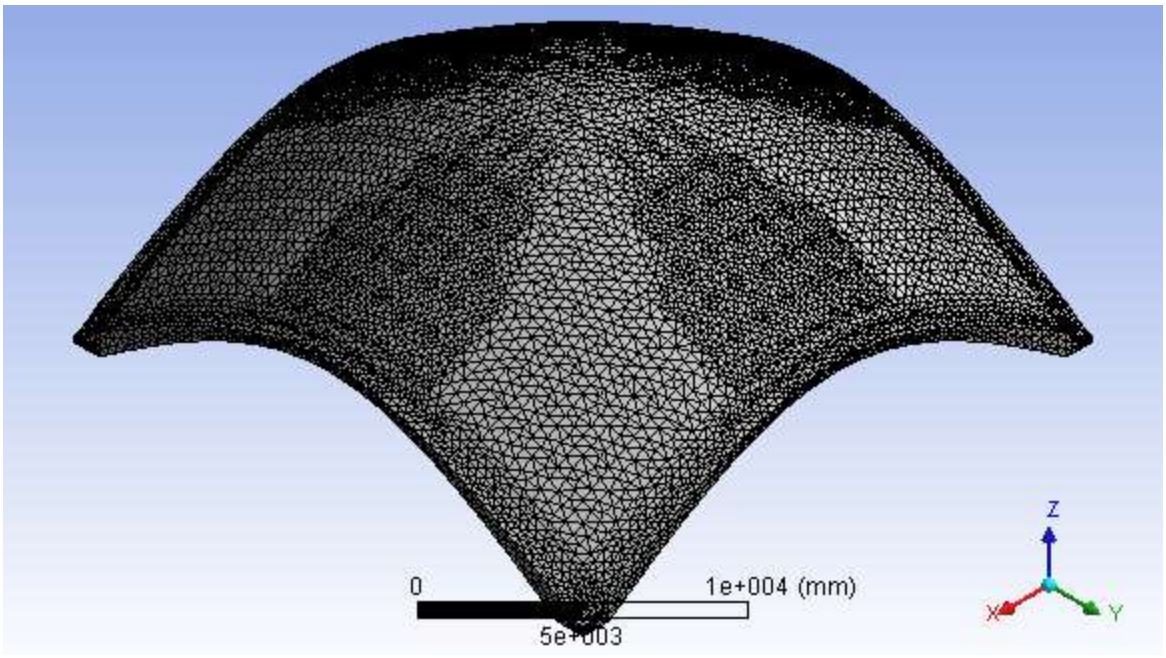


Figure 67: Further refined mesh of the finite element model

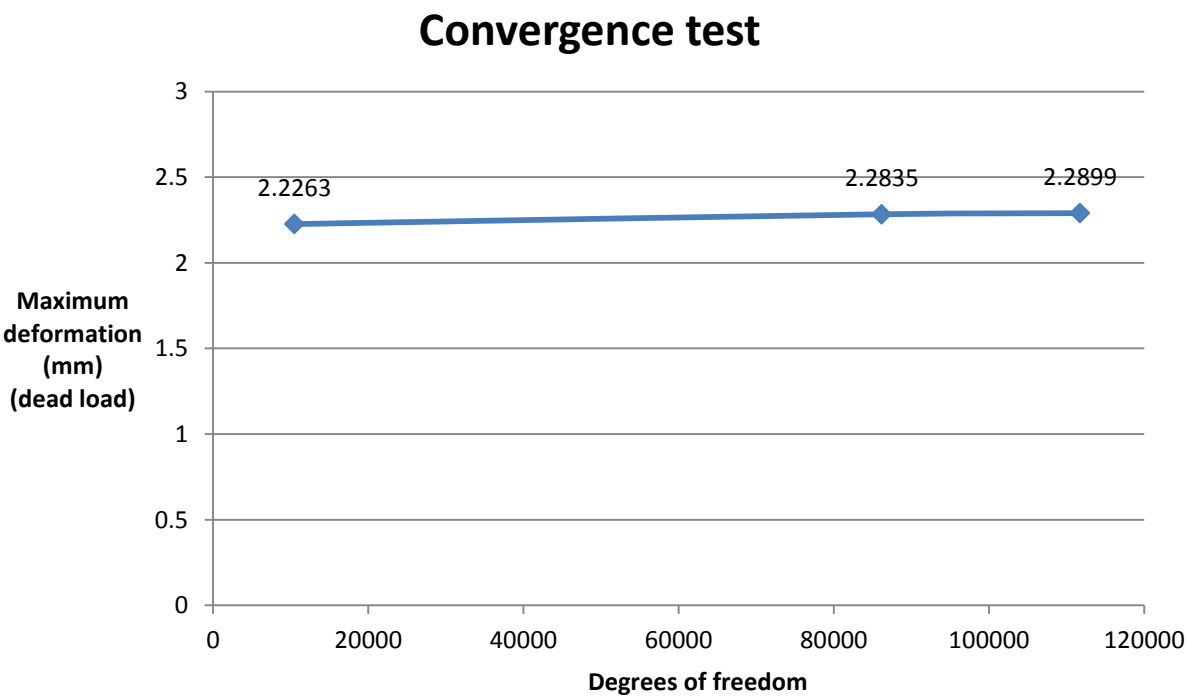


Figure 68: Convergence test graph of the finite element model

It has been shown through convergence testing of the structure that the initial mesh which ANSYS produced was within three percent error. This was due to all the elements being non-linear elements, thus the initial mesh gave near identical results to the mesh which was twice refined. Thus the initial mesh was used throughout the analysis to determine further results, as the computational time was significantly reduced.

## FEM Results

### Dead load

The finite element analysis produced compression stresses over most of the structure under dead load. However, there were areas where tension had developed in the shell which was expected, as I had noticed buckling of a handkerchief cloth material model when excessive plaster of Paris was placed on the model to stiffen the curves. These tensile stresses were a third of the ultimate tensile resistance of the material and may be attributed to Poisson's effect. The compression forces which had developed were also very small, and the material would absorb these stresses with ease. The following diagram illustrates the magnitude of the compression forces in relation to tensile stresses under dead load (note the diagram illustrates the deformation of structure in conjunction with the stresses);

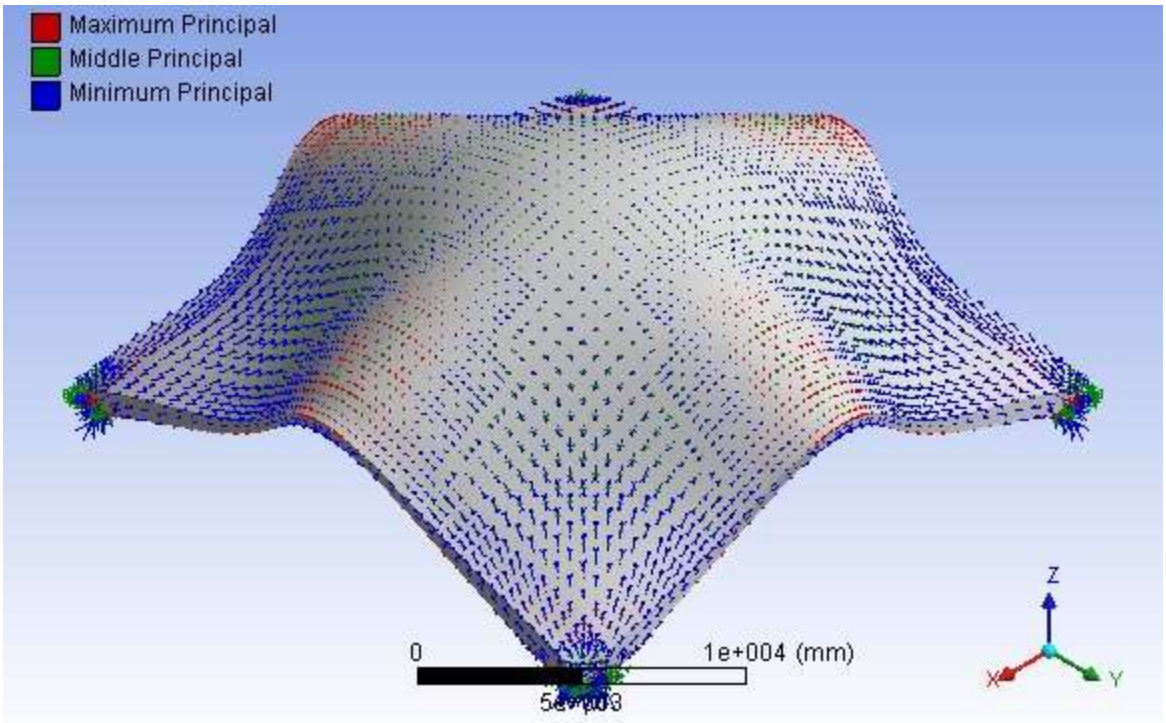


Figure 69: Vector principle stresses for the dead load

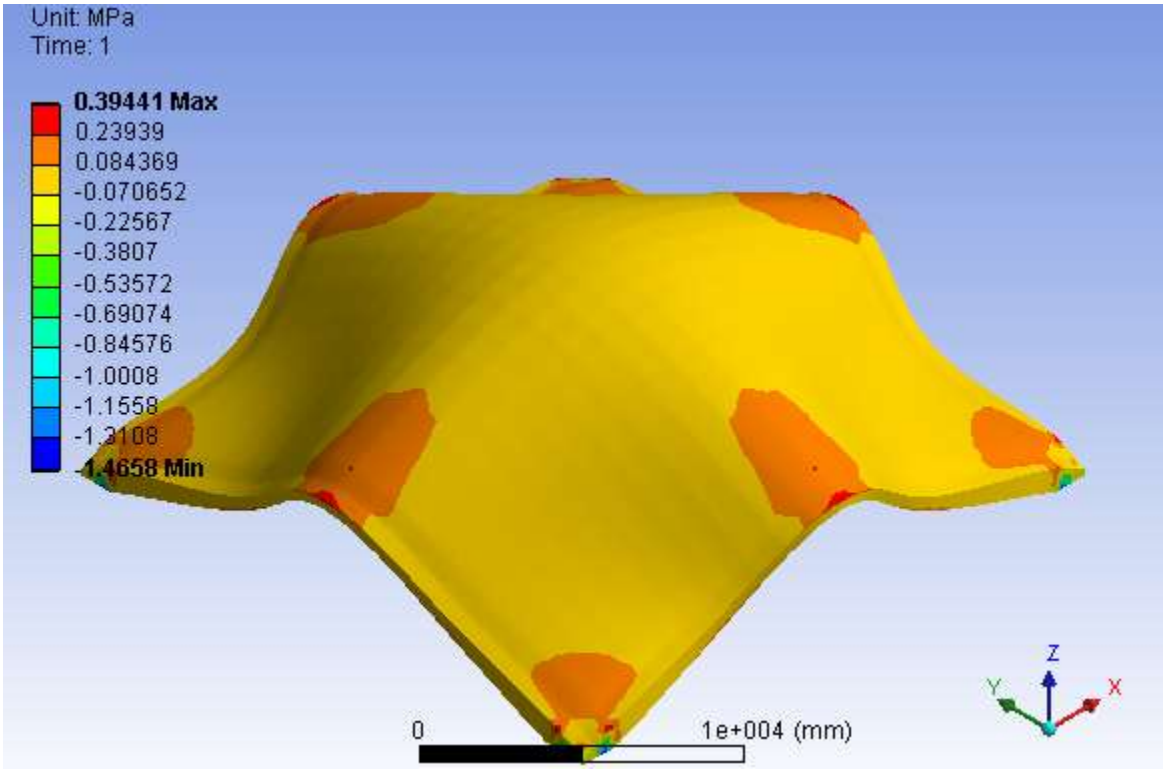


Figure 70: Outer surface maximum principal stresses for the dead load

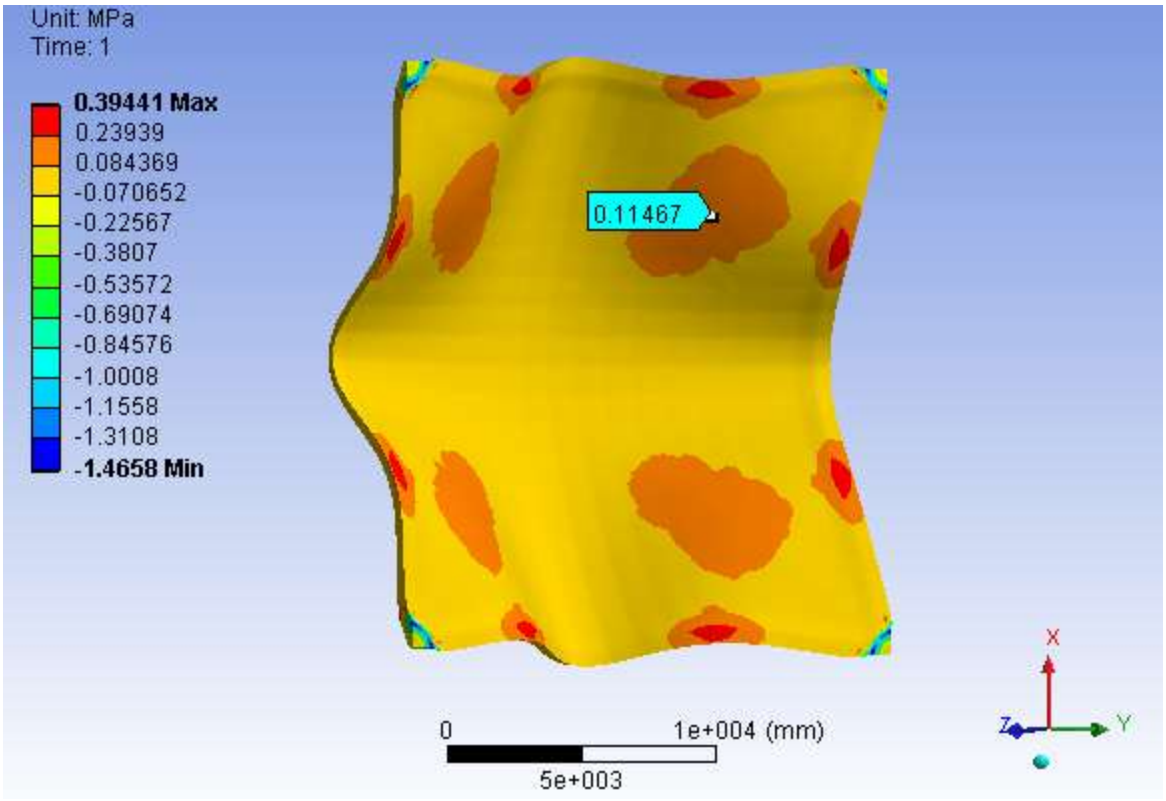


Figure 71: Inner surface maximum principal stresses for the dead load

According to the ANSYS sign convention, the minimum principle stresses are compressive. After careful observation of the vector principle stress diagram, it is observed that the shell is mainly in compression with very little tension, as expected. The maximum stress occurs at the support, the second highest at the tip of the outer arches as shown. As illustrated by the maximum principal stress diagram, majority of the structure is within the ultimate tensile stress limit. It is only by the supports where there is a huge increase in tensile stress, probably due to the high error at the supports as indicated by the program.

There is also some bending moments in the shell structure as indicated by the tension at the top and compression at the bottom of a cross section. These bending moments, albeit small, were not anticipated as I expected the shell to behave according to the catenary thin shell theory.

The development of tensile stresses under dead load alone raised the concern of extremely high tensile stresses developing in the dead and live load combination, according to the code.

This load combination was then applied to the roof structure and the tensile stresses were found to be seven percent higher for a live load of 2kN/m². Thus the structure's integrity was not affected by the dead and live load combination.

## Thermal loads

The thermal loading of the structure was analysed with no load safety factors in order to determine the effect of temperature on the structure. Multiple load scenarios were analysed in order to determine the highest thermal induced tensile stresses. The first load scenario which was analysed was the actual temperature distribution in the shell structure as obtained from the change in temperature contour plots in the winter months. It was in the winter months where the structure experienced the highest change in temperature.

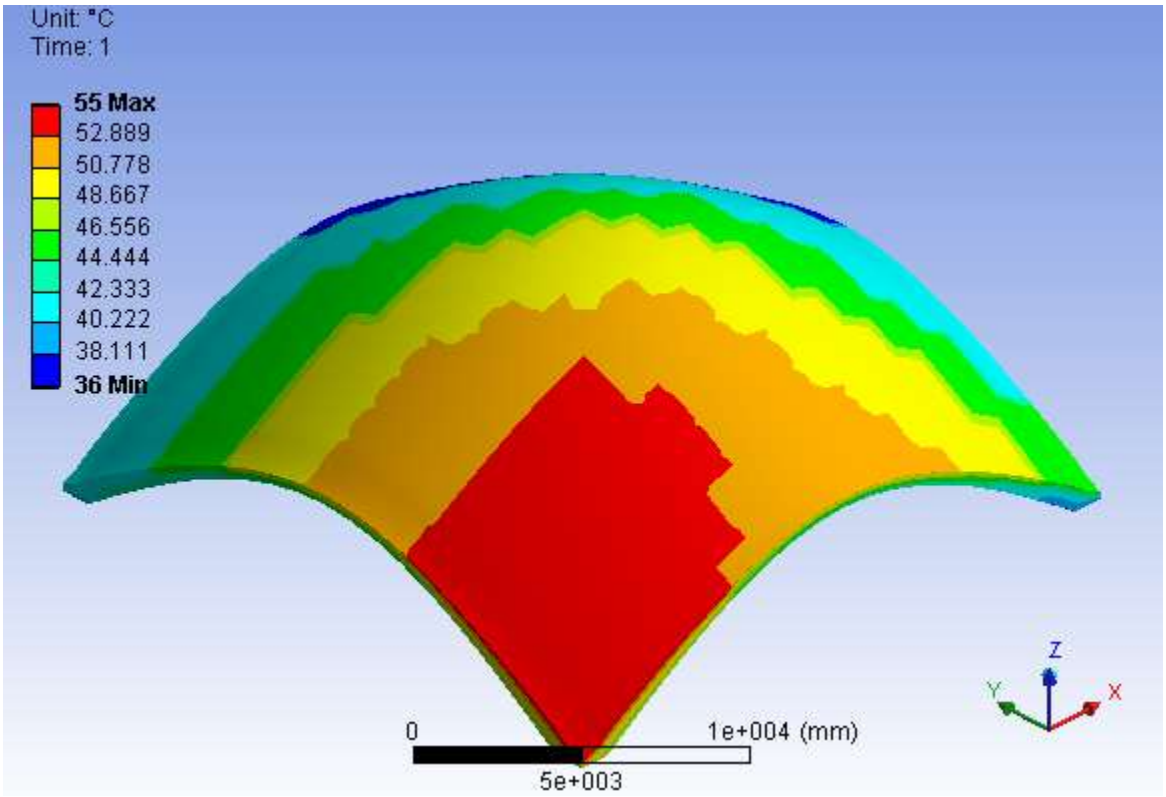


Figure 72: Change in temperature diagram for the finite element model in winter (note the varying temperature distribution in the cross-section of the structure)

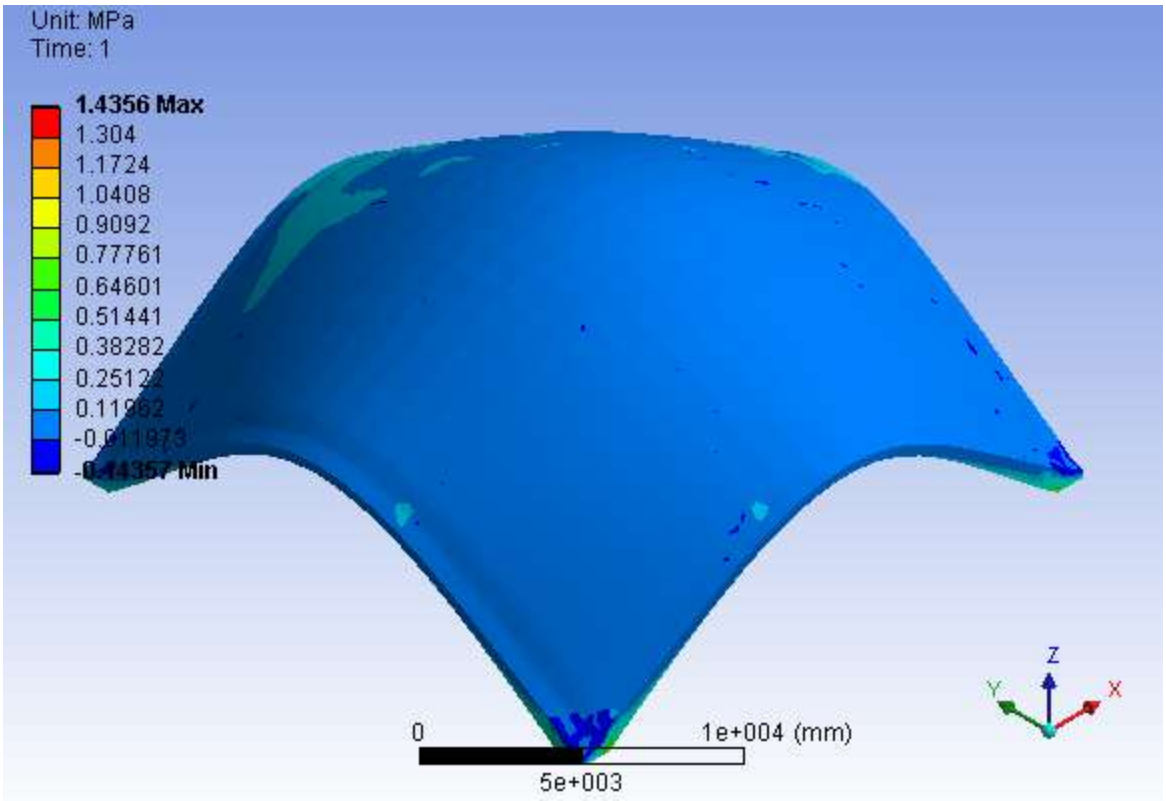


Figure 73: Outer surface maximum principle stress for the finite element model in winter

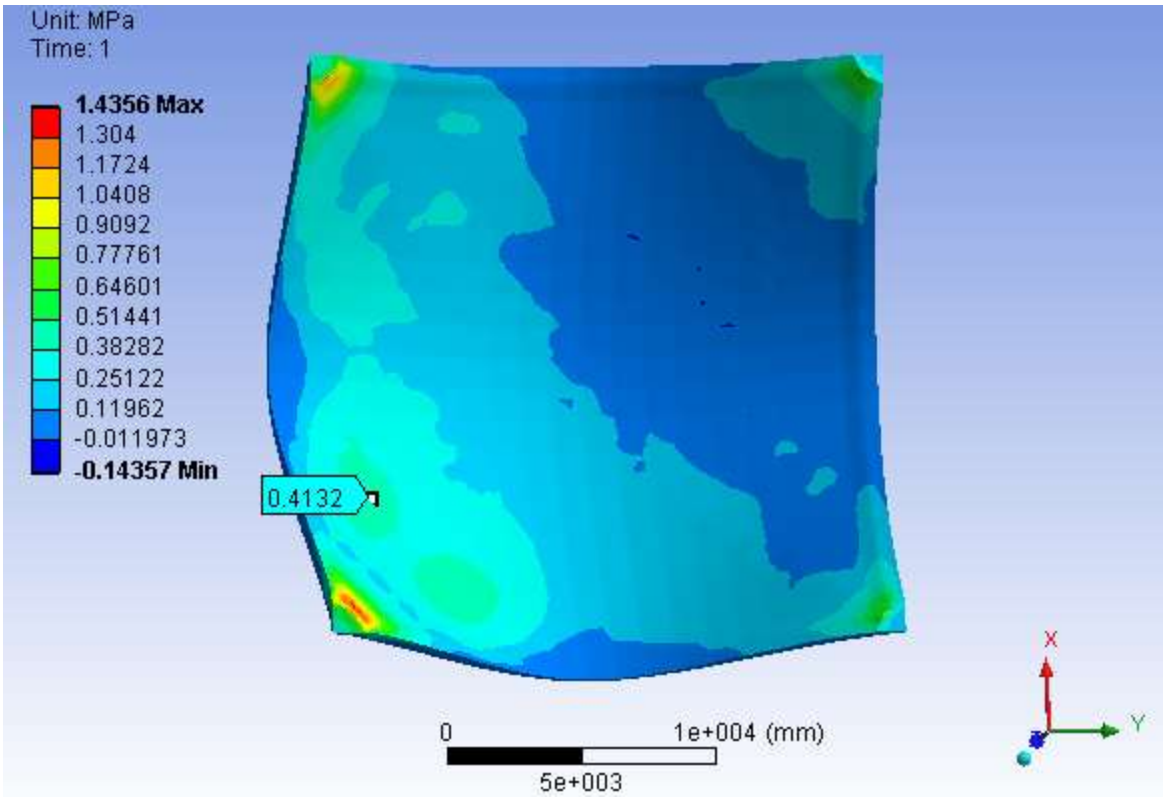


Figure 74: Inner surface maximum principle stress for the finite element model in winter

The result from this load scenario indicates that the tensile stresses on the outer surface of the structure are fairly low. However, on the inner surface some areas reach more than two thirds of the ultimate tensile strength. It was presumed that a concentration of high thermally induced tensile stresses would occur on the outer surface. However, as the analysis indicates the higher thermal stresses occur within the inner surface. This analysis indicates that the entire structure is within the tensile limit of the material, it is only close to the support where the extremely high tensile stresses occur, signifying a probable area of cracking in a real structure.

The second thermal load scenario which was analysed was the actual temperature distribution in the shell structure as obtained from the change in temperature contour plots in the summer months. The change in temperature was less in these months than the change in temperature winter, for that reason I presume the induced stresses are lower.

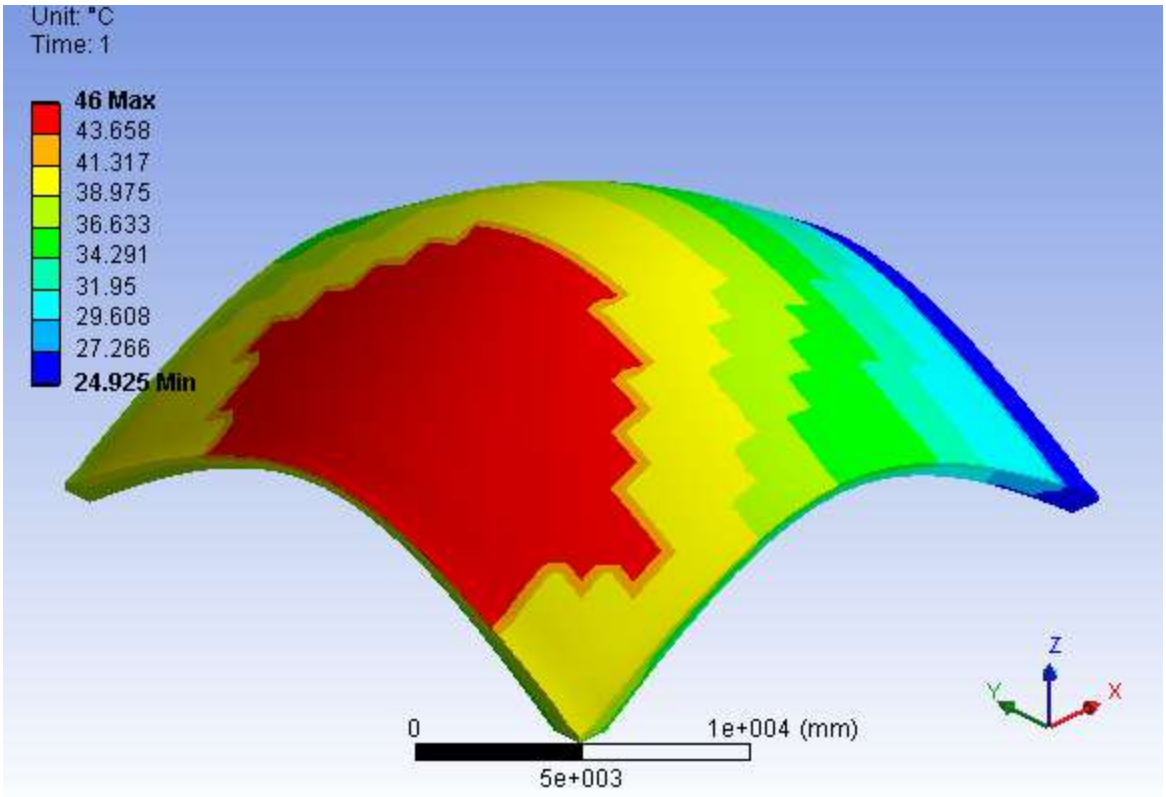


Figure 75: Change in temperature diagram for the finite element model in summer (note the varying temperature distribution in the cross-section of the structure)

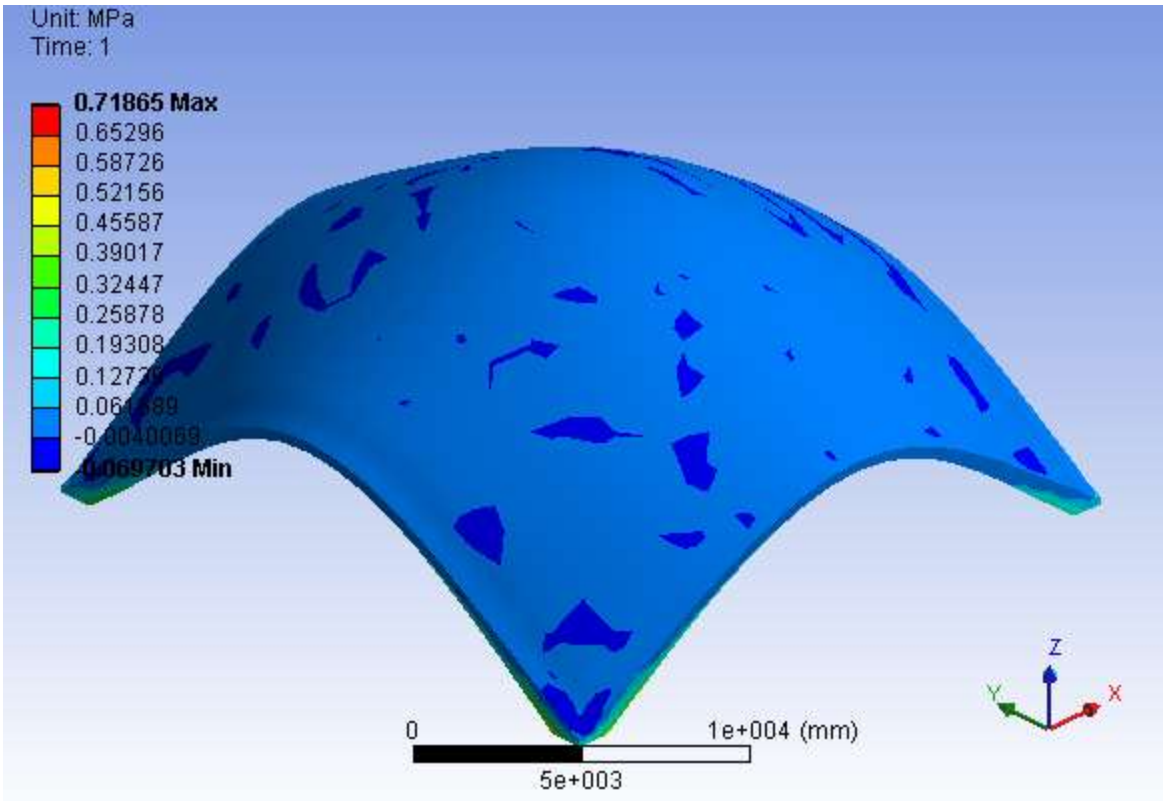


Figure 76: Maximum principle stress for the finite element model in summer

The result from this load scenario indicates again that the tensile stresses in the entire structure are fairly low with a few small areas on the inner surface of the structure reaching a third of the ultimate tensile strength. Most importantly the analysis indicates that the entire structure is within the tensile limit of the material. It is only by the support where the extremely high tensile stress occurs.

The third load scenario which was analysed was the plain surface of the structure with the design temperature loading derived previously. The maximum and minimum temperatures were determined in the winter months giving a maximum change in temperature of sixty degrees Celsius. This was processed in the temperature maps which produced the following results:

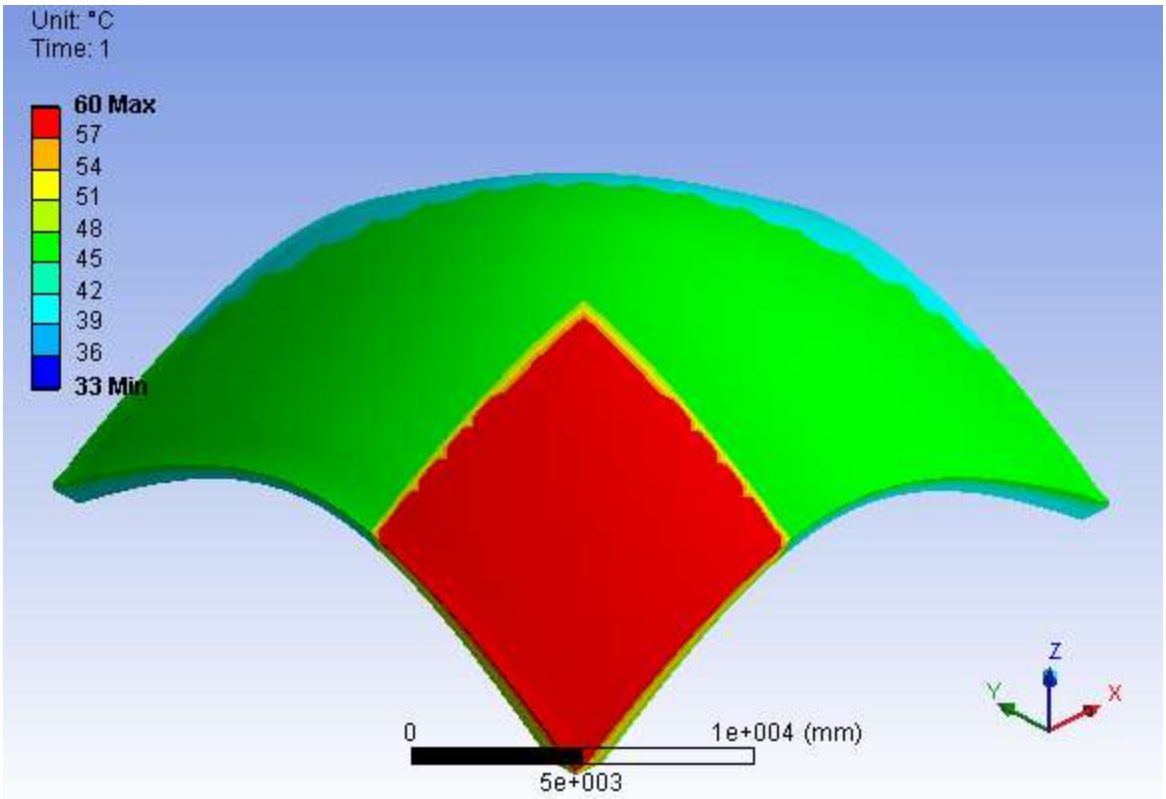


Figure 77: Change in temperature diagram for the finite element model according to the design temperature loading (note the varying temperature distribution in the cross-section of the structure)

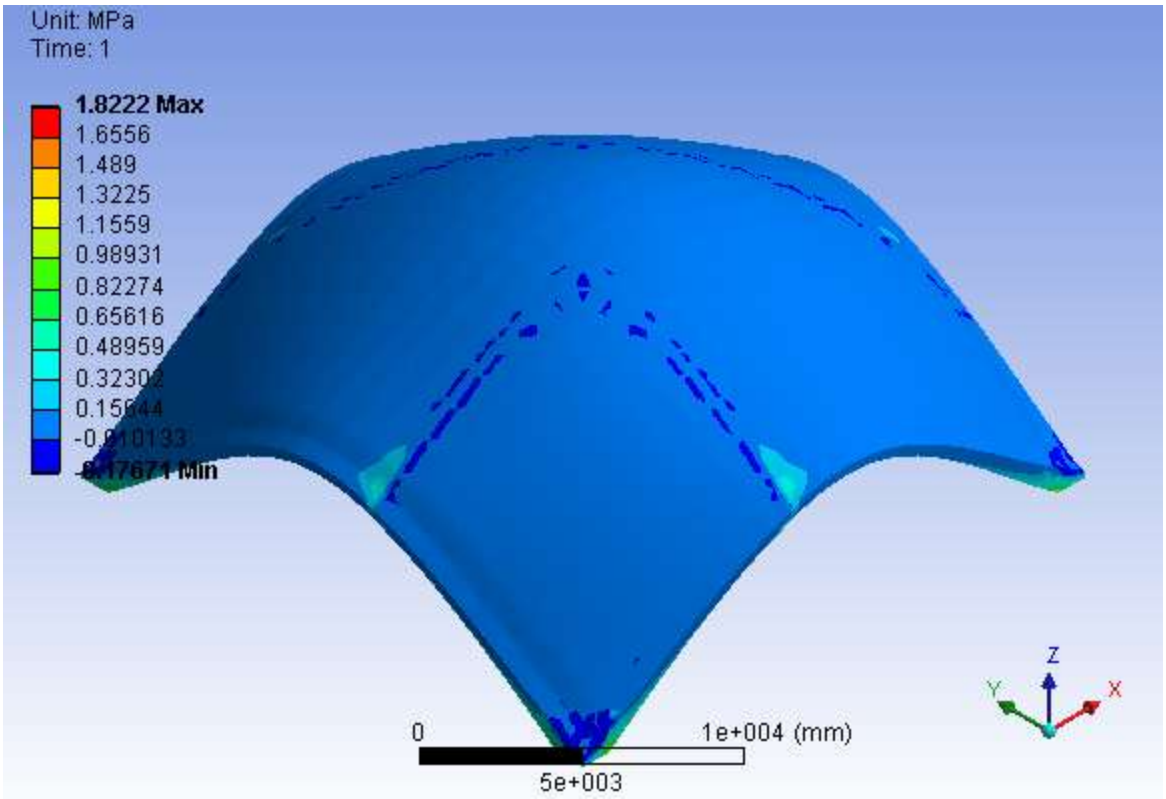


Figure 78: Outer surface maximum principle stress for the finite element model according to the design temperature loading

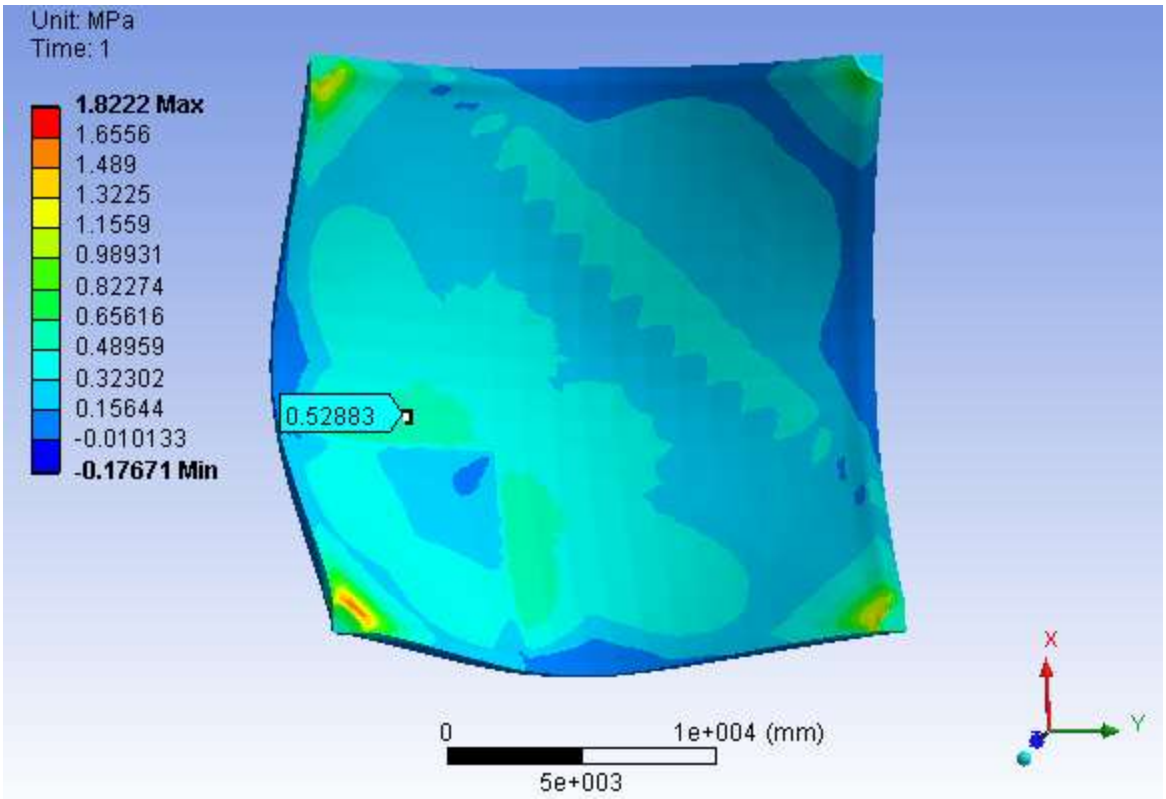


Figure 79: Inner surface maximum principle stress for the finite element model according to the design temperature loading

The change in temperature distribution design tool yielded fairly similar tensile stresses as compared to the actual temperature distribution in winter. A thermal induced tensile stress within a range of about twenty percent increase was observed in the design temperature loading. This implies that the prediction of the thermal induced stresses using the presented design tools are slightly conservative and may be applied in an actual design scenario.

The following load scenario which was analysed was the actual outer surface temperature distribution in the shell structure in the winter months, without the inner surface temperature distribution being applied to the structure. This was done to determine the effect of the varying temperature distribution through the cross section of the structure.

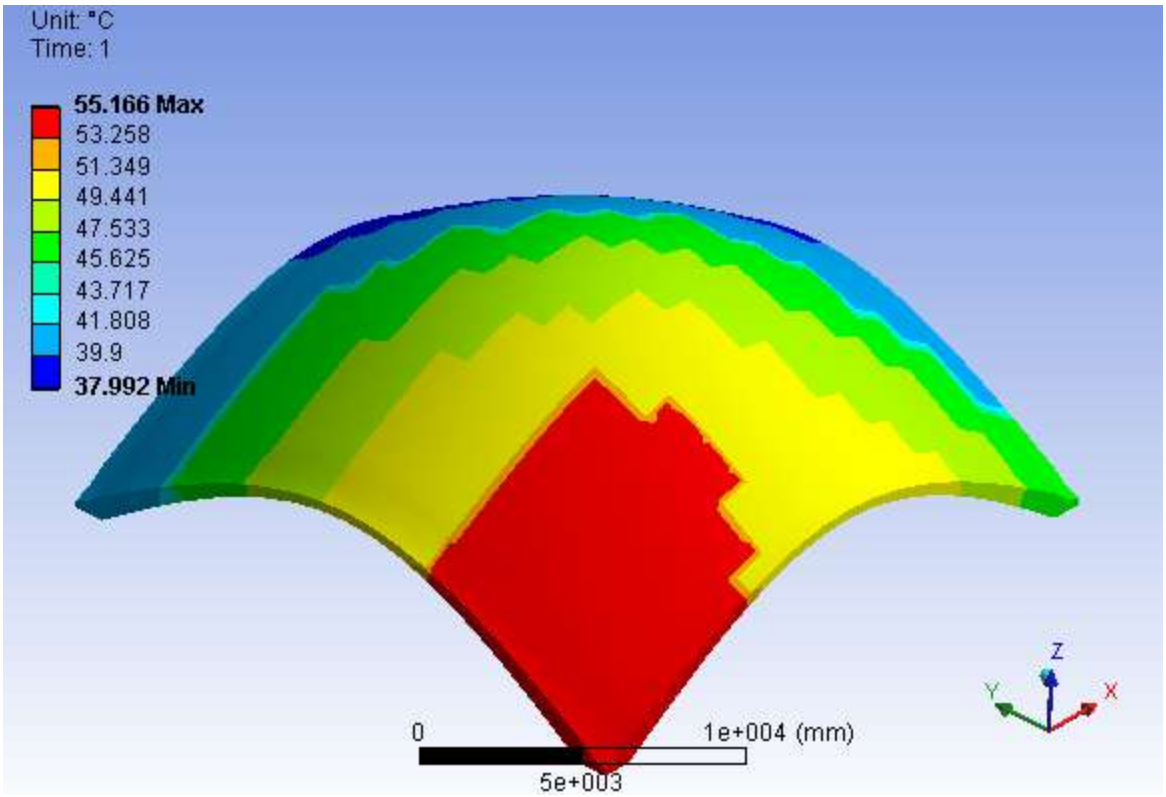


Figure 80: Change in temperature diagram for the finite element model, without the inner surface temperature distribution, in winter (note the constant temperature distribution in the cross-section of the structure)

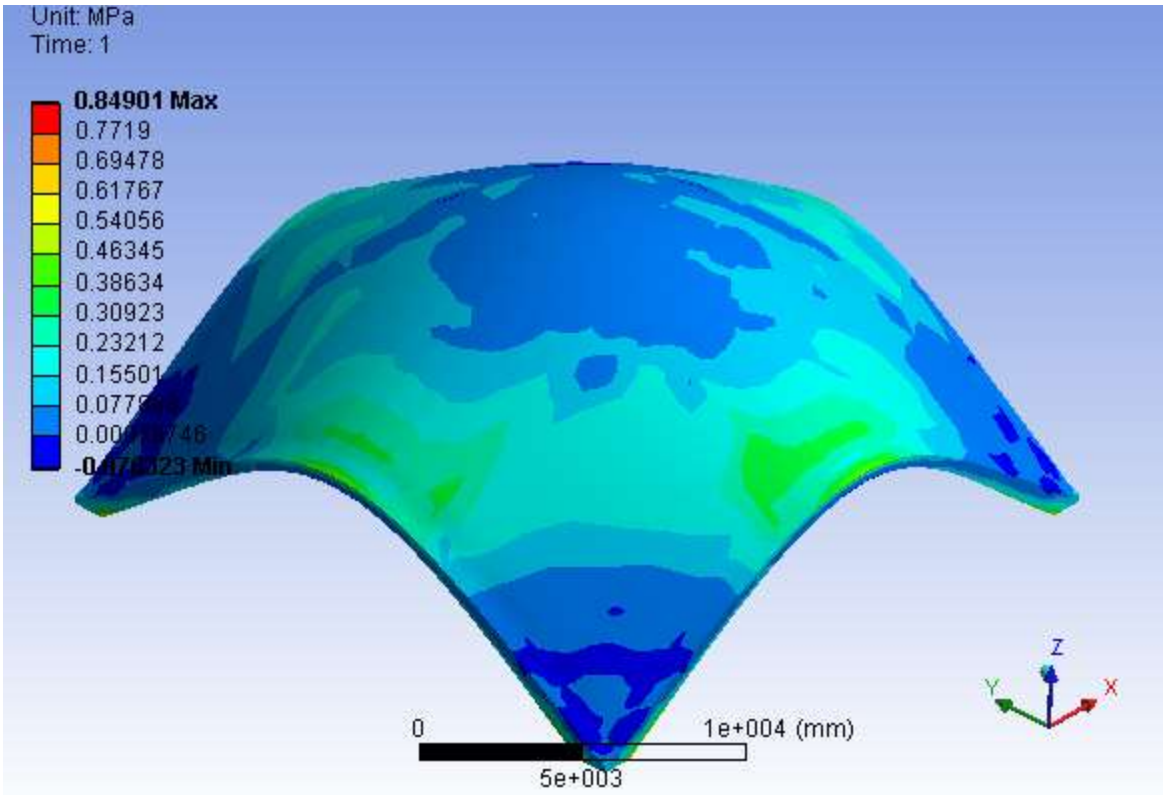


Figure 81: Maximum principle stress for the finite element model according to the outer surface temperature loading

It was expected that the varying temperature distribution would cause higher thermal induced tensile stresses on the outer surface of the structure. However, the constant temperature distribution through the cross-section of the structure produced much higher tensile stresses on the outer surface of the structure and much lower tensile stresses on the inner surface of the structure, as compared to the actual temperature distribtution. This is probably due to the inner surface temperature distribution reducing the change in temperature distribution in the structure, thus reducing the thermal induced stresses.

The constant temperature distribution behaves in the same way as the hanging handkerchief structure. Both structures are loaded essentially in the same direction and the stresses induced are tensile. Thus the handkerchief structure, or any other thin shell structure, would not appear to be a suitable structure under the presumed thermal loading. If the finite element model were represented by a middle surface or a shell element structure, much higher thermal

induced stresses would be observed as the cross-sectional temperature distribution in the model would be constant.

The next load scenario which was analysed was the actual winter thermal load in combination with the dead load of the structure. I did expect high thermal induced tensile stresses on the inner surface of the structure as there were tensile stresses on this inner surface in both load conditions. This load combination did not include any load safety factors so as to assume the induced stresses within the structure.

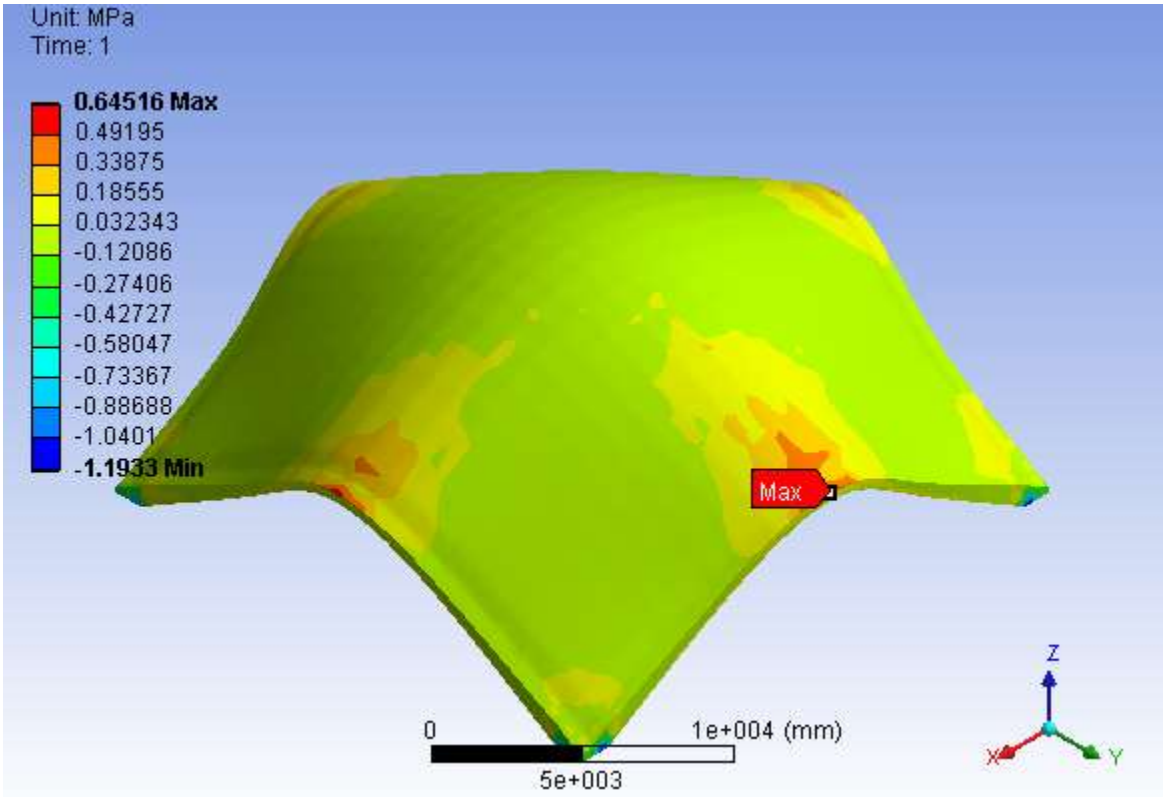


Figure 82: Outer surface maximum principle stress for the finite element model determined from the dead and temperature load combination

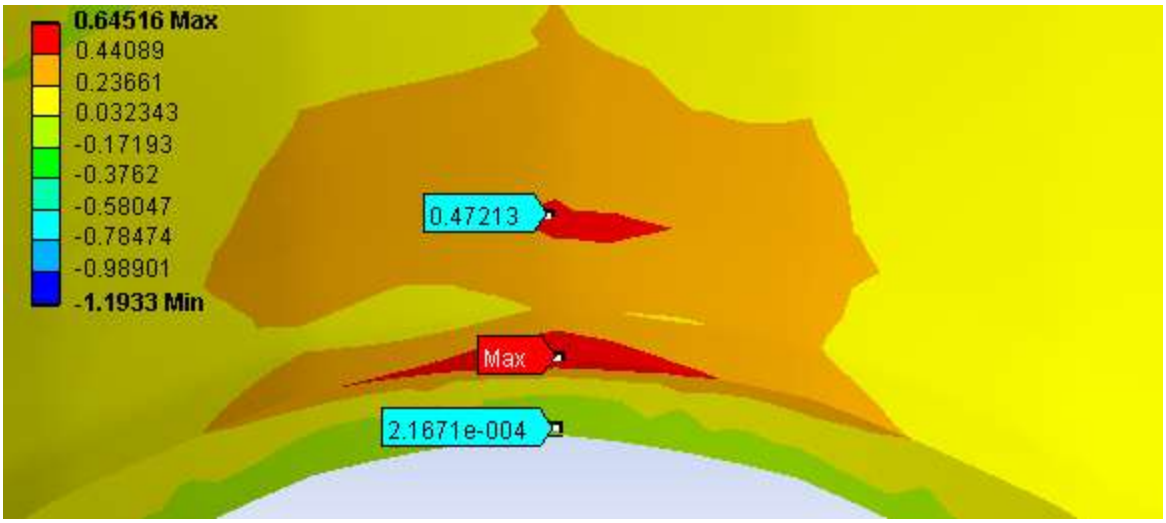


Figure 83: Arch tip maximum principle stress for the finite element model determined from the dead and temperature load combination

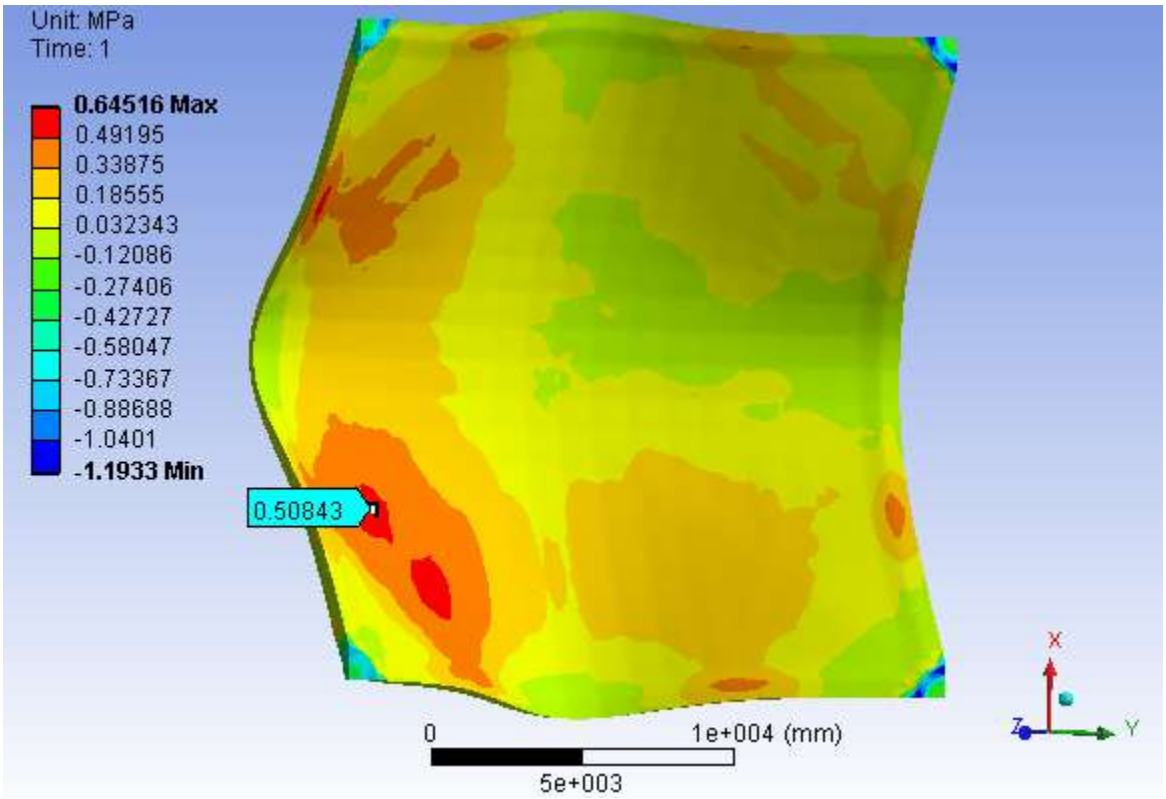


Figure 84: Inner surface maximum principle stress for the finite element model determined from the dead and temperature load combination

The result from this load scenario indicates that the tensile stresses on the outer surface of the structure are fairly low, except the tip of the arch with a tensile stress slightly higher than the ultimate tensile stress. It is clear from figure eighty three, a small and shallow crack on the outer surface will form. This crack may spread further or remain very small. On the inner surface there are some large areas reaching more than four fifths of the ultimate tensile strength.

The white surface temperature distributions were also mapped in the finite element model in combination with the dead load. This surface condition had a significant influence in summer reducing the thermal induced stresses by more than fifty percent. In the winter the thermal induced stresses were higher in a very small area at the tip of the arch at the end of the structure, but were significantly reduced on the underside of the structure as shown below:

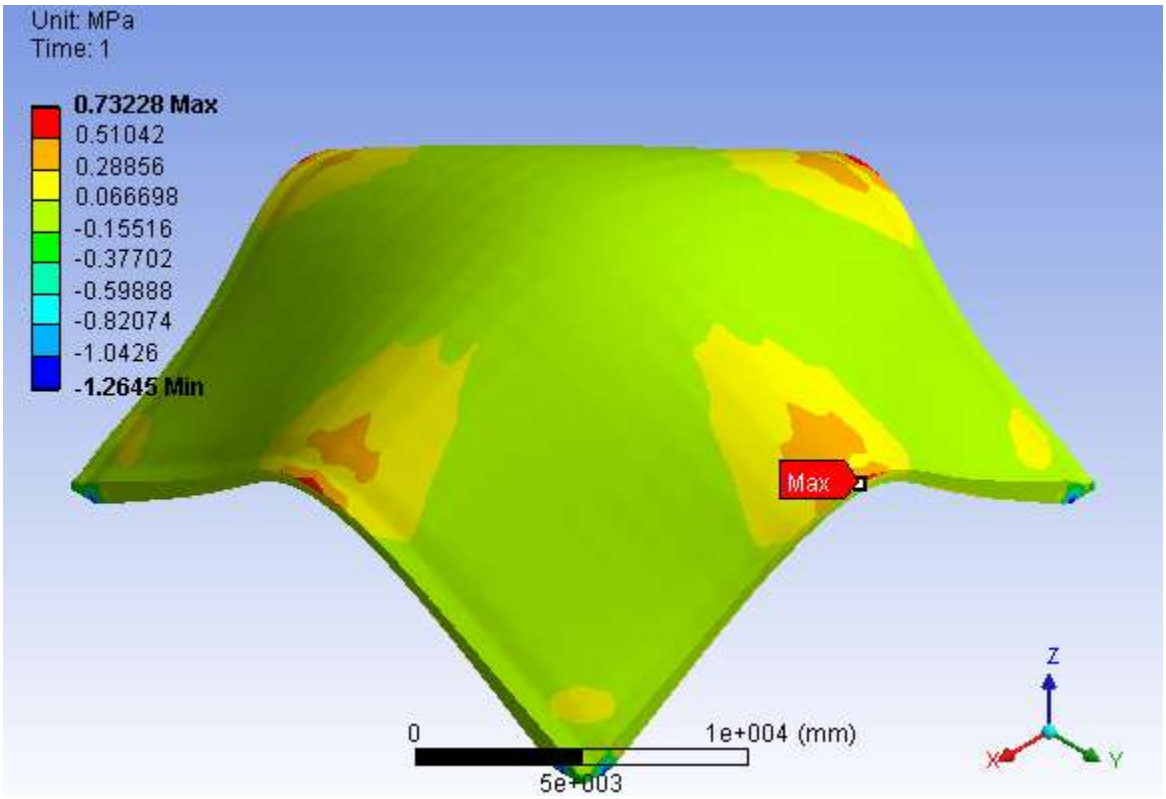


Figure 85: Outer surface maximum principle stress for a white surface structure

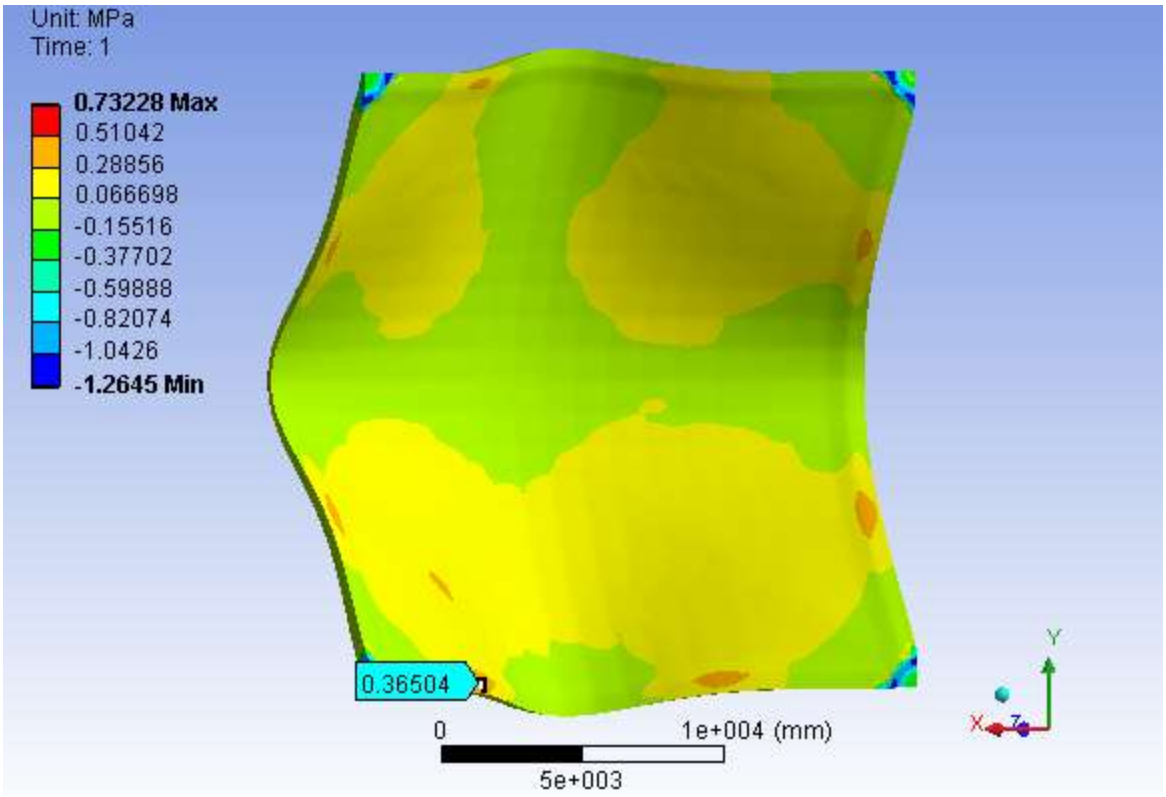


Figure 85: Inner surface maximum principle stress for a white surface structure

The white surface reduces the tensile stresses throughout the structure. However at the tip of the arch the stress is significantly increased indicating a crack at the tip larger than the plain surface crack.

## Discussion of FEM results

The finite element model results indicate that the maximum thermal induced tensile stresses within the handkerchief thin shell structure were above the ultimate tensile strength of the material. The area of this maximum tensile stress is also very small, the rest of the structure having a tensile stress below the ultimate tensile strength of the material. This in turn indicates that such a large structure may be erected with assumed minor thermal induced cracks at the tip of the arches at the ends, without any attenuation method being applied.

The extremely high stresses observed at the ends of the arches may be due to the discretized geometry of the structure. If a smooth geometry is applied in the finite element model, this tensile stress peak may diminish. The stresses on the inner surface of the structure do not

appear to be influenced by the discretized geometry as the geometry is smooth there, thus these stresses are presumed accurate.

If one would need to account for these thermal induced stresses with a safety factor, a bare minimum amount of reinforcement could be inserted by the areas of high tensile stress. This very small amount of reinforcement will not have a significant effect on the budget of a public building of this sort.

An alternative to reinforcement would be to include the mortar tensile strength in the design phase. Referring to “Structural Masonry Designers Manual” by W.G. Curtin et al, for clay bricks with a mortar of sixteen mega Pascal compressive strength, a designer is allowed four hundred kilo Pascal tensile strength. Crystacal has a compressive strength of forty four mega Pascal, using the ratio presented by the designers manual I expect a tensile strength of one thousand one hundred kilo Pascal. With the stabilized earth structure using Crystacal mortar in the first layer of tiles and other carefully determined areas (like the tip of the arches at the end of the structure), the induced thermal tensile stresses may be accounted for by the Crystacal mortar.

A white surface may be applied to the outer surface of the structure to attenuate the thermal induced stresses. With this surface and either of the two solutions mentioned above, I may be able to economically and adequately control the thermal induced tensile stresses in this handkerchief structure.

As thermal induced tensile stresses have been identified in thin shell structures to cause excessive cracking, these results display the ability of a thin shell structure constructed from stabilised earth to resist thermal induced tensile stresses by the carefully choosing the surface colour, support condition and shape of the structure. However, these results do not take into consideration the construction temperature of the structure.

The behaviour of the construction temperature induced stresses after placement is a complex problem. It is mainly affected by the temperature of the tiles at placement, the curing temperature of the mortar, the type and quantity of the binding materials, the solar radiation intensity and the boundary conditions of the structure. To capture this in a finite element

would be very complex and various models (FEM and real models) would need to be created to establish the effect of the initial temperature. The effect of the construction temperature is assumed to increase the total stress in the structure after completion. It is only the extent of this effect which needs to be determined.

## 7. Conclusion

From the beginning of this research project through to the apparent end, interesting results emerged from this project. I have found;

- High change in temperature distributions exist within stabilised earth, thin shell structures in the Gauteng region in South Africa, which causes cracking in these structures.
- The white surface attenuation method was able to control the most severe change in temperature distributions to an appreciable extent, more significantly though the thermal induced stresses were reduced considerably through most of the structure except for an extremely small portion.
- The stabilised earth, handkerchief shell structure performs excellently under self-weight and an imposed live load as expected; and even resists the actual temperature loading adequately as explained above.
- A conservative, change in temperature distribution design tool has been established for thin shell structures similar to the handkerchief shell structure, constructed from stabilised earth.

### Further research

In order to implement this design and construct proposal of thin shell structures using stabilised earth, further research is required in the design phase. A topic which may be the key to effectively and economically attenuating the thermal induced stresses may be found in optimising the shape of the thin shell structure.

Other methods of attenuating the thermal induced stresses may be explored, such as using thermal insulating paint which the manufacturers claim to reflect ninety nine percent of the

imposed heat. Support conditions may be varied and tested to allow the structure to expand freely when heated, and contract freely when cooled. Finally, considering trees and other landscape shading, which is an effective way of passively cooling the structure.

The only requirement which the research will require is a design and the construction of a life size structure. Although the results in this thesis indicate that there are methods of effectively controlling the thermal induced stresses in thin shell structures, a life size model would need to be designed, constructed and tested to determine the accuracy of these results. An example of this structure may be a low-cost house. With the construction of this structure the actual strains may be determined, cracking may be identified and the structure may be evaluated for adequate performance upon inspection, even among the communities who will receive these houses.

# 8. References


1. CRC Press - Technology and engineering, “Handbook of Structural Engineering”, Wai-Fah Chen, E.M. Lui
2. University of the Witwatersrand, School of Civil and Environmental Engineering, “Groin Vault Design”, CIVN4003: Design Project 2008, Adil Saloojee Daniel Cromberge Muhammad Bodhania Shaahid Hansa Zakarriyyah Ameen, Supervised by Professor M. Gohnert and Dr. A. Fitchett
3. University of the Witwatersrand, School of Civil and Environmental Engineering, “Skills development and employment creation through small public buildings in South Africa”, Anne Susan Fitchett
4. University of the Witwatersrand, School of Civil and Environmental Engineering, “Design & construction Criteria for domes in Low-cost housing”, G. Talocchino
5. CBS Publishers and distributors PVT. LTD., “Handbook of concrete engineering”, Second edition, Mark Fintel et al
6. California State Polytechnic University, “Physics, for scientist and engineers with modern physics”, Sixth edition, Raymond A. Serway, John W. Jewett Jr.
7. British Standards Institution, “BS 2846: Part 1: 1981 Guide to statistical interpretation of data, Part 1. Routine analysis of quantitative data”, United Kingdom
8. British Standards Institution, “BS 2846: Part 2: 1981 Guide to statistical interpretation of data, Part 2. Estimation of the mean: confidence interval”, United Kingdom
9. Statistics South Africa, “Methodology for Census 2001 South Africa: Applying the lessons learnt from Census '96”, Dr. Ros Hirschowitz
10. BSP Professional Books, “Structural masonry design manual”, Second edition, W.G. Curtain et al
11. Cement and concrete institute, Midrand, South Africa, “Fulton’s concrete technology”, Eighth edition, Brian Addis and Gill Owens et al

# 9. Appendices

## Selected temperature readings (raw data)

| Date | | |
|---|---|---|
| 15 | 2 | 2011 |

| Time | Ambient temperature | Description of weather |
|---|---|---|
| 14:25 | 27.7 | Sunny |

Model

Stone Surface

Outer surface

```
so3=[   53.5   50.5   51     46.5   43     37.5   ;
        55.5   56     55.5   52     47     39.5   ;
        55     54.5   53.5   51.5   46.5   37     ;
        52.5   56     52     47.5   45     38     ;
        51     55.5   51     48     42     36.5   ;
        49.5   49.5   45     43     38     33     ;];
```

Inner surface

```
si3=[   48.5   45.25   42    ;
        47     50.5    44.5  ;
        45.5   46.25   47    ;];
```

Plain Surface

Outer surface

```
po3=[   53     53     47.5   46     42     37     ;
        53     57     52     50.5   43     35.5   ;
        55.5   56.5   55.5   53     44.5   38     ;
        55     58.5   56     52.5   44     37.5   ;
        53.5   56     51     49.5   41     36.5   ;
        50     50     45     44     38.5   34     ;];
```

Inner surface

```
pi3=[   50.5    45.75    41   ;
        49.75   51       39.25;
        49      43.25    37.5 ;];
```

White Surface

Outer surface

```
wo3=[   33    33    32.5   30.5   30     30   ;
        34    34    34     31     30     27   ;
        34.5  35    34.5   31.5   27.5   27.5 ;
        34    34    34     32     29     28.5 ;
        32.5  33    32.5   31     30.5   27   ;
        31    31    31     30     29.5   27   ;];
```

Inner surface

```
wi3=[   33.5    31.5    29.5  ;
        31.5    33      27.75 ;
        29.5    27.75   26    ;];
```

| Time | Ambient temperature | Description of weather |
|---|---|---|
| 12:20 | 25.7 | Sunny |

Model

Stone Surface

Outer surface

```
so2=[   47.5  48  53  49  49  46 ;
        48    51  54  54  54  46 ;
        45    52  51  51  51  44 ;
        43    45  49  49  47.5 41 ;
        40    45  45.5 47 46  39 ;
        38    38  41  38  38  33 ;];
```

Inner surface

```
si2=[   43    41.5    40  ;
```

```
        40.25    41.5    37.5   ;
        37.5     36.25   35     ;];
```

Plain Surface

Outer surface

```
po2=[   42      50.5    51      52.5    52.5    46.5   ;
        46.5    53      53      54      51      46     ;
        47      52      52.5    54.5    52      45     ;
        44      50      51      52      48.5    44     ;
        42      47      46.5    48      47.5    41     ;
        38.5    39      39.5    41      40.5    36.5   ;];
```

Inner surface

```
pi2=[   45.5    44.25   43     ;
        44      45      40.75  ;
        42.5    40.5    38.5   ;];
```

White Surface

Outer surface

```
wo2=[   31      31.5    32      32.5    32.5    32.5   ;
        31      32      32      33.5    33      33     ;
        29.5    30      32.5    33      32.5    32     ;
        28.5    29      31.5    31.5    31.5    31     ;
        27.5    28      31      31      30.5    30.5   ;
        28      28.5    29      29      29      29     ;];
```

Inner surface

```
wi2=[   28.5    29.5    30.5   ;
        28.75   30      30.75  ;
        29      30      31     ;];
```

| Time | Ambient temperature | Description of weather |
|---|---|---|
| 06:00 | 15.2 | Clear, cool |

Model

Stone Surface

Outer surface

```
so1=[   11.1    11    11    11    11    11.1  ;
          11    11    11    11    11      11  ;
          11    11    11    11    11      11  ;
          11    11    11    11    11      11  ;
          11    11    11    11    11      11  ;
        11.1    11    11    11    11    11.1  ;];
```

Inner surface

```
si1=[   11.1    11    11.1  ;
          11    11      11  ;
        11.1    11    11.1  ;];
```

Plain Surface

Outer surface

```
po1=[     11    11    11    11    11      11  ;
          11    11    11    11    11      11  ;
          11    11    11    11    11      11  ;
          11    11    11    11    11      11  ;
          11    11    11    11    11      11  ;
          11    11    11    11    11      11  ;];
```

Inner surface

```
pi1=[     11    11    11  ;
          11    11    11  ;
          11    11    11  ;];
```

White Surface

Outer surface

```
wo1=[     11    11    11    11    11      11  ;
          11    11    11    11    11      11  ;
```

| | | | | | | |
|---|---|---|---|---|---|---|
| | 11 | 11 | 11 | 11 | 11 | 11 ; |
| | 11 | 11 | 11 | 11 | 11 | 11 ; |
| | 11 | 11 | 11 | 11 | 11 | 11 ; |
| | 11 | 11 | 11 | 11 | 11 | 11 ;]; |

Inner surface

| | | | | |
|---|---|---|---|---|
| wi1=[ | 11 | 11 | 11 | ; |
| | 11 | 11 | 11 | ; |
| | 11 | 11 | 11 | ;]; |

| Date | | |
|---|---|---|
| 19 | 7 | 2011 |

| Time | Ambient temperature | Description of weather |
|---|---|---|
| 13:45 | 25.4 | Sunny |

Model

Pumice Stone Surface

Outer surface

| | | | | | | | |
|---|---|---|---|---|---|---|---|
| so3=[ | 30 | 33 | 31 | 30 | 28.5 | 26 | ; |
| | 32 | 32 | 28 | 27 | 25.5 | 25 | ; |
| | 27.5 | 27.5 | 27 | 26 | 25 | 24 | ; |
| | 27.5 | 27 | 27 | 25.5 | 25 | 24 | ; |
| | 27.5 | 27 | 24.5 | 25 | 24.5 | 24 | ; |
| | 28.5 | 27.5 | 24.5 | 25 | 24.5 | 24 | ;]; |

Inner surface

| | | | | |
|---|---|---|---|---|
| si3=[ | 28 | 27 | 26 | ; |
| | 27 | 26 | 24.5 | ; |
| | 26 | 24.5 | 23 | ;]; |

Plain Surface

Outer surface

| | | | | | | | |
|---|---|---|---|---|---|---|---|
| po3=[ | 45 | 45 | 42.5 | 42 | 38 | 34 | ; |

```
                44.5    44.5    44      41      35      30  ;
                40.5    40.5    40      37      32.5    29  ;
                39      39      38.5    34      29      25.5;
                34.5    34.5    29.5    30      26.5    26  ;
                32      29.5    29      25.5    25      24.5;];
```

Inner surface

```
pi3=[           37      34      31  ;
                33      34.5    27.25;
                29      26.25   23.5;];
```

White Surface

Outer surface

```
wo3=[           33      33      33      32      32.5    30  ;
                32      31.5    31.5    30      29.5    29  ;
                30.5    30.5    30.5    28.5    28.5    28  ;
                29      29      29      27.5    27      27  ;
                28.5    28      28      26      26      26  ;
                27      26.5    26.5    26      26      26  ;];
```

Inner surface

```
wi3=[           31      29.75   28.5    ;
                29.5    27      27      ;
                28      26.75   25.5    ;];
```

| Time | Ambient temperature | Description of weather |
|---|---|---|
| 12:15 | 23.3 | Sunny |

Model

Pumice Stone Surface

Outer surface

```
so2=[           28      28      29      28      28      28  ;
                26      27      27      26      26      26  ;
```

```
                25      25      25      24.5      24      24  ;
                24      24      24      24        24      24  ;
                24      23.5    23.5    23        23      22.5;
               23.5     23      23      22        22      21.5;];
```

Inner surface

```
si2=[           27      27      27  ;
               24.5     24      24  ;
                22      21.5    21  ;];
```

Plain Surface

Outer surface

```
po2=[           40      40.5    40.5    41        41      38  ;
               36.5     37      37      39        38.5    34  ;
               34.5     35      35      34        35      32.5;
               31.5     31.5    31.5    33        32.5    32.5;
               27.5     27.5    27.5    28.5      28.5    28  ;
               24.5     24.5    24.5    25        24.5    24.5;];
```

Inner surface

```
pi2=[           33      33.5    34  ;
              28.75     30      29.5;
               24.5     24.75   25  ;];
```

White Surface

Outer surface

```
wo2=[         28.5      28.5    29      29        28.5    28.5;
              25.5      25.5    26.5    26.5      27      27  ;
              25.5      25.5    25.5    25.5      26      26  ;
               23       23      23      24.5      24.5    25  ;
               23       23      23      23        23      23.5;
              22.5      22.5    22.5    23        23      23  ;];
```

Inner surface

```
wi2=[     27.5    28.25     29   ;
          25.25   24.5      26   ;
          23      23        23   ;];
```

| Time | Ambient temperature | Description of weather |
|---|---|---|
| 06:00 | 1 | Clear, cold |

Model

Pumice Stone Surface

Outer surface

```
so1=[    -12.1    -12    -12    -12    -12    -12.1   ;
          -12     -12    -12    -12    -12     -12    ;
          -12     -12    -12    -12    -12     -12    ;
          -12     -12    -12    -12    -12     -12    ;
          -12     -12    -12    -12    -12     -12    ;
         -12.1    -12    -12    -12    -12    -12.1   ;];
```

Inner surface

```
si1=[    -12.1    -12    -12.1   ;
          -12     -12     -12    ;
         -12.1    -12    -12.1   ;];
```

Plain Surface

Outer surface

```
po1=[    -12.1    -12    -12    -12    -12    -12.1   ;
          -12     -12    -12    -12    -12     -12    ;
          -12     -12    -12    -12    -12     -12    ;
          -12     -12    -12    -12    -12     -12    ;
          -12     -12    -12    -12    -12     -12    ;
         -12.1    -12    -12    -12    -12    -12.1   ;];
```

Inner surface

```
pi1=[    -12.1    -12    -12.1   ;
```

```
        -12     -12     -12   ;
       -12.1    -12    -12.1  ;];
```

White Surface

Outer surface

```
wo1=[  -12.1    -12     -12     -12     -12    -12.1  ;
        -12     -12     -12     -12     -12     -12   ;
        -12     -12     -12     -12     -12     -12   ;
        -12     -12     -12     -12     -12     -12   ;
        -12     -12     -12     -12     -12     -12   ;
       -12.1    -12     -12     -12     -12    -12.1  ;];
```

Inner surface

```
wi1=[  -12.1    -12    -12.1  ;
        -12     -12     -12   ;
       -12.1    -12    -12.1  ;];
```

## Soil grading (raw data)

Soil Grading
60%
pit 40% river
Pit & River Sand

| Pan Mass | 274.11 | | Before wash | 782.51 | 508.4 | Actual mass | 508.4 |
|---|---|---|---|---|---|---|---|
| | | | After wash | 743.02 | 468.91 | | |

| Sieve size | Mass Retained | % Retained | % Retained (Whole) | % Passing | (check) |
|---|---|---|---|---|---|
| 6.7 | 0 | 0 | 0 | 100 | 100 |
| 4.75 | 6.5 | 1.27852085 | 1.27852085 | 98.72148 | 98.72148 |
| 2.36 | 63.1 | 12.411487 | 13.69000787 | 86.30999 | 86.30999 |
| 1.18 | 73.9 | 14.5357986 | 28.22580645 | 71.77419 | 71.77419 |
| 0.6 | 61.4 | 12.0771046 | 40.30291109 | 59.69709 | 59.69709 |
| 0.425 | 43 | 8.45790716 | 48.76081825 | 51.23918 | 51.23918 |
| 0.3 | 61 | 11.9984264 | 60.75924469 | 39.24076 | 39.24076 |
| 0.15 | 115.3 | 22.6789929 | 83.43823761 | 16.56176 | 16.56176 |
| 0.075 | 44.1 | 8.67427223 | 92.11250983 | 7.88749 | 7.88749 |
| pan | 0.6 | | | | |

Plaster Sand

| Pan Mass | 274.11 | | Before wash | 665.23 | 391.12 | Actual mass | 391.12 |
|---|---|---|---|---|---|---|---|
| | | | After wash | 632.32 | 358.21 | | |

| Sieve size | Mass Retained | % Retained | % Retained (Whole) | % Passing | Size difference |
|---|---|---|---|---|---|
| 6.7 | | | 0 | 100 | |
| 4.75 | 0 | 0 | 0 | 100 | 1.278521 |
| 2.36 | 2.34672 | 0.6 | 0.6 | 99.4 | 13.16902 |
| 1.18 | 4.30232 | 1.1 | 1.7 | 98.3 | 26.98454 |
| 0.6 | 17.99152 | 4.6 | 6.3 | 93.7 | 36.28913 |
| 0.425 | 40.28536 | 10.3 | 16.6 | 83.4 | 38.56213 |
| 0.3 | 62.5792 | 16 | 32.6 | 67.4 | 41.77929 |
| 0.15 | 142.7588 | 36.5 | 69.1 | 30.9 | 46.40206 |
| 0.075 | 44.9788 | 11.5 | 80.6 | 19.4 | 59.34283 |
| | | | | | 32.97594 |

## Design surface temperature graph (raw data)

Plain surface

| x | Temperature readings y |
|---|---|
| Ambient temperature (°C) | Temperature (°C) |
| 32.3 | 54.5 |
| 32.1 | 54.2 |
| 28.8 | 53 |
| 28.7 | 52.8 |
| 27.7 | 58.5 |
| 27.5 | 59 |
| 27.9 | 59 |
| 25.7 | 52 |
| 25.4 | 45 |
| 25.2 | 49 |
| 23.3 | 40 |
| 23.2 | 40 |
| 22.1 | 41 |
| 22 | 40 |
| 21.9 | 40 |
| 21.9 | 40 |
| 15 | 11 |
| 15 | 11 |
| 15 | 11 |
| 14 | 11 |
| 14 | 11 |
| 14 | 11 |
| 13 | 10 |
| 13 | 10 |
| 13 | 10 |
| 2 | -12 |
| 2 | -12 |
| 1 | -13 |
| 1 | -13 |

| | | |
|---|---|---|
| Slope, m | m | 2.586182 |
| Intercept, b | b | -20.4294 |
| Observations, n | n | 29 |
| std error Syx | SYX | 5.322615 |
| Average x | XAVG | 18.88621 |
| Std deviation squared | SSX | 2418.254 |
| t(alpha,df) | t | 2.042272 |
| t(0.05,n+1) | | |

The values of t are those of Student's t distribution

| x | CI | y+CI |
|---|---|---|
| 0 | 4.63716 | -15.7922 |
| 5 | 3.673764 | -3.8247 |
| 10 | 2.816551 | 8.248998 |
| 15 | 2.193741 | 20.5571 |
| 20 | 2.03351 | 33.32777 |
| 25 | 2.429188 | 46.65436 |
| 30 | 3.179602 | 60.33568 |
| 35 | 4.09413 | 74.18112 |

White surface

| | Temperature readings |
|---|---|
| x<br>Ambient temperature (°C) | y<br>Temperature (°C) |
| 32.3 | 33 |
| 32.1 | 32.5 |
| 28.8 | 31 |
| 28.7 | 30 |
| 27.7 | 35 |
| 27.5 | 34 |
| 27.9 | 35 |
| 25.7 | 30 |
| 25.4 | 30 |
| 25.2 | 29 |
| 23.3 | 25.5 |
| 23.2 | 25 |
| 22.1 | 23 |
| 22 | 23 |
| 21.9 | 23 |
| 21.9 | 23 |
| 15 | 11 |
| 15 | 11 |
| 15 | 11 |
| 14 | 11 |
| 14 | 11 |
| 14 | 11 |
| 13 | 10 |
| 13 | 10 |
| 13 | 10 |
| 2 | -12 |
| 2 | -12 |
| 1 | -13 |
| 1 | -13 |

| | | |
|---|---|---|
| Slope ,m | m | 1.605458 |
| Intercept, b | b | -12.8038 |
| Observations, n | n | 29 |
| std error Syx | SYX | 2.469808 |
| Average x | XAVG | 18.88621 |
| Std deviation squared | SSX | 2418.254 |
| t(alpha,df) | t | 2.042272 |
| t(0.05,n+1) | | |

The values of t are those of Student's t distribution

| x | CI | y+CI |
|---|---|---|
| 0 | 2.151742 | -10.652 |
| 5 | 1.704706 | -3.07178 |
| 10 | 1.30694 | 4.557747 |
| 15 | 1.017943 | 12.29604 |
| 20 | 0.943593 | 20.24898 |
| 25 | 1.127196 | 28.45988 |
| 30 | 1.475404 | 36.83538 |
| 35 | 1.899765 | 45.28703 |